Low Speed Avian Maneuvering Flight

Low Speed Avian Maneuvering Flight

A dissertation presented

by

Ivo Ros

to

The department of Organismic and Evolutionary Biology

in partial fulfillment of the requirements

for the degree of

Doctor of Philosophy

in the subject of

Biology

Harvard University

Cambridge, Massachusetts

October, 2013

Dissertation Advisor: Professor Andrew A. Biewener Ivo Ros

Low Speed Avian Maneuvering Flight

Abstract

Low speed avian maneuvering flight is an ecologically crucial behavior that has contributed to the explosive diversification of several avian taxa by allowing access to complex spatial environments. Negotiating a sharp aerial turn requires finely tuned interactions between an animal's sensory-motor system and its environment. My thesis work focuses on how aerodynamic forces, wing and body dynamics, and sensory feedback interact during aerial turning in the pigeon (*Columba livea*).

Using high-speed kinematics and inertia data, I resolve the aerodynamic forces during low speed turns. The pigeons' tip-reversal upstroke is found to be aerodynamically active, indicating its role for increased power production. The overall turning strategy consists of body rotations that redirect aerodynamic forces to change flight trajectory, followed by body rotations that re-establish forward flight posture upon exiting the turn.

Through mechanical modeling, I separate aerodynamic from inertial effects, showing that aerodynamic torques dominate in pigeon flight. Contrary to previous findings, contra-lateral asymmetries in wing speed do not appear to underlie aerial turns, and surprisingly, nor do contra-lateral differences in wing area, angle of attack, wingbeat amplitude, or timing. The pigeons simply reorient their wing trajectories toward the desired direction. As a result, the aerodynamic

force, which acts above the center of mass, is redirected into the turn, generating the torques required to turn.

Detailed measurements of body, wing and head orientations and velocities confirm a functional decoupling between head and body motions, allowing insight into sensory control principles. Brief head motions (saccades) during aerial turns provide visual feedback to control the bird's flight trajectory and, likely, cervical mechanosensory feedback to control body orientation.

Visual (versus vestibular) cues dominate in the perception of motion in birds. To test whether vision is used to stabilize flight, I present freely hovering hummingbirds (*A. colubris*) with rear-projected, artificial, rotating panoramas. The hummingbirds separate optical cues that arising from self-rotation from those arising from translational flight, and use both visual inputs to stabilize their vision and control their hovering flight. Similar visual-motor principles have been observed in insects, suggesting that these may be robust control strategies common to a wide range of flying animals.

TABLE OF CONTENTS

ACKNOWLEDGEMENTS

Phrasing my thesis in the singular first person narrative misrepresents the many instrumental contributions from those such as my thesis advisor, wife, colleagues, friends and thesis committee. To give at least some credit where lots of credit is due, I would like to say a few words of acknowledgement. I undoubtedly will inadvertently omit several contributors, and apologize in advance.

First and foremost a most heartfelt thank you to my advisor Andy Biewener. Andy epitomizes what a student could want in an advisor: A combination of tremendous scientific insight and expertise and personal warmth and understanding. Great patience when more time is needed, and expedited assistance when time is running short. I thoroughly appreciate the freedom to work independently as well as the ever ready guidance and hands-on enthusiastic experimental help. Thank you very much!

My graduate school experience has been life changing, quite literally. I now live with the love of my life (we met at CFS) and we are about to welcome a daughter to our family, in addition to our son Riley. I thank you, Anna, for your loving support, countless comments and (mostly) tireless ear and attention for me talking about birds.

Only while raising my own offspring have I truly come to learn and appreciate the dedication of my parents. I proudly thank them, pa and ma, for their unconditional support and hope their dispersed nest has lead and continues to lead to an overall increase in their happiness.

Although the saying “Choose a job you love, and you will never work a day in your life” (purportedly by Confucius) probably only extremely rarely transcends the proverbial into the literal, I feel very privileged to have relatively few days that feel like ‘work’. In no small part this is due to the phenomenal Concord Field Station and its staff. I would like to thank Pedro Ramirez, Ken Wilcox, Lisa Litchfield, Peg Hedström and Somer O’Brien for all their help, both scientifically and personally.

Furthermore, throughout the years, I feel lucky to have met the many other grad students and post docs at the Concord Field Station. I am indebted to each and every one for sharing their knowledge and friendship. I particularly thank: Trevor Higgins for showing a foreigner life outside of CFS; Andrew Carrol for exploring lakes near Bedford while talking physiology, you are missed; Dave Lee for the combination of Kung Fu movies and great whisky; Russ Main for soccer; Craig McGowan for countless rides and surgery guidance; Jen Carr for teaching teaching; Ed Yoo for amazing pictures; Carlos Moreno for lengthy discussions of goats and birds; Chris Richards for not letting those conversations bother him (too much), and for phenomenal music; Monica Daley for coding; Glenna Clifton for bridging the distance; Andrew Mountcastle for combining science and humor; Huai-Ti Lin for good food and electronics; Ty Hedrick for discussions and for his famous 3D reconstruction methods. The list gets long fast, illustrating the collective effort of research, but I also specifically thank Carolyn Eng, Allison Arnold-Rife, Talia Moore, Dave Williams, Sridhar Ravi, David Lentink, Mary Salcedo, Jake Peters and Callin Switzer.

The thesis work would not be complete without the indispensable contributions of and fun interactions with the many students during my graduate school experience. In particular, I thank Marc Badger, Alyssa Pierson and Yeahmoon Hong, as well as Annika Eberle, Charles Gastil, Alex Randall and Emmett Kistler.

The members of my thesis committee, in addition to Andy Biewener, namely Stacey Combes, George Lauder, Bence Ölveczky and Doug Warrick have been most helpful and supportive, with their insightful questions and suggestions significantly improving my thesis work. Much obliged.

I would also like to express my gratitude to Eize Stamhuis and John Videler, who trained me prior to my graduate studies and taught not only science but life-lessons along the way.

I thank Dan Lieberman for generously allowing the use of his high speed camera system as well as for intriguing conversations. Which brings up Fuzz Crompton: always graciously interested and helpful in putting the research in a broad perspective.

In addition to the department of Organismic and Evolutionary Biology here at Harvard, I thank the National Science Foundation, the Office of Naval Research and the Robert A. Chapman Memorial Scholarship Fund for making the research possible.

"Perfect as the wing of a bird may be, it will never enable the bird to fly if unsupported by the air. Facts are the air of science. Without them a man of science can never rise”

~ Ivan Pavlov

CHAPTER 1

Introduction

Well known derived features of birds are asymmetrical flight feathers and the fusion of lightweight bones (Gill, 1995). These adaptations to flight illustrate strong selective evolutionary pressures. An enlargement of the keel and pectoralis muscles predominantly evolved to generate the high mass-specific power required for slow flight (Gill, 1995). Adaptations allowing for the ability to maneuver are anatomically less obvious. However, this does not imply that adaptations for flight control carry less evolutionary weight. It is suggested that the ability to maneuver allowed for the explosive diversification of certain avian taxa by lifting the constraint to large spatial environments (Warrick et al. 1998).

For a flying animal, negotiating a sharp turn requires many finely tuned interactions between the external environment, the animal's sensory systems, central nervous system and musculo-skeletal system. Understanding the organization and constraints of these systems benefits greatly from an integrative approach, in which the systems are not only investigated individually, but also as a collective (figure 1).

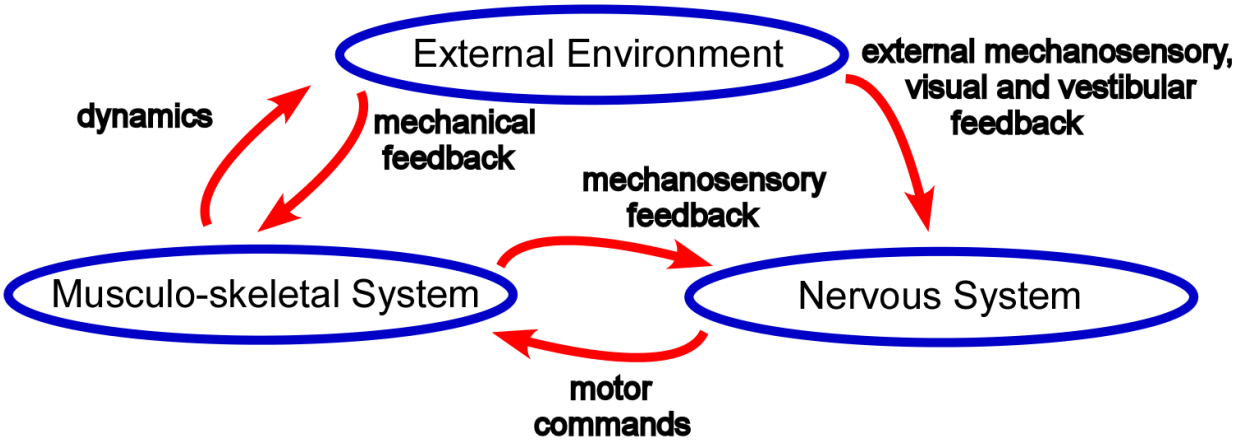

Figure 1_1. The interactions between various components of the avian flight system.

Flapping flight is an intense mode of locomotion, due to both fluctuating aerodynamic forces and inertial consequences of moving wings which each comprise about 6 % of the body mass at high frequencies. These mechanical challenges in combination with the control requirements of moving through a three-dimensional environment with many degrees of freedom across the avian body plan, and high mass-specific power requirements, make low speed maneuvering flight an especially complex sensorimotor behavior.

Chapter 1 Introduction

The pigeon is an ideal animal and species model system in which to examine maneuvering flight. Much of the influential past work on avian neural organization, perception, behavior, motor control, and muscle physiology has been performed on pigeons (see Zeigler and Bischof, 1993; Davies & Green, 1994). Furthermore, specimens are readily available, reasonably sized, trainable and, last but not least, very adept at low speed maneuvering, which is required in their natural habitats of cliffs and rock ledges (Baptista et al., 1997). In addition to the pigeon, I use the hummingbird to study the involvement of optic flow in flight stabilization.

Hummingbirds excel at hovering among birds, with several specializations, such as in their in their skeletal morphology (Stolpe & Zimmer, xxxx), neuroanatomy (Iwaniuk) and wing stroke kinematics (Hedrick *et al*., 2012).

In Chapter 2 the role of body rotations in relation to aerodynamic force production is investigated to obtain a fundamental understanding of turning flight. Aerodynamic forces are found to be produced in a uniform anatomical direction, emphasizing the central role of body rotations in low speed aerial turning. Two functionally separate body rotations are identified, separating analysis of flight trajectory, or course, from analysis of angular body positioning. The relationship between these body rotations and aerodynamic force production elucidates that turning pigeons prioritize changes in flight course over angular positioning of the body, or flight posture. Furthermore, the functionally distinct body rotations allow for targeting of sensory feedback specific to the control of course, or flight path, and body orientation in chapter 4.

The mechanisms of torque generation crucial to aerial turns are investigated in chapter 3. From chapter 2 it follows that torques, which underlie body rotations, play a cardinal role in flight control. To separate aerodynamic from inertial bases for these torques, in chapter 3, aerodynamic and inertial accelerations of pigeons turning during low speed flight are separately calculated using segment masses, moments of inertia and time-varying wing and body configurations. Directly measured body accelerations were predicted by aerodynamic torques, with aerodynamic torques correlating with contralateral asymmetries in swept wing trajectories and wing long axis rotation angles. No contra-lateral asymmetries were found in wing speed, wing area, angle of attack, wingbeat amplitude, or timing. Instead of using mosaic of kinematic variables, turning pigeons appear to generate aerodynamic torques by simply reorienting their wing trajectories toward the desired direction. The thereby initiated body rotations are subsequently arrested through aerodynamic damping, resulting in the previously described impulsive nature of low speed aerial turns in pigeons.

In chapter 4 I investigate head stabilization in relation to the sensory control of turning flight. Based on previous observations that the eyes remain fixed relative to the head, control inputs are inferred from detailed head and body orientations and velocities during 90-degree aerial turns. Visual cues induced by rapid head reorientations, or saccades, predict changes in flight trajectory, whereas the magnitude of neck bending predicts changes in angular positioning of the body.

Expanding on the visual control of flight, in chapter 5, the role of optic flow in flight stabilization is investigated in ruby-throated hummingbirds. I present freely hovering ruby-throated hummingbirds with projected virtual panoramas, or surrounds, rotated in different directions and at different speeds. The birds counter these illusory self-motions by rotating their head and body, and by flying with the surround. The hummingbirds apparently separate rotational from translational optic flow and use both these visual cues to stabilize their vision and control hovering flight, much like insects.

The collective goal of the thesis work is to expand on the current understanding of maneuvering flight and provide insight into general principles in areas such as muscle and general physiology, control theory, neurobiology and the evolution of animal flight.

CHAPTER 2

Pigeons steer like helicopters

and generate down- and upstroke lift during low speed turns

Ivo G. Ros[1], Lori C. Bassman[2], Marc A. Badger[2], Alyssa N. Pierson[2]

and Andrew A. Biewener[1]

Published in *PNAS* **108**, 19990-19995
doi: 10.1073/pnas.1107519108

ABSTRACT. Turning is crucial for animals, particularly during predator-prey interactions and to avoid obstacles. For flying animals, turning consists of changes in 1) flight trajectory, or path of travel, and 2) body orientation, or 3D angular position. Changes in flight trajectory can only be achieved by modulating aerodynamic forces relative to gravity. How birds coordinate aerodynamic force production relative to changes in body orientation during turns is key to understanding the control strategies used in avian maneuvering flight. We hypothesized that pigeons produce aerodynamic forces in a uniform direction relative to their body, requiring changes in body orientation to redirect those forces to turn. Using detailed 3D kinematics and body mass distributions, we examined net aerodynamic forces and body orientations in slowly flying pigeons (*Columba livia*) executing level 90º turns. The net aerodynamic force averaged over the downstroke was maintained in a fixed direction relative to the body throughout

the turn, even though the body orientation of the birds varied substantially. Early in the turn, changes in body orientation primarily redirected the downstroke aerodynamic force, affecting the bird's flight trajectory. Subsequently, the pigeons mainly reacquired the body orientation used in forward flight without affecting their flight trajectory. Surprisingly, the pigeon's upstroke generated aerodynamic forces that were approximately 50% of those generated during the downstroke, nearly matching the relative upstroke forces produced by hummingbirds. Thus, pigeons achieve low speed turns much like helicopters, by using whole-body rotations to alter the direction of aerodynamic force production to change their flight trajectory.

INTRODUCTION. Maneuverability is critical to the movement of animals in their natural environment. Turning represents a basic maneuver that is particularly relevant to predator-prey interactions and obstacle avoidance. To begin to understand the mechanisms by which birds achieve and control aerial turns, we examine the role of body rotations in relation to aerodynamic force production to alter the flight *trajectory*, or path of travel, during turns. More specifically, we ask whether body rotations serve to redirect aerodynamic forces during low speed 90° level turns in pigeons.

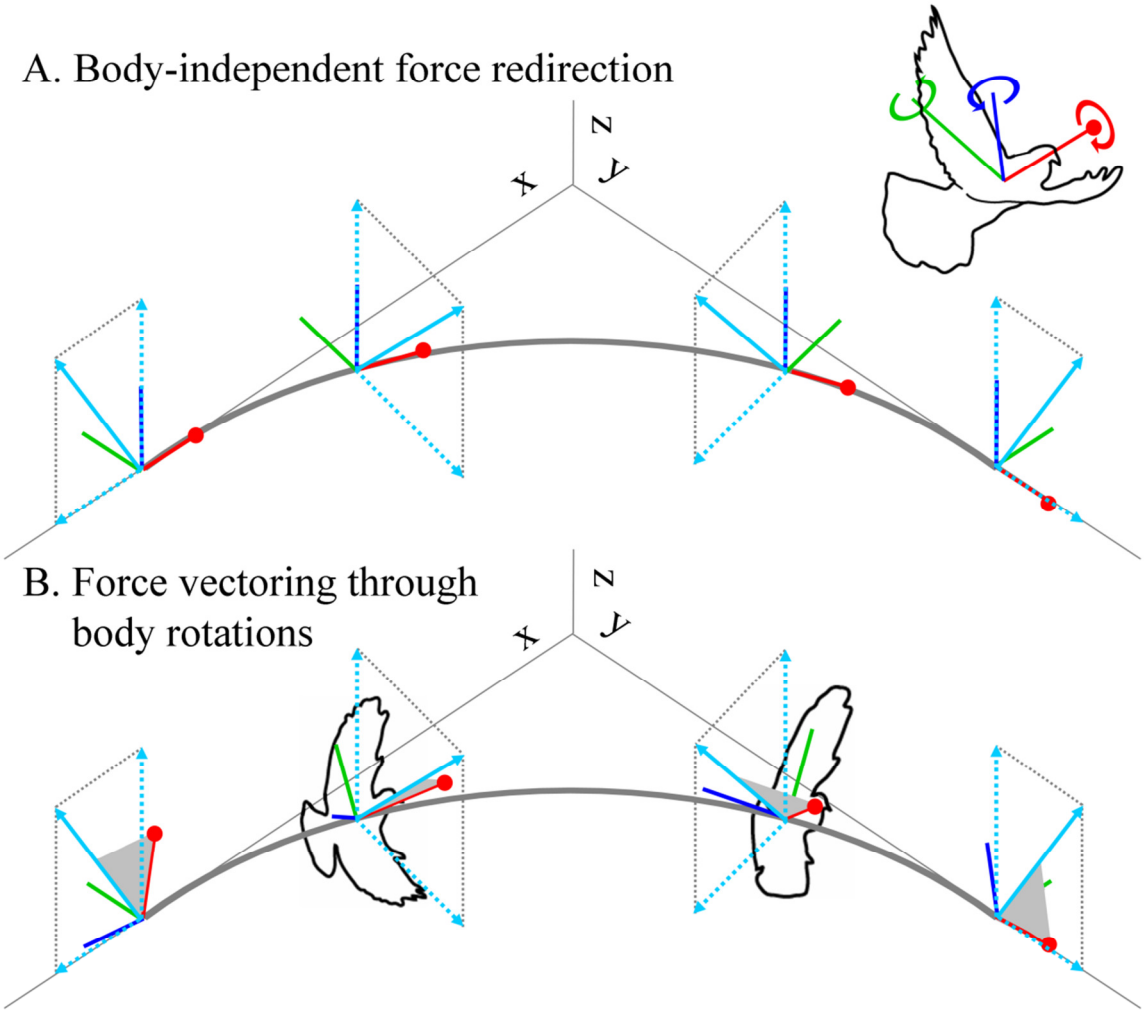
A. Body-independent force redirection
Z
X
Y
B. Force vectoring through
body rotations
Z
X
Y

Figure 2_1.

Figure 2_1 (Continued). Schematic representation of the experimental hypotheses. The global frame (thin grey lines) with z (vertical) defined in line with gravity, and x and y defined along the two perpendicular horizontal axes of the flight corridor (Fig. 2_2). Upper right inset: The bird's body frame with antero-posterior (along the spine), medio-lateral and dorso-ventral axes in red, green and blue, respectively. Rotations about these anatomical axes are defined as roll, pitch and yaw (red, green and blue circular arrows). (A, B) Hypothetical aerodynamic forces (solid light blue vectors) in the global frame (thin solid grey lines) during a level, 90° aerial turn to the right. Horizontal and vertical global projections (dashed blue vectors) of the aerodynamic forces early, during and upon completion of the turn provide braking, centripetal and accelerating forces, respectively, as well as vertical forces. (A) $H_{0:}$ Birds produce aerodynamic forces in variable directions in the body frame, requiring only realignment of the antero-posterior body axis with the flight trajectory. (B) Force-vectoring Hypothesis: Birds produce aerodynamic forces in a uniform direction in the body frame, requiring body rotations to redirect aerodynamic forces in the global frame to change flight trajectory (grey curved line). NB: the grey triangles shown between the antero-posterior body axis and resultant aerodynamic force vector are of identical dimensions in each of the four represented positions of the turn, emphasizing the anatomically fixed direction of aerodynamic force.

The three dimensional (3D) nature of flight requires analyses of aerodynamic force production in relation to body motions not only in a global reference frame, but also in a local, body reference frame (Fig. 2_1). The global frame allows for application of Newton's laws of motion, which for a flying bird means that the resultant of aerodynamic and gravitational forces can be estimated from accelerations of the whole body center of mass (CM). However, the bird's torso moves relative to the CM, primarily due to the time-varying wing configurations during the wingbeat cycle. Therefore, localization of the CM cannot rely solely on the torso, but requires detailed assessment of the motions of the head and wings as well. The body frame corrects for the displacements and rotations of the torso, allowing for analyses of head and wing motions and forces relative to the body, which subsequently can be related to underlying musculoskeletal and sensory-

motor function. The combination of global and local frames therefore can reveal how aerodynamic force production is coordinated with a bird's 3D *body orientation*, or body angular position, during aerial turns.

There are two major reasons for animals to change their body orientations during turns: 1) to reacquire their preferred body orientation for forward movement, and 2) to alter the direction of propulsive force needed to change their movement trajectory. Bilaterally symmetric animals have body plans that are best suited for forward locomotion with a particular 3D body orientation (Arbib *et al*., 1997). Consequently, this preferred body orientation must be reacquired during a turn to move along the new movement trajectory. Additionally, body rotations must also occur to redirect the animal's propulsive turning forces, if these forces are directionally constrained within the animal's body frame. Redirecting resultant forces in the global frame due to changes in body orientation is referred to as *force vectoring* (Fig. 2_1). In fact, flying insects have been argued to turn primarily by force vectoring, meaning that the majority of the redirection of aerodynamic forces is based on changes in body orientation, and not on changes in the direction of aerodynamic forces relative to the insect's body (Dudley, 2000).

Even though quantifying the time-varying aerodynamic forces produced during flapping flight is challenging, estimates of aerodynamic force production during flight maneuvers have been made in insects (Blondeau, 1981; Götz & Wandel, 1984; Sugiura & Dickinson, 2009; Wagner, 1986). Turning calliphorid, muscid and drosopholid flies

support the use of force vectoring as a means to redirect aerodynamic force, as the aerodynamic forces produced by their wings operate within a limited range relative to their bodies. Most of the redirection of aerodynamic force within the body frame occurs within the animal's mid-sagittal plane, varying over a range of merely 20°; although fruit flies also generate moderate lateral forces with respect to their body. Notable exceptions are hover flies (Syrphidae), which seem to achieve a wider variation in aerodynamic force orientation relative to their body (Collet & Land, 1975, Nachtigall, 1979), though these findings have been questioned (Wagner, 1986).

Vertebrate fliers also appear to have a limited ability to redirect aerodynamic force relative to their body. Horseshoe bats, fruit bats, pigeons and rose-breasted cockatoos roll during aerial turns (Aldridge, 1986; Warrick & Dial 1998; Hedrick & Biewener, 2007; Iriarte-Diaz & Swartz, 2008), indicating that they likely rely on force vectoring to turn. Fruit bats rotate their bodies in the direction of the turn in addition to rolling, increasing their centripetal acceleration (Iriarte-Diaz & Swartz, 2008). Finally, pigeons appear to redirect aerodynamic forces to accelerate after flight take-off and brake prior to landing by pitching movements of their bodies (Berg & Biewener, 2010).

Here, we ask whether pigeons redirect aerodynamic forces (in the global frame) by redirecting aerodynamic forces relative to their body (Fig. 2_1A), or by rotating the body itself (Fig. 2_1B). Given the constrained musculoskeletal and stereotypical kinematic features of the avian wingstroke (Sy, 1936; Rayner, 1988; Dial *et al*., 1991; Gatesy & Baier, 2010), we hypothesize that pigeons generate aerodynamic forces in a

uniform direction relative to their body (*i.e.* in the body frame), necessitating the use of force vectoring to turn (Fig. 2_1B). To test this hypothesis, we used high-speed videography to obtain 3D positions of body markers of pigeons performing low speed, 90º level turns within a netted, 10m long, square-corner corridor (Fig. 2_2). Detailed analysis of the pigeons' whole-body mass distributions enabled their non-body-fixed CM to be accurately tracked, from which time-varying, whole-body, or net, aerodynamic forces were assessed (Fig. 2_2-2_5). To interpret the functional significance of changes in body orientation made throughout the turn, body rotations of the pigeons were quantified relative to the redirection of aerodynamic force averaged over successive downstrokes. Specifically, for each downstroke in the turn the component of the body rotation that redirected the average aerodynamic force was mathematically separated from the component of the 3D body rotation that had no effect on the direction of the average downstroke force. This approach allowed any 3D body rotation to be decomposed into two complementary body rotation fractions, one that redirected and one that rotated about the downstroke average aerodynamic force (Fig. 2_6).

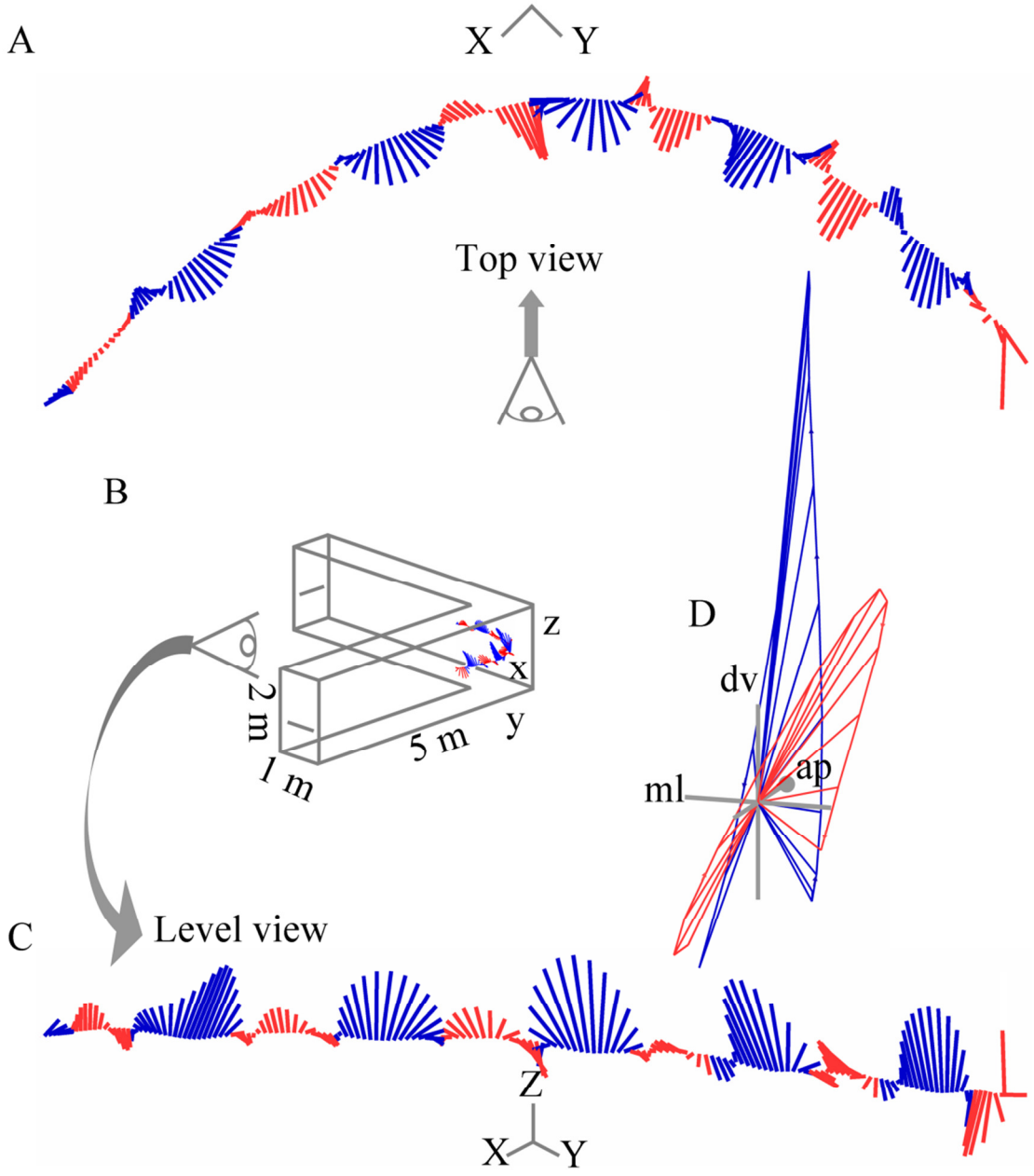

Figure 2_2. Instantaneous net aerodynamic forces (F) visualized on corresponding center of mass (CM) positions throughout a representative right 90° turn. Downstroke forces in blue and upstroke forces in red, plotted at 4 ms intervals. (A-C) **F** in the global frame with axes x, y and z. (A) Top view. (B) Schematic of the flight corridor with viewpoints for (A) and (C). (C) Level view. (D) Caudo-lateral view of **F** for a single wingbeat in the body frame with antero-posterior (ap, red), medio-lateral (ml, green) and dorso-ventral (dv, blue) axes. Arrows connecting vector tips indicate temporal sequence. (A,C,D) Axes lengths represent two body weights of force.

RESULTS. Three pigeons with a mean body mass of 319 $\pm$ 33 g (all results are expressed as mean $\pm$ SD) negotiated the 90° level turn at a CM speed of 3.3 $\pm$ 0.2 ms^{-1}, with mean flight trajectory slopes relative to the global horizontal plane of 2.5 $\pm$ 0.2^{o}, and a wingbeat frequency of 8.3 $\pm$ 0.3 Hz. Combined wing mass distal to the shoulder comprised 12.5 $\pm$ 1.4% of total body mass.

Aerodynamic forces are reaction forces resulting from the interactions of the animal's body, wings and tail with the surrounding air. In mid-air, an animal's flight trajectory can only be changed by gravity or the aerodynamic forces produced by the animal. Since the external force on an object equals the product of its mass and acceleration, the instantaneous aerodynamic force acting on the pigeon's center of mass (CM) can be estimated after factoring out gravity (see methods for details). However, the time-varying configurations of the bird's wings and head relative to its torso cause the whole-body, or net, CM to vary in position with respect to the torso through time. This non-body-fixed CM therefore requires estimates based on detailed 3D kinematics and body mass distributions (Fig. 2_3). Using a mass-distribution model then provides estimates of instantaneous net aerodynamic forces (**F**) throughout the turns. The aerodynamic origin of these forces and any force components that cancel out internally, however, cannot be identified by this method.

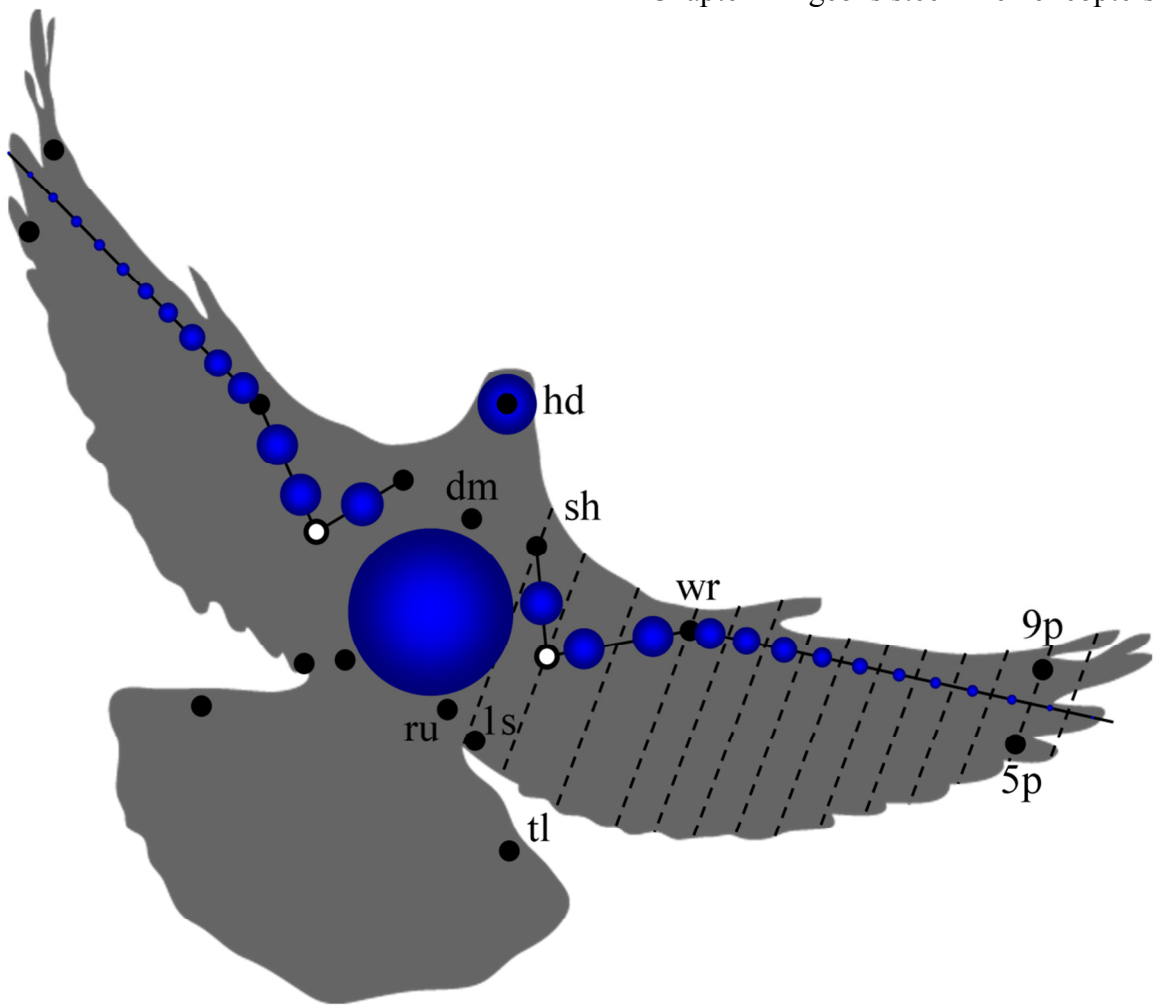

Figure 2_3. Pigeon marker locations and mass-distribution model. Silhouette at mid downstroke with sixteen marker locations (solid black circles) and calculated elbow locations (open circles). The approximate wingstrip edges (dashed lines) and marker descriptors are provided for the bird's right side (dm: dorsal midshaft; ru: rump; sh: shoulder, 5p: fifth primary; 9p: ninth primary; tl: tail; 1s: innermost secondary; see methods for details). Modeled point masses (blue spheres), with size representing relative mass. Note that the tail is considered part of the torso mass (largest blue sphere).

Pigeons turn with an aerodynamically active upstroke. Throughout the 90^{o} turn the pigeons produced aerodynamic forces during the upstroke as well as the downstroke (Fig. 2_2, 2_4). In the global frame, aerodynamic forces were directed

vertically to support the pigeon's body weight and horizontally to change its flight trajectory during the turn (Fig. 2_2).

Table 2_1. Body rotations accumulated throughout the turn. Mean ± SD of means of three individuals for both continuous and net wingbeat effects in terms of roll, pitch and yaw.

Body rotations	Continuous effects (deg)	Net wingbeat effects (deg)
Roll	143 ± 16	77 ± 14
Pitch	125 ± 24	43 ± 2
Yaw	81 ± 10	58 ± 4

Substantial body rotations occur about all three anatomical axes. The 3D body rotations of the turning pigeons consisted of substantial roll, pitch and yaw components, defined as rotations about the antero-posterior (along the spine), the medio-lateral and dorso-ventral body frame axes, respectively (Phillips, 2004) (Table 2_1; Fig. 2_1). During the turn, body rotations oscillated back and forth within wingbeats, but led to net changes in body orientation between successive wingbeats. The pigeons' 3D body rotations predominantly consisted of roll, both continuously and on a net wingbeat basis; although pitch and yaw components were also substantial (Table 1). Over the course of a turn, early wingbeats rolled the pigeons into the turn, with subsequent wingbeats producing net roll rotations out of the turn. In contrast, net wingbeat rotations about the pitch and yaw axes were directed upwards and into the turn, respectively, throughout turning. Oscillations of body rotations within wingbeats were larger in pitch and roll (16 ± 5 and 13 ± 6 °/wingbeat, respectively), and smallest in yaw (4 ± 3 °/wingbeat), indicating yaw angular velocities were most uniform.

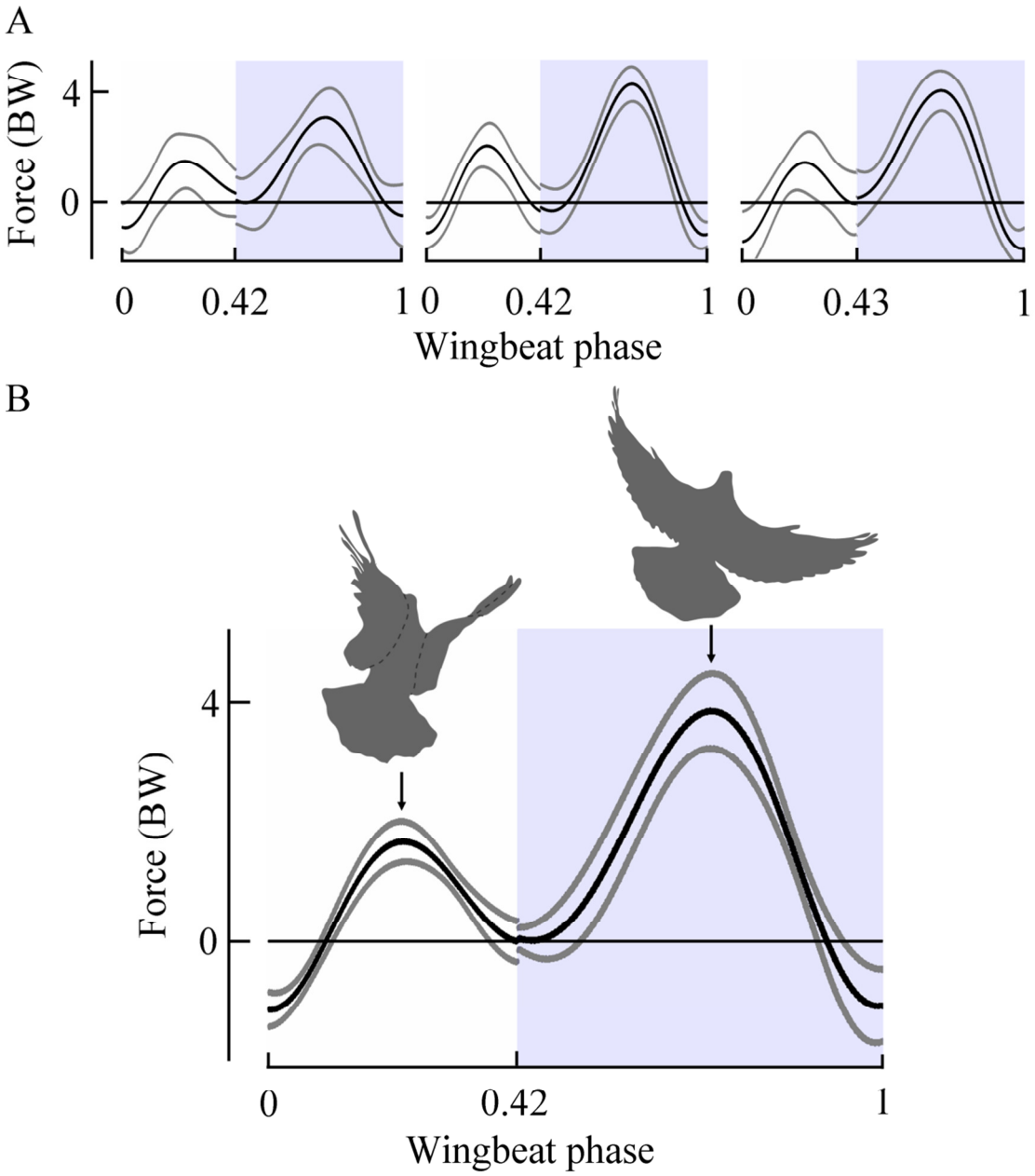

Figure 2_4. Net aerodynamic force magnitude (|F|) in line with the stroke averaged aerodynamic force for turning pigeons. The force magnitude is normalized to body weight (BW) and wingbeat duration. Grey shading indicates downstroke. (A) Mean |**F**| ± SD (N=20) for each of 3 individual pigeons. (B) Pooled mean ± SD of the mean |**F**| across the three pigeons. Representative silhouette at both phases of upstroke and downstroke peak force (black arrows) illustrates timing with respect to wing configuration. Note that the discontinuity between upstroke and downstroke traces results from normalization to the half-stroke phases, necessitated by variations in stroke durations.

Pigeons produce consistent patterns of aerodynamic force. The directions and magnitudes of instantaneous net aerodynamic force (**F**) exhibited stereotypic patterns within the body frame during both downstroke and upstroke. (Fig. 2_2D, 2_4, 2_5). During downtroke **F** was directed mainly in the midsagittal plane of the birds, whereas during upstroke **F** was more variably directed. Net aerodynamic force magnitude (|**F**|) approximated zero at the upstroke-downstroke transition, before peaking near mid-downstroke (4.5 $\pm$ 0.4 body weights (BW) at 53% of the downstroke period; Fig. 2_4). At the downstroke-upstroke transition, **F** momentarily opposed the stroke average. Throughout the remainder of the upstroke, however, the pigeons produced aerodynamic force in support of body weight, in line with the stroke average. |**F**| reached a maximum at mid-upstroke (2.3 $\pm$ 0.3 BW, Fig. 2_4), coinciding with tip-reversal (Fig. 2_4B, left silhouette). Although upstroke peak |**F**| averaged about half the downstroke peak |**F**|, the aerodynamic impulse generated during upstroke averaged 27 $\pm$ 4% of the impulse generated during downstroke. Aerodynamic forces averaged 1.33 $\pm$ 0.07 BW over the full wingbeat cycle, consistent with the pigeons' need for centripetal forces in addition to weight support to fly through the turn. A sensitivity analysis consisting of a decrease and an increase of the wing masses by 10% resulted in an increase and a decrease of upstroke peak force estimate by approximately 5%, respectively, indicating the robustness of our findings for upstroke aerodynamic force based on a full body and wing mass distribution model of the birds.

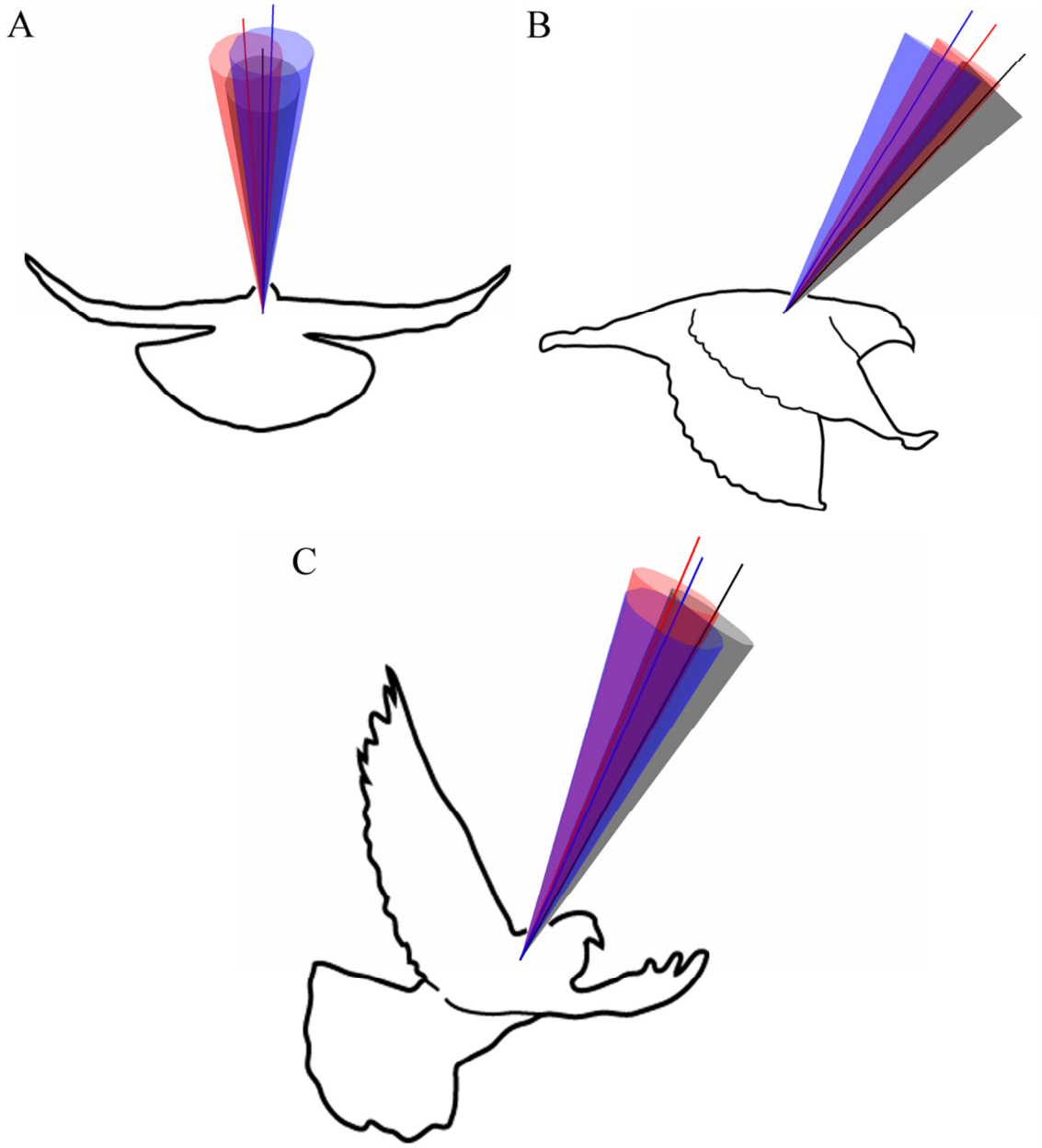

Figure 2_5. Mean net downstroke aerodynamic forces (F_d) for three turning pigeons expressed in the body frame and superimposed on a pigeon outline. The mean ± SD vector cone is depicted by a different color for each individual averaged for all analyzed wingbeats of the turns. For clarity, three views are provided. (A) rear view, (B) side view and (C) oblique view.

As the pigeon rotated its body and changed its flight trajectory, downstroke-averaged aerodynamic forces ($\mathbf{F}_d$) were produced in a uniform direction with respect to the pigeon's body during the five sequential wingbeats of the turn (Fig. 2_5). $\mathbf{F}_d$ were oriented in the mid-sagittal plane of the bird's body and directed anterior to the dorso-ventral body axis by 38 + 7° (Fig. 2_5), consistent with the 'pitched-up' body orientation of pigeons during slow steady flight (~ 32° at a flight speed of 5-6 ms^{-1} (Biewener *et al*., 1998)). During slow flight aerodynamic drag is small and, by approximation, only gravity needs to be countered by near vertical aerodynamic forces.

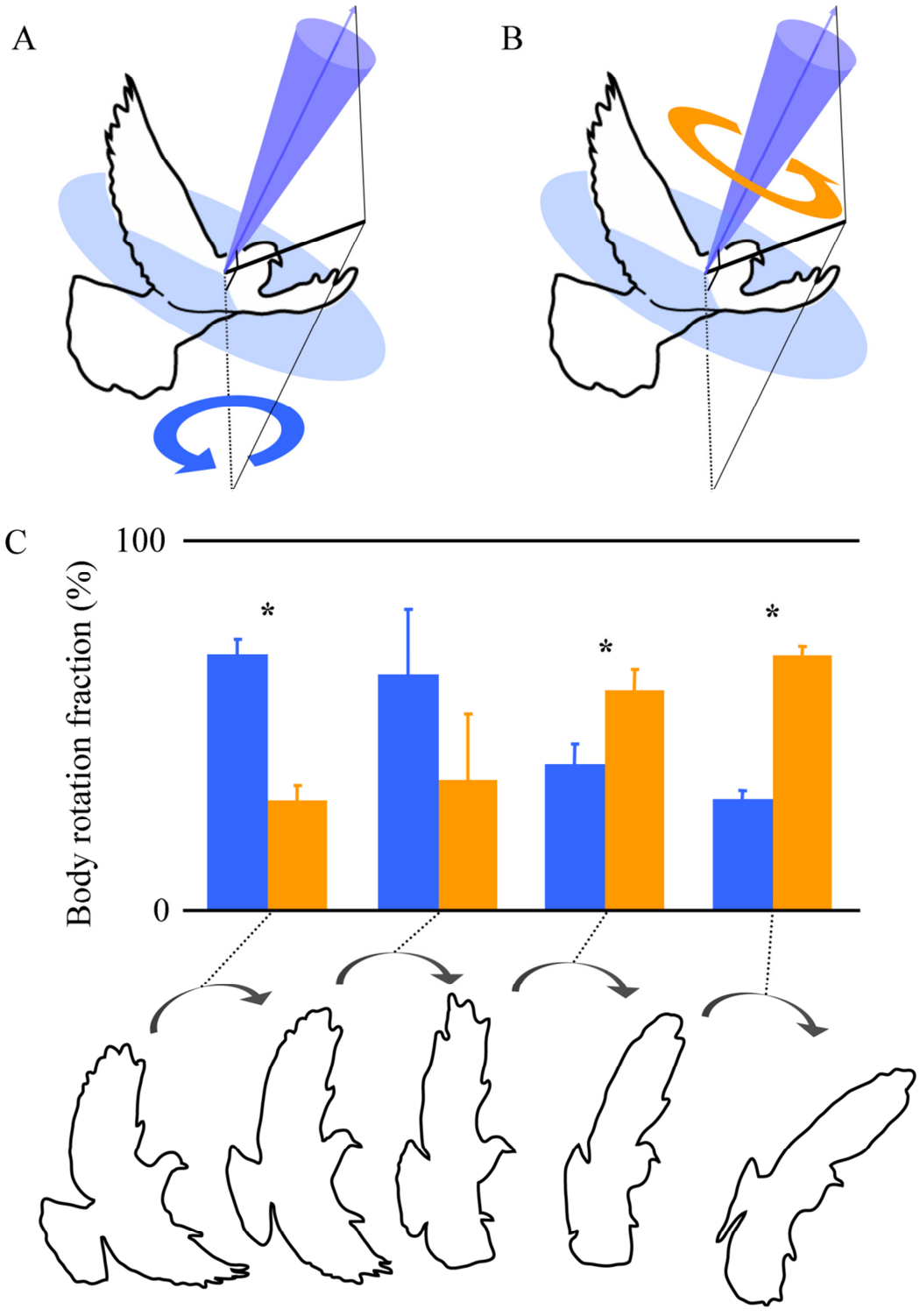

Figure 2_6.

Figure 2_6 (Continued). Decomposition of sequential body rotations of a turning pigeon. (A,B) Outline of a pigeon, with superimposed $\mathbf{F}_d$ and SD vector cone, as well as the plane to which $\mathbf{F}_d$ is normal, and an exemplary axis of body rotation (thick black line), all in the body frame. (A) The component of the body rotation that redirects $\mathbf{F}_d$ (blue circular arrow). Note that the axis describing this rotation fraction lies within the circular blue plane. (B) The component of the body rotation about $\mathbf{F}_d$ (orange circular arrow). (C) Fractions of body rotation for four sequential, complete wingbeats of the turn, showing the orthogonal components of body rotations that redirect $\mathbf{F}_d$ (blue fraction) versus which occur about $\mathbf{F}_d$ (orange fraction). Pooled mean $\pm$ SD of means of three individuals. Mid-downstroke outlines of five sequential wingbeats, as seen from a single elevated viewpoint from inside the turn. Grey arrows and dotted lines link colored bars to positions in the turn. Asterisks indicate significant differences between body rotation fractions.

Turning pigeons prioritize changes in trajectory over angular positioning of the body. By comparing rotations of the pigeon's torso with respect to redirection of $\mathbf{F}_d$ over the course of a wingbeat in the global frame, we evaluated the extent to which pigeons relied on body rotations to redirect $\mathbf{F}_d$ versus to what extent body rotations occurred about the direction of $\mathbf{F}_d$ (see methods for details). Body rotations that redirect $\mathbf{F}_d$ alter flight trajectory, but body rotations about $\mathbf{F}_d$ leave the direction of $\mathbf{F}_d$ in the global frame unaffected, and therefore do not change flight trajectory. This analysis revealed that for each sequential wingbeat of the turn, the pigeon's body progressively rotated about an axis that was increasingly aligned with the direction of $\mathbf{F}_d$ (Fig. 2_6). Body rotations produced over the course of the first two wingbeats of the turn predominantly redirected $\mathbf{F}_d$ (70.1 $\pm$ 4.1 % and 64.4 $\pm$ 17.8 %, respectively), whereas body rotations during the last two wingbeats occurred predominantly about $\mathbf{F}_d$ (60.2 $\pm$ 5.6 % and 69.4 $\pm$ 2.3 %) (Fig. 2_6C).

In summary, during turning flights the pigeon's torso oscillated vigorously due to the combined effect of the flapping wings (resulting from inertial forces) and aerodynamic forces in relation to gravity. Aerodynamic forces accelerating the bird's center of mass peaked during downstroke, but also peaked during upstroke and were roughly half the downstroke magnitude. These aerodynamic forces serve to offset gravity and change the bird's flight trajectory to achieve level 90° turns. Even though the pigeon's orientation changed significantly about all three body-axes, downstroke-averaged aerodynamic forces were produced in a uniform anatomical direction. Decomposition of successive wingbeat 3D body rotations revealed that early in the turn body rotations of the pigeon mainly redirected downstroke-averaged aerodynamic forces, reflecting anatomical constraints on the direction of aerodynamic force production. However, later in the turn body rotations mainly served to reorient the bird's body for straight flight, and had little effect on the direction of aerodynamic force production.

DISCUSSION. Using an analytical approach based on high-speed 3D kinematics and detailed body mass distributions, we determined the time-varying net aerodynamic forces produced by slowly flying pigeons as they negotiated 90^{o} level turns (Fig. 2_2_2). We identified the tip-reversal upstroke as aerodynamically active (Fig. 2_2, 2_4B), indicating its role for increased power production and control of body position. Net aerodynamic forces were produced in a uniform direction within the pigeon's body frame, requiring that changes in flight trajectory be mediated by body rotations that redirect aerodynamic force in the global frame (Fig. 2_5). Consistent with our hypothesis, the overall turning strategy consisted of force vectoring to change the pigeon's flight trajectory, followed by re-acquisition of the bird's preferred body orientation for forward flight (Fig. 2_6).

Substantial rotations occurred about all three anatomical axes indicating that 1) pigeons are not restricted to a particular anatomical axis to change their body orientation, and 2) body rotations function to redirect net aerodynamic forces as needed to negotiate the turn (Table 1). That body rotations occurred mainly about the birds' roll axis does not necessarily reflect a preference for this axis, but may simply reflect the birds' body orientation upon entering the turn and the reliance on force vectoring to negotiate the turn.

Net Aerodynamic force magnitude (|**F**|) varied consistently, with minima and maxima occurring at wingbeat phases as predicted by aerodynamic theory (Greenewalt, 1975), across all individuals and trials. The average net aerodynamic force per wingbeat was greater than one BW because turning birds need to accelerate themselves to redirect their flight trajectory, as well as offset their weight due to gravity. The small negative peak in |**F**|, opposing the stroke-averaged aerodynamic force, may well reflect an aerodynamic consequence of strong supination of the wings near the downstroke-upstroke transition (Brown, 1963).

Positive aerodynamic force during the upstroke coincided with wing tip-reversal (Fig. 2_4B, left silhouette). During an upstroke with tip-reversal, the elbow and wrist are flexed, and the hand-wing is supinated, causing it to be inverted. Elbow and wrist flexion effectively moves the point of wing rotation from the shoulder during the downstroke towards the wrist during the upstroke, facilitating the upward 'back flick' of the hand-wing. This tip-reversal mechanism is found in the slow to intermediate flight of birds with relatively pointed wings, as well as some birds with rounded wings (Brown, 1963; Zimmer, 1943; Tobalske, 2007), and bats (Aldridge, 1986; Norberg, 1976; 1990). The functional significance of wing tip-reversal has been the subject of debate since the pioneering work of Brown (Brown, 1948), and has been proposed by others in prior studies of avian flight to be aerodynamically active (Aldridge, 1986, Tobalske, 2007; Norberg, 1976; 1990; Brown, 1948; Alexander, 1986; Azuma, 1992; Bundle & Dial, 2003; Hedrick *et al*., 2004; Iriarte-Diaz *et al*., 2011; Lorenz, 1933; Spedding *et al*, 1984).

Until now, however, aerodynamic force production of the tip-reversal upstroke had not been convincingly demonstrated during vertebrate flight.

The consistent force patterns observed here across wingbeats of all three pigeons provide the first definitive evidence for upstroke aerodynamic force production during slow flight in birds larger than hummingbirds (Fig. 2_2, 2_4). Useful contributions of an active tip-reversal upstroke to weight support can therefore be expected during other modes of flight where tip-reversal is present, such as hovering, landing and steady slow flight. This is reinforced by the fact that we observed no significant differences in upstroke force patterns across the five wingbeats during which birds entered, executed and left the 90° turn. Aerodynamic force generation by the tip-reversal mechanism also agrees with recent force measurements of pigeon wings spun like a propeller, while positioned in an upstroke configuration (Crandell & Tobalske, 2011).

Although maximum **F** during the upstroke reached 50% of maximum **F** during the downstroke (Fig. 2_4), the upstroke generated only 27 $\pm$ 4% of the downstroke impulse. The smaller impulse of the upstroke reflects its shorter period (42% of the wingbeat duration), as well as the opposing aerodynamic force production relative to weight support early in the upstroke (Fig. 2_4B).

In a comparative context, the relative contribution of upstroke aerodynamic force to total impulse in pigeons is nevertheless surprisingly high. Hummingbirds operate at temporal and spatial scales similar to insects (2), and, until recently, were thought to share weight support between the two halves of the wingbeat (Weis-Fogh, 1972).

However, hovering rufous hummingbirds generate only 33% of the downstroke impulse during upstroke ((Warrick *et al*, 2005), based on wake measurements). With an upstroke that generates 27% of their downstroke impulse, pigeons achieve a similar impulse distribution to that found in rufous hummingbirds, which is remarkable since hummingbirds are thought to have evolved a highly derived upstroke (Stolpe & Zimmer, 1939).

Our hypothesis that pigeons produce aerodynamic forces in a uniform anatomical direction is also clearly supported (Fig. 2_5). $\mathbf{F}_d$ was oriented within the mid-sagittal body plane and directed antero-dorsally, with little variation across successive turning wingbeats. Thus, during low speed flight, pigeons exhibit a consistent direction of net aerodynamic force production with respect to their body, reflecting the fundamental anatomical features that underlie powered avian flapping flight.

The constrained direction of force production in the body frame indicates that pigeons turn much like insects and helicopters. Helicopters redirect aerodynamic forces relative to their fuselage (in the body frame) within relatively narrow ranges (roughly 20°; (Talbot & Corliss, 1977)), meaning that maneuvers with more substantial redirections of resultant forces in the global frame require force vectoring, as we found for pigeons. Airplanes, with decoupled wing lift and engine thrust, can redirect resultant forces to a larger degree within the body frame, particularly in the fore-aft direction (for modern fighter planes this can be > 90° (Winchester, 2006)), reducing their reliance on force vectoring to maneuver.

The turning strategy of pigeons appears to prioritize trajectory changes over readjustments of body orientation. Body rotations of the pigeons early in the turn mainly contribute to changes in flight trajectory, whereas body rotations progressively later in the turn predominantly serve to realign the body for subsequent forward flight, having a smaller effect on redirecting aerodynamic force (Fig. 2_6C). This turning strategy likely arises from constraint of $\mathbf{F}_d$ direction with respect to the bird's body, which requires force vectoring to redirect $\mathbf{F}_d$. However, body rotations that redirect $\mathbf{F}_d$ during the first part of the turn result in a body orientation that is not well suited for the bird's new flight trajectory. Therefore, once the bird achieves its new target flight trajectory, its preferred body orientation for forward flight must be reacquired by rotating its body about $\mathbf{F}_d$. Only body rotations that occur about $\mathbf{F}_d$ leave the newly acquired flight trajectory unaffected, which explains why these body rotations predominantly occur later in the turn.

To the extent that aerodynamic force production may be anatomically constrained in avian flapping flight, it seems likely that the pattern of early flight trajectory adjustment followed by reacquisition of a preferred forward flight body orientation observed here for slow turning flight may also apply for fast turning flight. At higher flight speeds, however, changes in wings and/or tail configurations are likely to produce more substantial changes in aerodynamic force with respect to the bird's body (Rüppell, 1977), allowing for changes in aerodynamic force direction, independent of force vectoring, to achieve a turn. Additionally, given that flight power requirements are lowest at intermediate speeds (Tobalske *et al*., 2003), birds may be able to redirect aerodynamic

force within the body frame by differentially activating flight muscles between their inside and outside wings. This could enable an alternative turning strategy to that observed here. For instance, during flight versus when flap-running, chukars produced aerodynamic forces roughly in the same global direction, yet body pitch orientation differs by about 30° between these behaviors (Dial *et al*., 2008). These findings indicate that birds may be able to re-direct aerodynamic forces more variably with respect to the body depending on behavior or power output.

At the low flight speeds examined here, pigeons operate much like helicopters, which have limited capacity to redirect aerodynamic forces relative to their body, relying on whole-body force vectoring to change flight trajectory, similar to fruit flies, blow flies and house flies (Götz & Wandel, 1984; Wagner, 1986; Fry *et al*., 2003; Vogel, 1966). The moderate redirection of $\mathbf{F}_d$ with respect to the pigeon's body that does occur, may contribute to body torques required to produce the body rotations needed for turning (Warrick & Dial, 1998; Hedrick & Biewener, 2007). Understanding flight control will therefore require insight into the specific mechanisms used by pigeons to generate the torques that produce the observed body rotations. However, torques cannot be inferred from Newton's second law of motion because the distribution of applied forces remains unknown. Nevertheless, by limiting the direction of aerodynamic force production to a single main axis relative to the body, our results indicate that birds may simplify the problem of controlling turns from six to four degrees of freedom (LaValle, 2006).

METHODS. Three rock doves (*Columba livia*) were selected from ten wild-caught individuals, based on subjective assessment of their initial turning flight performance during training. These pigeons were housed, trained and studied at the Concord Field Station (Bedford, MA, USA) in accordance with protocols approved by Harvard University's Institutional Animal Care and Use Committee. The pigeons were trained to fly back and forth between two perches situated at either end of two 5m long by 1m wide by 2m high netted sections, connected by a 90º turn midway (Fig. 2_2B). The symmetrical, square-corner corridor was constructed of lightweight, 2-cm mesh nylon deer netting supported by a PVC frame consisting of 4-cm diameter piping.

Using nine synchronized, high-speed cameras, 3D positions of body markers were collected within a calibrated 1.8 m^3 cubic volume that encompassed the turn. Trials accepted for analysis were those in which the birds 1) did not contact the netting, and 2) maintained a turning flight trajectory relative to global horizontal of < 5°. The pigeons were marked at 16 anatomical locations (Fig. 2_3): Dorsum at the second thoracic vertebra (dm); Left and right rump (4-cm lateral to the vertebral column over the synsacrum) (ru); Center of head (hd); Left and right wing roots (sh); Left and right wrists (wr); Tip of left and right 5^{th} primary feathers (5p); 67% of the length of left and right 9^{th} primary feathers (9p); 67% along the length of left and right outer tail feathers (tl); Left and right tip of the innermost secondary feathers (1s). Elbow position was determined trigonometrically based on two lengths and three positions: brachial and ante- brachial segment lengths and wing root, wrist and tip of the innermost secondary feather

positions. Flights were recorded with two camera systems: A high-speed light video system recording at 250 Hz with 0.001 sec exposure time, consisting of one FastCam-X 1280 PCI and two FastCam 1024 PCI cameras (Photron USA Inc., San Diego, CA, USA), and an infrared-based auto-tracking system recording at 240 Hz with 0.0004 sec exposure time, consisting of six ProReflex MCU240 cameras (Qualisys AB, Gothenburg, Sweden), was used to track flight kinematics. The two camera systems were synchronized using a start trigger signal. The visible-light videos were digitized using DLTdv3 (Hedrick, 2008). Calculations were performed in Matlab (Mathworks Inc., Natick, MA) using custom-written scripts. Positional data were filtered with a fourth-order Butterworth filter using a low-pass cutoff frequency three times the wingbeat frequency. Cutoff frequency was determined by residual analysis (Winter, 2005).

Rotations. The sum of absolute back and forth rotations within a wingbeat and the net change in body orientation over a wingbeat period were defined as continuous and net wingbeat body rotations, respectively, about each of the body axes. For each turn, five sequential wingbeats were analyzed, during which continuous and net wingbeat body rotations about each axis were accumulated.

Aerodynamic Forces. The position of the net CM was approximated throughout the turn using a mass-distribution model of the body and tail, head, and wings (Fig. 2_3). The torso and tail were represented by a single point-mass, because the effect of tail movements on net CM were assumed to be minor and are difficult to model. The head and 14 chord-wise strips per wing were modeled as point-masses, with time-varying

positions based on segment kinematics (Fig. 2_3). The two wings together constitute approximately $1/8^{th}$ of a pigeon's body mass. The motion of the flapping wings causes the net CM to move substantially relative to a pigeon's torso CM, necessitating the time-dependent, non-body-fixed CM calculations.

Wingbeats were partitioned into upstroke and downstroke phases, based on reversal of the major bending direction of the primary feathers. This bending-reversal of the primary feathers coincided with the instant the primary feather markers moved laterally relative to the body, in both ventral (start of upstroke) and dorsal (start of downstroke) positions.

Instantaneous net aerodynamic forces (**F**) were determined throughout the turn based on net CM accelerations relative to gravity, because the CM of a freely flying bird can only be accelerated by external gravitational and aerodynamic forces. **F** vectors were normalized to wingbeat phase and expressed in the body frame. The net aerodynamic forces averaged over the duration of the downstroke ($\mathbf{F}_{d)}$ act in line with the main impulse vector, the time integral of force, produced during each wingbeat.

Redirection of aerodynamic forces versus rotation about aerodynamic forces. Identification of $\mathbf{F}_d$ allowed for decomposition of body rotations relative to this direction of main aerodynamic impulse imparted during each downstroke. Body rotations of the bird were analyzed with respect to $\mathbf{F}_d$ over the five wingbeats of the turn. Two 3D rotations were calculated between successive mid-downstroke instants of each wingbeat: a 3D body rotation and a 3D redirection of $\mathbf{F}_d$. Body rotations identical to the redirection of $\mathbf{F}_d$ were designated as representing 100% redirection of $\mathbf{F}_d$. Conversely, if body rotations did not redirect $\mathbf{F}_d$, body rotations were designated as representing 100% rotation about $\mathbf{F}_d$. Mathematically, this approach is identical to expressing the 3D body rotation as a vector in the body frame and determining the relative magnitudes of two perpendicular projections of this vector: 1) The projection of the 3D body rotation vector on the plane normal to $\mathbf{F}_d$ represents the component of the body rotation that redirects $\mathbf{F}_d$ (force vectoring), and 2) The projection of the 3D body rotation vector on $\mathbf{F}_d$ represents the component of the body rotation about $\mathbf{F}_d$. This approach allowed any 3D body rotation to be decomposed into two complementary body rotation fractions, one that redirected $\mathbf{F}_d$ and one that rotated about $\mathbf{F}_d$ (Fig. 2_6A, 2_B).

Statistics. All results were based on five complete wingbeats nearest the center of each of two left and two right turns for each individual (20 wingbeats per bird, N=3) expressed as mean $\pm$ SD. Paired t-tests (JMP, SAS Institute, Cary, NC) were used to compare group means for the three individuals. Differences were considered significant when $p<0.05$.

ACKNOWLEDGMENTS. We thank P.A. Ramirez for care of the animals, D.E. Lieberman for shared use of the Qualysis cameras, and A.N. Ahn, D.R. Warrick, A.S. Arnold-Rife, C.A. Moreno, T.E. Higgins, A. Eberle, C. Gastil, and A. Randall for helpful discussions and informal contributions to this work. We furthermore thank three anonymous reviewers for their constructive suggestions. This research was funded by NSF IOS-0744056 to AAB.

CHAPTER 3

Pigeons in low speed aerial turns produce aerodynamic torques through wing trajectory changes

Ivo G. Ros, Lori C. Bassman, Marc A. Badger, Alyssa N. Pierson and Andrew A. Biewener

Summary

The complexity of low speed maneuvering flight is apparent from the combination of two critical aspects of this behavior: high power and precise control. To understand how such control is achieved we examined the underlying kinematics and resulting aerodynamic mechanisms of low speed turning flight. Three rock pigeons (*Columba livia*) were trained to perform a 90-degree level turn in a stereotypical fashion and detailed three-dimentional (3D) kinematics at high speeds were recorded. Applying the angular momentum principle, we used mechanical modeling based on time-varying 3D moments of inertia and mass distributions to separate aerodynamic from inertial accelerations of the turning pigeons' bodies.

Directly measured body accelerations were predicted by aerodynamic torques, justifying an exploratory comparison of inside wing versus outside wing kinematic proxies for aerodynamic torque generating mechanisms. Contrary to previous findings, contra-lateral asymmetries in wing speed did not appear to underlie the 90-degree aerial turns, and surprisingly, nor did contra-lateral differences in wing area, angle of attack, wingbeat amplitude,

or timing. However, body accelerations into the turn were associated with the outside wing sweeping more anteriorly, compared to a more laterally-directed inside wing. Together with the relatively more retracted path, the inside wing pronated about the wing long axis more strongly than the outside wing, offsetting any difference in angle of attack that would arise from the observed asymmetry in wing trajectory.

To generate a roll and pitch torque into the turn, the pigeons simply reorient their wing trajectories toward the desired direction. As a result, the aerodynamic force, which acts above the center of mass, redirects inward, generating the torques required to turn.

Introduction

High power and precise control are two critical aspects of low speed maneuvering flight. Insight into the control of flight maneuvers requires understanding the mechanics and aerodynamics involved, which to date, has received little attention compared with steady forward flight.

Mechanistically, the task of turning can be decomposed in two sub-objectives.

1) Re-direction of the flight path (*translational movement*): During this change in course, any linear momentum present upon entering the turn that is not in the direction of the new desired course must be transferred to the surrounding air. Additionally, any 'new' required momentum to successfully negotiate the turn must be acquired. To achieve this change in direction of momentum, slowly flying vertebrates, including horseshoe bats, pigeons, fruit bats and cockatoos, all bank, redirecting the resultant aerodynamic force into the turn, analogous to turning fixed-wing aircraft (Aldridge, 1989; Warrick & Dial, 1998; Hedrick & Biewener, 2007;

Iriarte-Diaz & Swartz, 2008; Chapter 2). Fruit bats also reorient their body towards the turn using thrust as an additional source of centripetal acceleration (Iriarte-Diaz & Swartz, 2008).

2) Reorientation of the body (*rotational movement*): There are two mechaniss by which a flying animal can rotate its body: (i) aerodynamic reorientation, achieved by generating aerodynamic forces that are not directed through the center of mass (CM), resulting in an aerodynamic moment arm and subsequent torque, and (ii) inertial reorientation, due to phasic changes in the moments of inertia (I) of moving appendages, which result in inversely related phasic changes of angular velocity of the body leading to net changes in orientation (Frolich, 1980). The mass distributions and time varying configurations of head, body and wings determine both aerodynamic and inertial maneuvering in flying birds.

Irrespective of the nature of the torque generating mechanisms, initiation and active control of maneuvering flight requires asymmetries in the locomotor system. Resolving maneuvering mechanisms on a fine timescale (within wing beats) is necessary to identify the mechanisms involved in turning flight that require differential neuromuscular control.

Pigeons and cockatoos redirect net aerodynamic forces through bilateral asymmetries in both downstroke velocity and angular momentum of the two wings (Warrick & Dial, 1998; Hedrick *et al.* 2007). Furthermore, pigeons maneuvering through a course with multiple turns generate small, sequential, pectoralis muscle force asymmetries to bank and navigate through the course (Warrick *et al.* 1998).

The generation of torques that rotate the bird are integral to low speed avian turning flight (Chapter 2). Here we seek to characterize the key mechanism of low speed turning in the pigeon, by investigating whether the relevant turning torques are of aerodynamic or inertial nature, and which contralateral wing and/or tail asymmetries are associated with these torques.

Based on previous findings in pigeons, cockatoos and bats (Warrick & Dial, 1998; Hedrick *et al.* 2007; Iriarte-Diaz *et al*., 2011), we expect inertial and aerodynamic effects to act synergistically in rotating the body, with a greater influence of the aerodynamic reorientations. We further hypothesize that aerodynamic torques are generated through contralateral asymmetries in wing velocity and aerodynamic angle of attack.

To test these hypotheses, we record detailed kinematics of three pigeons negotiating a level 90-degree turn. By merging morphological mass-distribution measurements with these kinematic data we generate a full three-dimensional (3D) dynamics model that can separate aerodynamic from inertial accelerations of the turning pigeon's body, based on application of the angular momentum principle. A determination of the timing and magnitude of both inertial and aerodynamic body accelerations is expected to provide a more accurate description of the rotational component of the maneuver, as well as allow for more a detailed identification of the wing and tail kinematics underlying these body accelerations.

Materials and Methods

Three rock doves (*Columba livia*) were selected from 10 wild-caught individuals, based on their turning flight performance during training. These pigeons were housed, trained, and studied at

the Concord Field Station (Bedford, MA) in accordance with protocols approved by Harvard University's Institutional Animal Care and Use Committee. The pigeons were trained to fly back and forth between two perches situated at either end of two 5-m-long by 1-m-wide by 2-m-high netted sections, connected by a 90° turn (Fig. 3_1). The symmetrical, square-corner corridor was constructed of lightweight, 2-cm mesh nylon deer netting supported by a PVC frame consisting of 4-cm diameter piping.

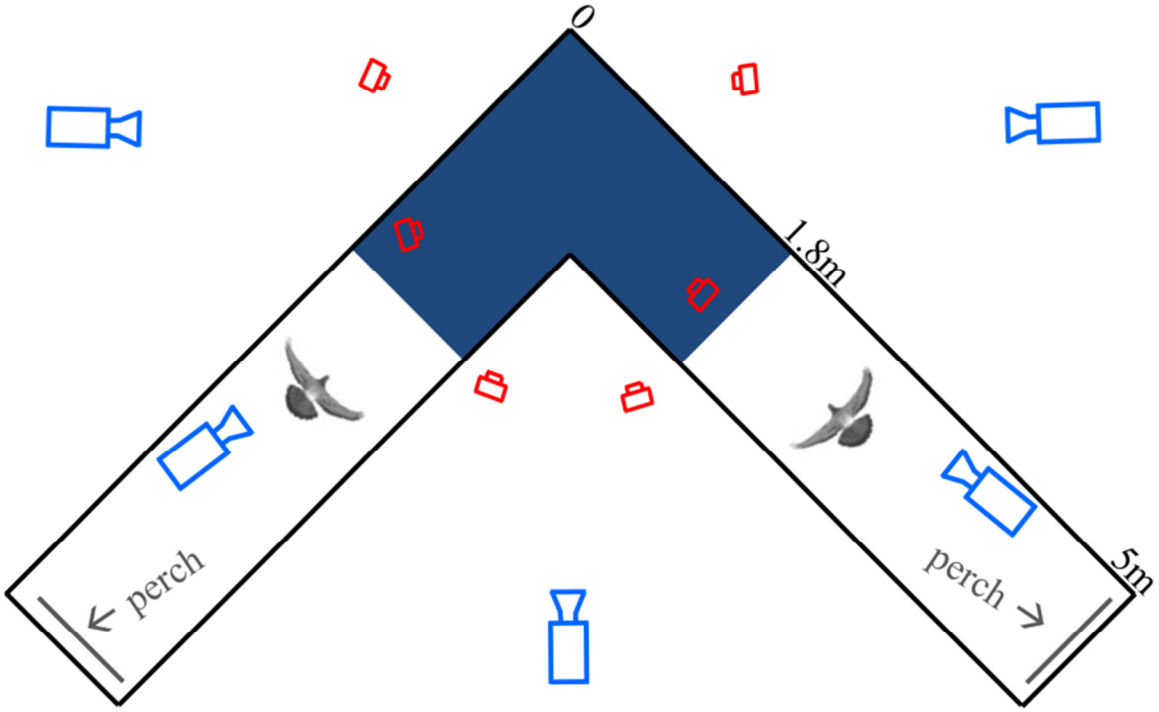

Figure 3_1. Schematic top view of the flight corridor. Camera outlines represent viewing angles, with camera distances underrepresented by 50%, for the high-speed (blue) and infrared-based auto-tracking (red) systems. The spatially calibrated section of the 90-degree turn (dark blue), pigeon silhouettes, and perches (grey lines) are drawn to scale. Dimensions are noted along the outside of one leg of the symmetrical corridor.

Flights were recorded with two camera systems. A high-speed light video system recording at 250 Hz with 0.001 sec exposure time consisted of one FastCam-X 1280 PCI, two FastCam 1024 PCI cameras (Photron USA Inc., San Diego, CA, USA), and two RedLake PCI 500 cameras (RedLake Inc., San Diego, CA, USA). An infrared-based auto-tracking system recording at 240 Hz with 0.0004 sec exposure time consisting of six ProReflex MCU240 cameras (Qualisys AB, Göteborg , Sweden) was used simultaneously. The two camera systems were synchronized using an electrical pulse trigger.

Using the eleven synchronized high-speed cameras, time-varying positions of 10 mm diameter torso and tail markers, as well as 4 mm diameter head and wing markers were collected within a calibrated 1.8 m^3 cubic volume that encompassed the turn. Trials accepted for analysis were those in which the birds (*i*) did not contact the netting and (*ii*) maintained a turning flight trajectory relative to global horizontal of <5°. The markers were adhered at 16 anatomical locations (see Fig. 2_3*)*: dorsum at the second thoracic vertebra; left and right rump (4-cm lateral to the vertebral column over the synsacrum); center of head; left and right wing roots; left and right wrists; tip of left and right fifth primary feathers; 67% of the length of left and right ninth primary feathers; 67% along the length of left and right outer tail feathers; left and right tip of the innermost secondary feathers. Elbow position was determined trigonometrically based on two lengths and three positions: brachial and antebrachial segment lengths and wing root, wrist, and tip of the innermost secondary feather positions. The maximum mass added to a bird was 14 g, or 4% of the body mass.

The 3D marker positions were reconstructed based on the volumetric calibration, using freely available digitization software (Hedrick, 2008). Calculations were performed in Mathematica (Wolfram Research, Champaign, IL, USA) and Matlab (Mathworks Inc., Natick, MA, USA) using custom-written scripts. Positional data were filtered with a fourth-order Butterworth filter using a low-pass cutoff frequency three times the wingbeat frequency. Cutoff frequency was determined by residual analysis (Winter, 2005). Correlations were tested with standard least squares regression models with individual effect leverage (JMP, SAS Institute, Cary, NC). Unless noted otherwise, results were expressed as mean ± SD.

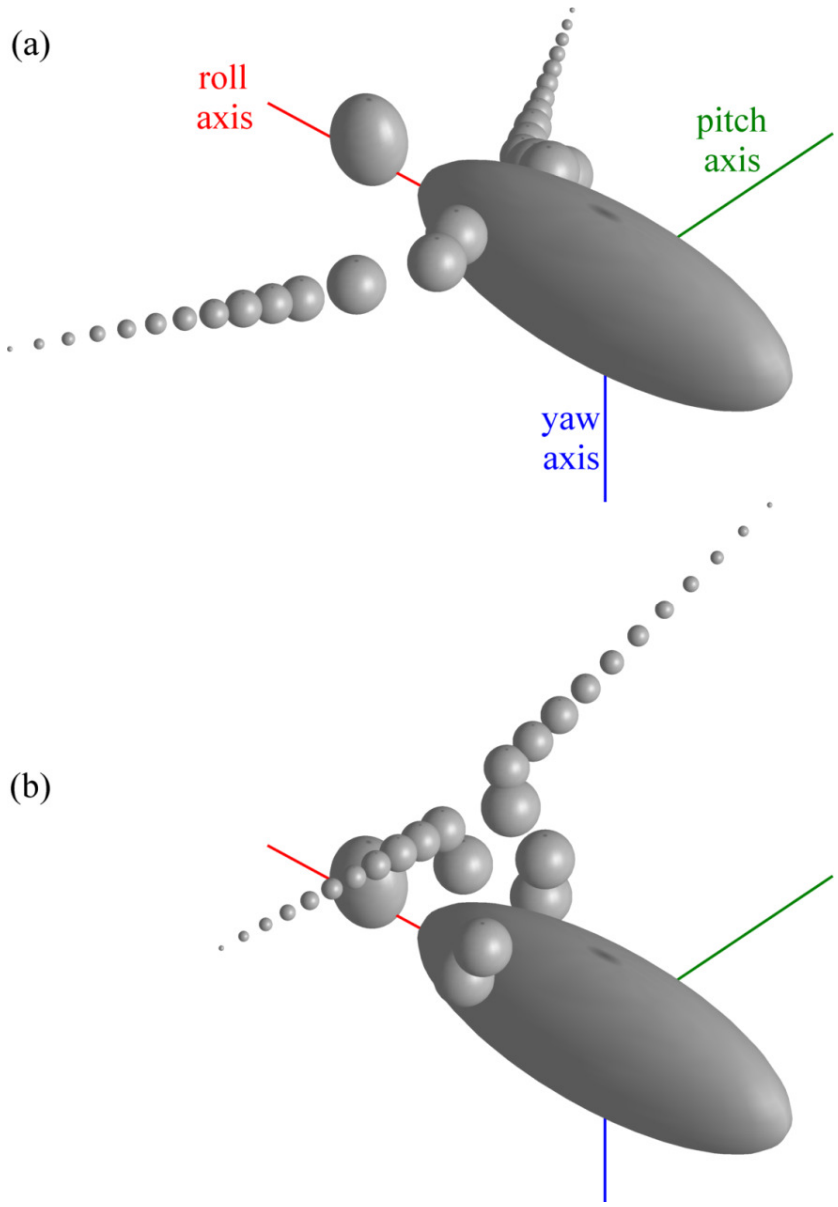

Figure 3_2. Dynamics model of a pigeon. Representations of the mass distribution and moments of inertia of a pigeon in late downstroke (a), and near mid-upstroke (b). The body and head (large and small grey ellipsoids) were treated as rigid objects for which the moments of inertia were assigned about the principal axes: anterior-posterior (roll, red line), medio-lateral (pitch, green line) and dorso-ventral (yaw, blue line). Point-masses represent three articulating segments of each wing: the brachium (two masses), antebrachium (one mass) and the hand wing distal to the wrist (eleven masses). The volumes of the spheres and ellipsoids represent relative masses.

Applying the angular momentum principle (Pratab & Ruina, 2009along with wing-segment masses and moments of inertia for the body and head, to the time-varying 3D marker positions allowed for calculations of aerodynamics- and inertia-based accelerations of the body. The principle of conservation of angular momentum states that the rate of change of the angular momentum of a system, *e.g.*, an entire bird, is equal to the sum of all torques acting about the center of mass (Mitiguy, 2008). For the body plan of a pigeon, with many spatial degrees of freedom, the angular momentum can be calculated through summation of the angular momentum of each body segment about the collective, or system, center of mass (S_{CM}). Note that S_{CM} can move relative to the torso, due to varying wing and head positions.

Table 3_1. Inertial morphological properties measured for Columba livia (N=4): segment masses.

segment	% of S_{CM}
torso (including tail)	83.6 ± 1.3
head	3.9 ± 0.3
brachium	1.5 ± 0.3
ante-brachium	2.9 ± 0.4
hand wing	1.9 ± 0.1

Table 3_2. Inertial morphological properties measured for *Columba livia* (N=4): mass moments of inertia.

(*10-5 kg*m^2)	roll	pitch	yaw
torso	20.98 ± 3.75	56.38 ± 0.28	71.19 ± 8.62
head	3.90 ± 0.45	5.93 ± 0.90	4.42 ± 0.13

To calculate the system angular momentum, a mass-distribution model was created that treated the torso/tail (body), and head, as rigid objects, and modeled the wings as a series of point masses positioned along the wing segment (Fig. 3_2; Table 3_1). Here, the head was assumed to remain in a fixed orientation with respect to the body and the inertial effect of tail movement to be negligible. The wing masses were measured as described in Ros et al. (2011) (Chapter 2). The moments of inertia about the antero-posterior (roll), medio-lateral (pitch), and dorso-ventral (yaw) axes of the head and body (Table 3_2) were calculated from the angular swing periods during two-point suspensions (see Newman and Searle, 1957 and Alexander, 1968). Additionally, the centers of mass of the head and body were determined by multiple single-point suspensions as the intersection of the direction of gravity.

The expanded angular momentum principle for the pigeon system about S_{CM} was given by:

$$\frac{{}^{N}d\,{}^{N}\vec{H}^{S/S_{\mathrm{CM}}}}{\mathrm{dt}} = \Big(\sum_{i=1}^{n}\Big(m^{P_i} * \Big[\Big(\vec{r}^{\,P_i/\mathrm{Body}_{\mathrm{CM}}} - \frac{1}{m^{S}} * \Big(\sum_{i=1}^{n}\big(m^{P_i} * \vec{r}^{\,P_i/\mathrm{Body}_{\mathrm{CM}}}\big)\Big)\Big) \times$$

$$\Big(\Big(\Big(-\frac{1}{m^{S}} * \Big(\sum_{i=1}^{n}\Big(m^{P_i} * \big(\big({}^{\mathrm{Body}}\vec{a}^{\,P_i} + {}^{N}\vec{\omega}^{\mathrm{Body}} \times {}^{\mathrm{Body}}\vec{v}^{\,P_i}\big) + \big({}^{N}\vec{\alpha}^{\mathrm{Body}} \times \vec{r}^{\,P_i/\mathrm{Body}_{\mathrm{CM}}}\big) + \big({}^{N}\vec{\omega}^{\mathrm{Body}} \times {}^{\mathrm{Body}}\vec{v}^{\,P_i}\big)\big)\Big)\Big)\Big) +$$

$${}^{N}\vec{\alpha}^{\mathrm{Body}} \times \vec{r}^{\,P_i/\mathrm{Body}_{\mathrm{CM}}} + {}^{N}\vec{\omega}^{\mathrm{Body}} \times \big({}^{N}\vec{\omega}^{\mathrm{Body}} \times \vec{r}^{\,P_i/\mathrm{Body}_{\mathrm{CM}}}\big)\Big) + {}^{\mathrm{Body}}\vec{a}^{\,P_i} + 2\,{}^{N}\vec{\omega}^{\mathrm{Body}} \times {}^{\mathrm{Body}}\vec{v}^{\,P_i}\Big]\Big)\Big) +$$

$$\Big(\big(\underline{\boldsymbol{I}}^{\mathrm{Body}/\mathrm{Body}_{\mathrm{CM}}} \cdot {}^{N}\vec{\alpha}^{\mathrm{Body}}\big) + \big(m^{\mathrm{Body}} * \Big(-\frac{1}{m^{S}} * \Big(\sum_{i=1}^{n}\big(m^{P_i} * \vec{r}^{\,P_i/\mathrm{Body}_{\mathrm{CM}}}\big)\Big)\Big) \times$$

$$\Big(-\tfrac{1}{m^{S}} * \Big(\sum_{i=1}^{n}\big(m^{P_i} * \big(\big({}^{\mathrm{Body}}\vec{a}^{\,P_i} + {}^{N}\vec{\omega}^{\mathrm{Body}} \times {}^{\mathrm{Body}}\vec{v}^{\,P_i}\big) + \big({}^{N}\vec{\alpha}^{\mathrm{Body}} \times \vec{r}^{\,P_i/\mathrm{Body}_{\mathrm{CM}}}\big) + \big({}^{N}\vec{\omega}^{\mathrm{Body}} \times \big({}^{\mathrm{Body}}\vec{v}^{\,P_i} + {}^{N}\vec{\omega}^{\mathrm{Body}} \times \vec{r}^{\,P_i/\mathrm{Body}_{\mathrm{CM}}}\big)\big)\big)\big)\big)\big)\big)\big)\big), \quad (1)$$

with:

$\frac{{}^{N}d\,{}^{N}\vec{H}^{S/S_{\mathrm{CM}}}}{\mathrm{dt}}$ = rate change of angular momentum in the inertial frame (N) about S_{CM};

m^{P_i} = mass of particle P_i;

m^{S} = mass of the system (entire bird);

$\underline{\boldsymbol{I}}^{\mathrm{Body}/\mathrm{Body}_{\mathrm{CM}}}$ = inertia dyadic of the body about the center of mass of the body;

$\vec{r}^{\,P_i/\mathrm{Body}_{\mathrm{CM}}}$ = vector from the body center of mass to P_i;

${}^{\mathrm{Body}}\vec{v}^{\,P_i}$ = velocity of P_i, relative to the body;

${}^{N}\vec{\omega}^{\mathrm{Body}}$ = angular velocity of the body;

${}^{\mathrm{Body}}\vec{a}^{\,P_i}$ = acceleration of Pi, relative to the body;

${}^{N}\vec{\alpha}^{\mathrm{Body}}$ = angular acceleration of the body.

Because only external torques can change the angular momentum of the entire bird, a bird in mid-air can only be rotationally accelerated by aerodynamics. Gravity, by definition, acts through S_{CM} and therefore does not apply a torque about S_{CM}. The rate change of the angular momentum solved in three dimensions for the pigeon (Eq. 1) therefore is equivalent to the aerodynamic torque acting about S_{CM}.

Similarly, in a hypothetical absence of air, any changes in the angular momentum of the wings will be matched by an equal and opposite change in the angular momentum of the rest of the bird (torso, head and tail), referred to here as the body. By equating the entire right hand side of equation (1) to 0, ${}^{N}\vec{\alpha}^{\mathrm{Body}}$ can be solved between each time step. Furthermore, by comparing the expected angular velocity from inertial reorientation to the measured angular velocity, body accelerations based on aerodynamics can be deduced. These aerodynamic body accelerations closely matched measured aerodynamic torques, and were used for further analysis, since they allowed for a direct comparison with inertial body accelerations.

Table 3_3. Net wingbeat reorientations accumulated throughout the turn.

body rotation components	reorientation (deg) (mean ± SD)
roll	76.8 ± 13.6
pitch	42.6 ± 1.6
yaw	58.1 ± 4.3

Wingbeats were partitioned into upstroke and downstroke phases, based on reversal of the major bending direction of the primary feathers. This bending reversal of the primary feathers coincided with the instant the primary feather markers moved laterally relative to the body, in both ventral (start of upstroke) and dorsal (start of downstroke) positions. Net wingbeat body rotations were defined as the resulting changes in body orientation over entire wingbeat periods and were calculated about each of the body axes. For each turn, five sequential wingbeats were analyzed, during which net wingbeat body rotations about each axis were accumulated (Table 3_3).

Potential wing and tail kinematic predictors were compared on an inside vs outside wing basis by averaging between left turn and right turn wingbeat cycle pairs. Due to the incremental, yet impulsive nature of pigeon turning flight (Warrick *et al.,* 1998), wingbeat characteristics, such as variations in aerodynamic power output from one wingbeat to the next, could lead to higher wing speeds or angles of attack of both the inside and outside wing in a left turn as compared to a right turn (or *vice versa*), without accurately reflecting torque-related contra-lateral asymmetries. To account for such potential differences between left and right wingbeat cycles, as well as differential left-right marker placement, wing kinematics were averaged over the left turn and right turn inside wings. Outside wing kinematics were averaged accordingly.

Averaging for inside versus outside wing comparisons was performed over wingbeat cycles, which were identified by the occurrence of head saccades. Turning pigeons tend to rotate their body to redirect aerodynamic force production during a wingbeat cycle immediately following a head saccade, which is consistently made into the direction of the turn (Chapter 4).

Results

The three pigeons negotiated the 90° level turn at a CM speed of 3.3 ± 0.2 ms^{-1} and a wingbeat frequency of 8.3 ± 0.3 Hz. Of the whole-body mass of 319 ± 33 g, each wing (distal to the shoulder) comprised 6.3 ± 0.7 % and the head 3.9 ± 0.3 % (Table 3_1).

The low-speed, level turns in pigeons were predominantly driven by roll and yaw rotations (Fig. 3_3). Only pitch fluctuated with consistent periodicity within the wingbeat cycle. Body orientations about all three anatomical axes fluctuated within wingbeats independent of changes in body orientation across wingbeats (net wingbeat reorientations). Net wingbeat reorientations, summed throughout the turn, about the roll and yaw body axes comprised the majority of the body reorientations (Table 3_2). The birds consistently yawed into the turn, whereas roll changed direction, initially being directed into the turn, and later directed outwards. Pitch reorientations were generally directed upwards (head-up).

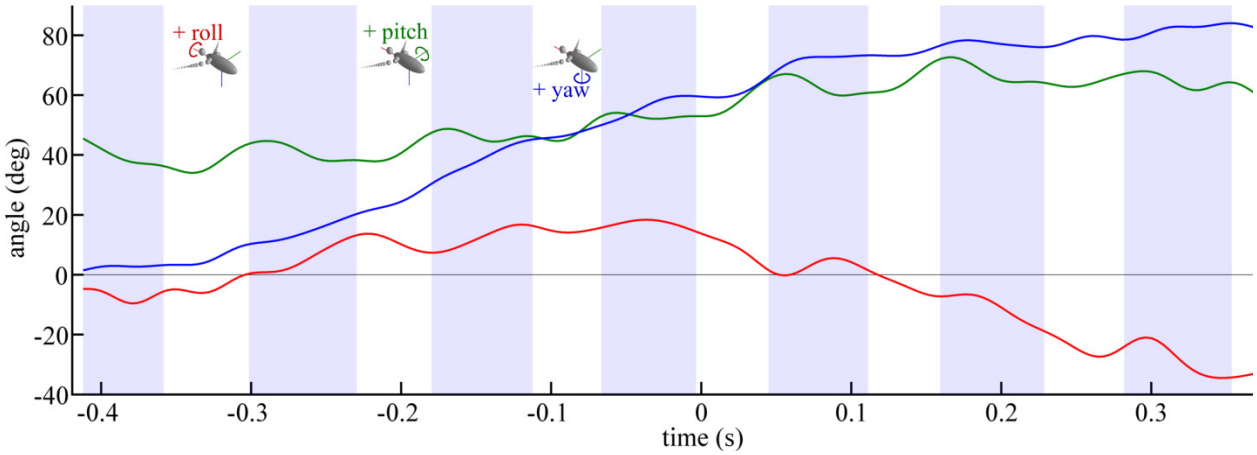

Figure 3 3. Low-speed, level turns in pigeons are predominantly based on roll and yaw rotations. Integrated angular velocities about the principal body axes throughout a representative right turn, with positive roll and yaw into the turn, as well as head-up pitch (small depictions, and Fig. 2-2a). Initial angles are based on the inclinations of the corresponding body axes with respect to the horizontal at the start of recording. The majority of body reorientations occurs about the roll and yaw axes. Only pitch varies periodically with the wingbeat cycle (blue shading represents downstroke phases). The bird's center of mass passes the midpoint of the turn at t = 0 s.

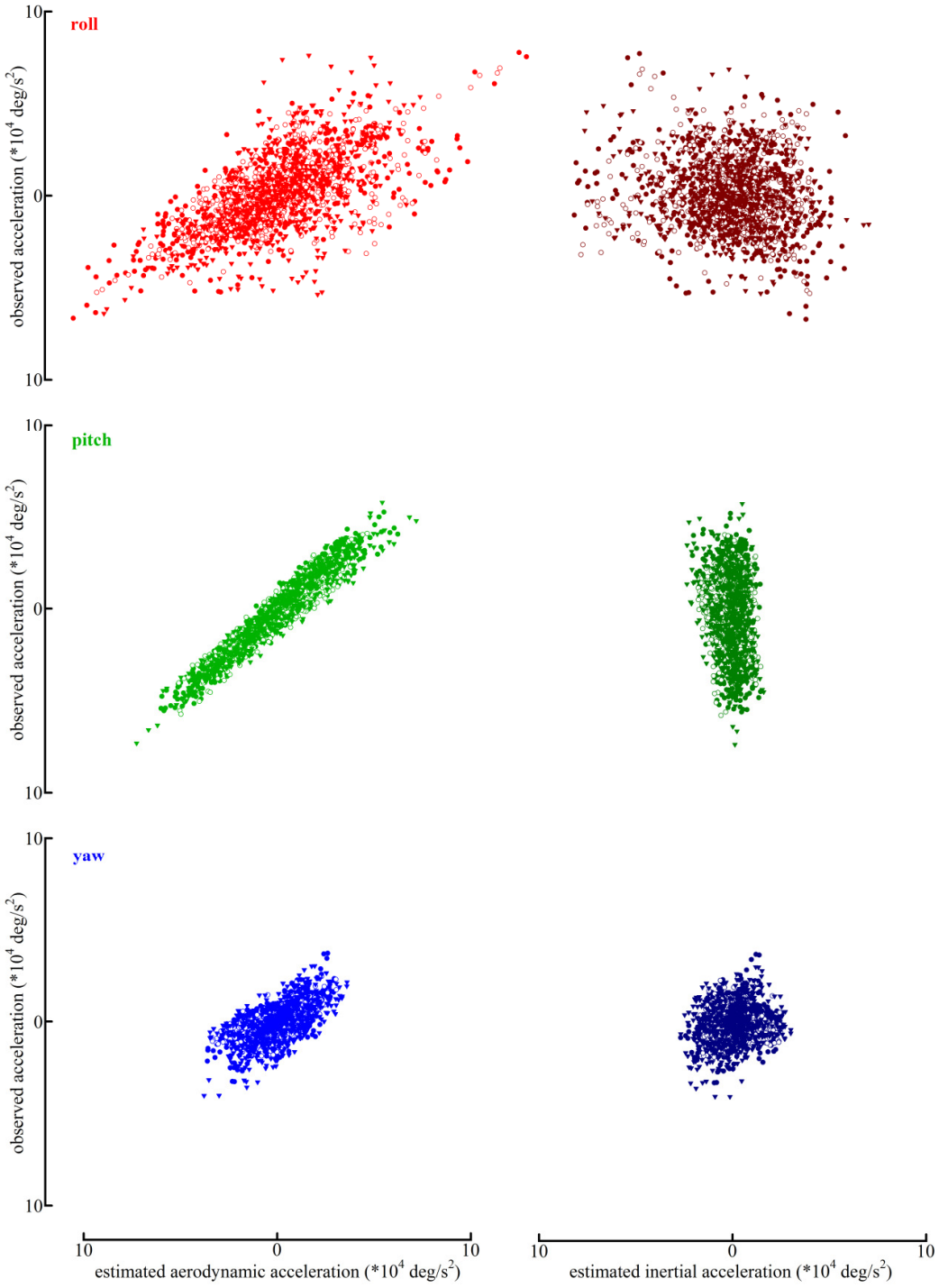
roll
pitch
yaw
observed acceleration (*10^4 deg/s^2)
10
0
10
estimated aerodynamic acceleration (*10^4 deg/s^2)
estimated inertial acceleration (*10^4 deg/s^2)

Figure 3_4.

Figure 3_4 (Continued). Aerodynamic estimates predict body accelerations. Body accelerations based on aerodynamic torque estimates predict measured body accelerations throughout left and right turns for three individuals (plotted symbols), about roll (red; R^2=0.44, p<0.01), pitch (green; R^2=0.93, p<0.01) and yaw (blue; R^2=0.43, p<0.01) axes. Body accelerations based on rate of momentum exchange (inertia) between the wings and the body (right panels) are either not correlated (roll), weakly correlated (yaw: R^2=0.01, p=0.02), or weakly, negatively correlated (pitch: R^2=0.02, p<0.01) with observed body accelerations.

Aerodynamic torques, not inertia-based momentum exchanges between the wings and body, predicted body accelerations (Fig. 3_4). Estimated aerodynamic accelerations of the body correlated positively with measured body accelerations about each of the principal body axes. Aerodynamic estimates most reliably predicted pitch rotations (p<0.01, R^2 = 0.93), with body acceleration correlations about both roll (p<0.01, R^2 = 0.44) and yaw (p<0.01, R^2 = 0.43) of similar strength. The range of estimated aerodynamic accelerations was smallest about the yaw body axis. Inertial roll did not correlate with observed accelerations (p=0.82), but inertial and observed body accelerations did correlate about pitch (p<0.01) and yaw axes (p=0.02), although with extremely low predictive power (R^2 = 0.02 and 0.01, respectively).

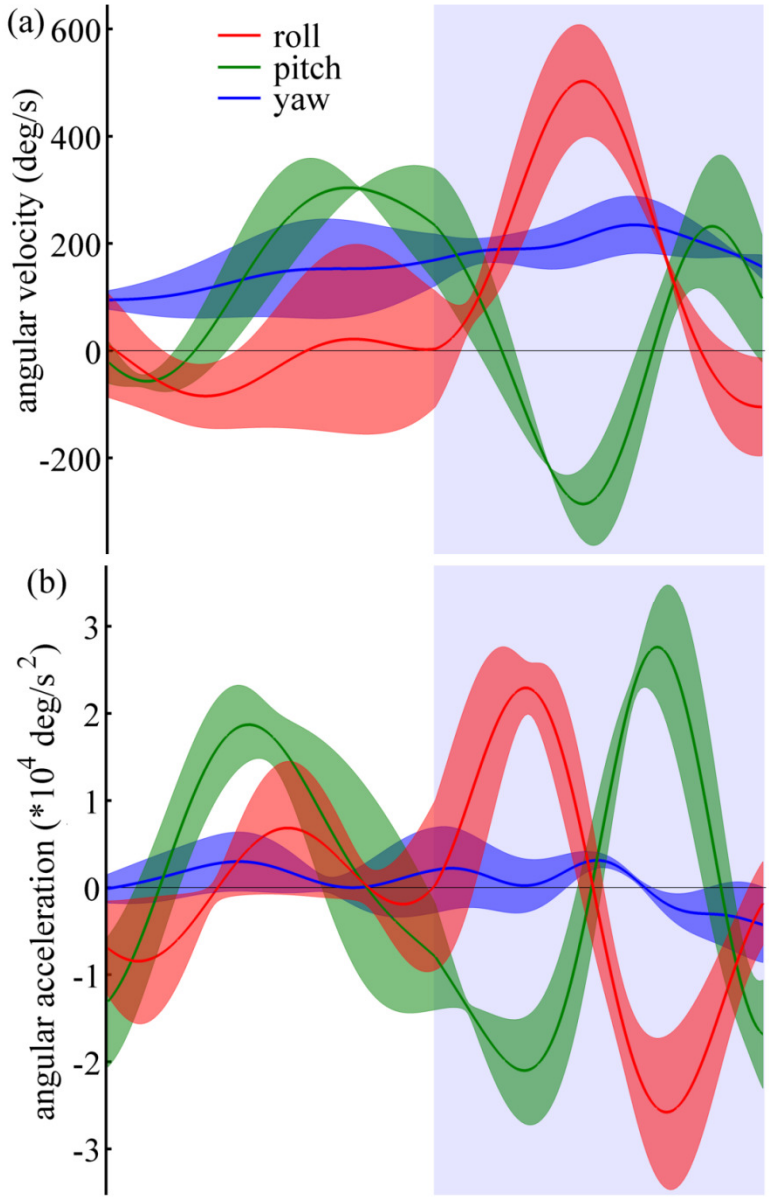

Figure 3_5. Roll velocity is initiated early and arrested late in the downstroke. (a) Mean ± sd of individual mean body velocities in roll (red), pitch (green) and yaw (blue) throughout three left and three right wingbeats early in the turn, and normalized to the wingbeat cycle period. Near the middle of the downstroke (blue shading) the body pitches bill-down (-) and rolls into the turn (+). (b) The mean individual roll and pitch accelerations peak in the first half of the downstroke (red and green, respectively), with extremes reversed in the second half of the downstroke, arresting the roll velocity and reversing the pitch velocities in (a), respectively. Pitch accelerations also show peaks near mid-upstroke, whereas roll accelerations are more variable during the upstroke.

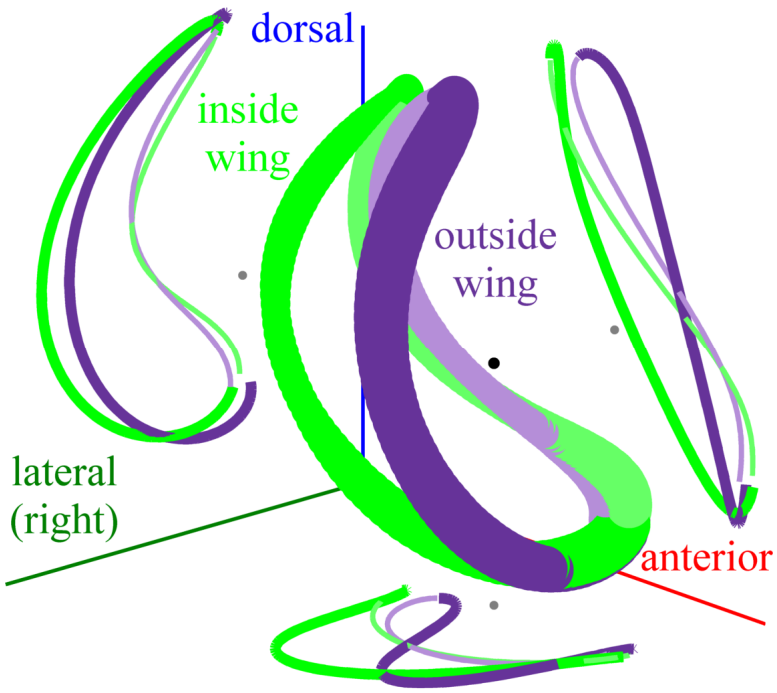

Figure 3_6. Turning wingbeats are characterized by differentially swept wing trajectories. Mean ± sd (trace thickness) of individual mean trajectories of the distal wing marker for the inside (green) and outside (purple) wing for the same wingbeats as in Fig. 2-5. Both trajectories are represented as a right wing. The trajectories are displayed relative to the body frame, represented by the anterior (red), right (green) and dorsal (blue) directions, as well as the right shoulder location (black sphere). The means of the 3D trajectories, with the upstroke in a lighter shade, are projected on each of the anatomical planes, emphasizing the more protracted (anteriorly projected) path of the outside wing early in the downstroke.

During the turning wingbeats selected for analysis (Fig. 3_5-3_7), *i.e.* those following head saccades, roll velocity was initiated early and arrested late in the downstroke, with a peak in angular velocity into the turn occurring at mid downstroke (Fig. 3_5a, b). Roll velocities varied and were of much smaller magnitude during the upstroke. Body pitch velocities and accelerations consistently varied with wingbeat phase: head-up pitch acceleration peaked near the temporal middle of the upstroke and approximately two-thirds into the downstroke, whereas

a head-down pitch acceration peak coincided with the peak in roll acceleration near the first third of the downstroke. These pitch patterns were consistent for all wingbeat cycles analyzed, whereas body roll and yaw angular movements were more variable throughout the turn (not shown). Yaw velocity was consistently positive and directed into the turn over the full wingbeat cycle, with a moderate deceleration phase near the end of the downstroke.

Turning wingbeats were characterized by differentially swept wing trajectories, or paths relative to the body, accompanied by contralateral differences in axial wing orientation. Corresponding with the roll acceleration early in the downstroke phase (Fig 3_5b), the outside wing was swept and initiated relatively more anteriorly, compared to a more laterally directed inside wing trajectory (Fig 3_6). In concert with the contra-lateral asymmetry in wing trajectories, the inside wing was more strongly pronated, or rotated forward (leading-edge down) about the long axis of the wing during the first half of the downstroke (Fig 3_7a). This contra-lateral difference in axial wing rotation was reversed in the second half of the downstroke through supination of the inside wing and pronation of the outside wing near the middle of the downstroke (Fig 3_7a). As the body rolled into the turn in the downstroke, the inside wing also acquired a higher speed (Fig 3_7b), and became oriented more laterally (Fig 3_7c).

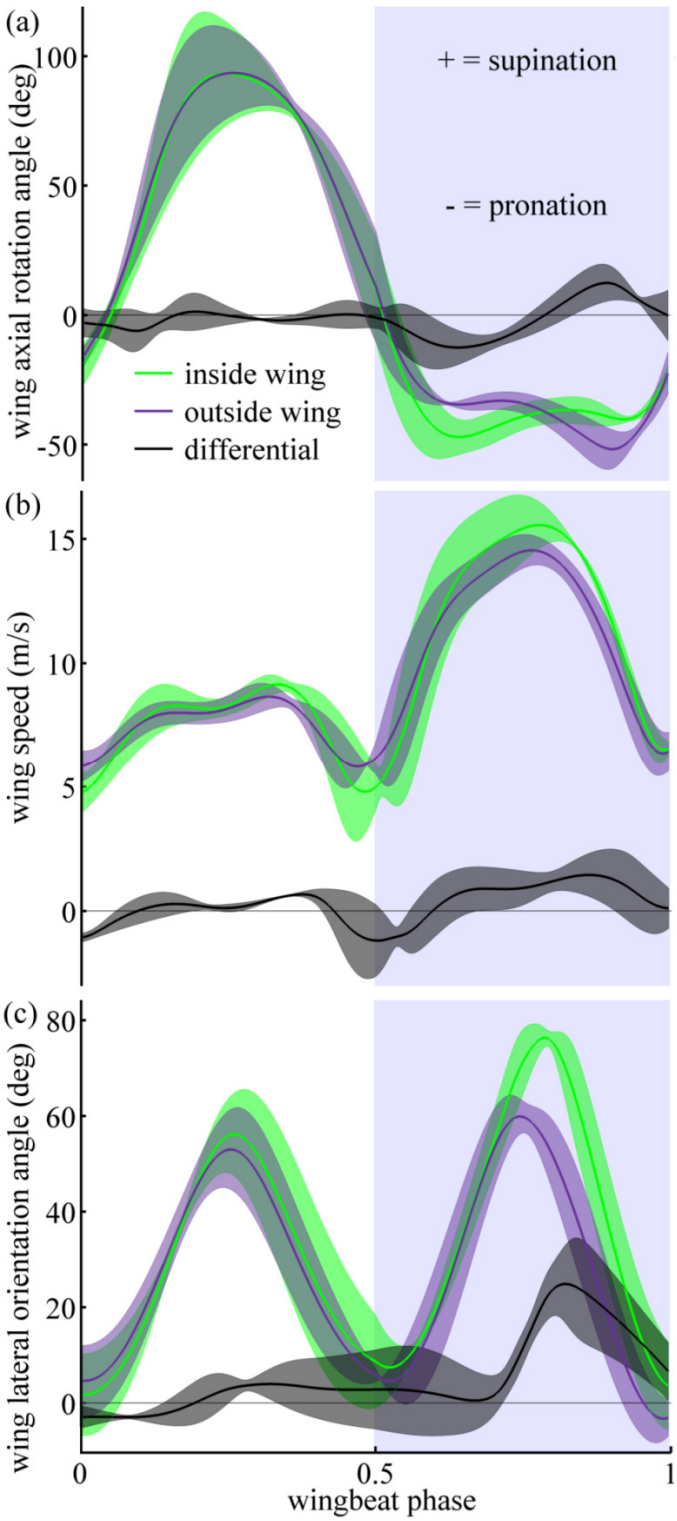
(a)
+ = supination
- = pronation
wing axial rotation angle (deg)
100
50
0
-50
inside wing
outside wing
differential
(b)
wing speed (m/s)
15
10
5
0
(c)
wing lateral orientation angle (deg)
80
60
40
20
0
0
0.5
1
wingbeat phase

Figure 3_7.

Figure 3_7 (Continued). Wing pronation accompanies a more caudally swept inside wing, whereas a greater wing speed and later projection aerodynamically dampen roll velocity. (a) For the same wingbeats as in Fig. 2-5; 2-6, during the upstroke, the inside wing (green) and outside wing (purple) supinate and subsequently pronate about the wing long-axis in synchrony. Early in the downstroke, the inside wing pronates to a larger degree than the outside wing (purple), resulting in an inside versus outside wing differential that is negative, or pronated (black trace ± sd). The more pronated inside wing in combination with the contra-lateral difference in wing trajectory maintains comparable angles of attack between the wings. However, these wing-configuration and kinematic differences likely results in aerodynamic forces that act above the center of mass to be directed upwards and to the right side of the body, causing the pitch down and roll torques into the turn. (b) Inside wing speed starts surpassing outside wing speed as the roll velocity (a) increases towards the inside wing. The higher speed of the inside wing persists longer than the roll velocity, indicating its contribution to passive aerodynamic roll damping, aided by a more lateral orientation angle (e) of the inside wing (the angle between the wing long axis and the sagittal plane of the body).

Discussion

Aerodynamic and inertial accelerations of pigeons turning during low speed flight were calculated using segment masses, moments of inertia and time-varying wing and body configurations. Directly measured body accelerations correlate with aerodynamic torques, justifying an exploratory comparison of inside wing versus outside wing kinematic proxies for aerodynamic torque generating mechanisms. Contrary to previous findings (Warrick & Dial, 1998), contra-lateral asymmetries in wing speed do not appear to underlie these aerial turns, and surprisingly, nor do contra-lateral differences in wing area, angle of attack, wingbeat amplitude, or timing. To generate roll and pitch torques into the turn, the pigeons reorient their wing trajectories toward the desired direction (Fig. 3_6-3_7). As a result, the aerodynamic force, which acts above the center of mass, is redirected into the turn, generating the torques required to turn.

Pigeons use a complex combination of roll, pitch and yaw body rotations to turn, with the largest contribution resulting from roll reorientations (Fig 3_2; Table 3_3). The roll rotations likely serve to redirect aerodynamic force production and therefore change the flight path (Chapter 2), since during the first half of the turn the birds roll into the turn, whereas during the second half they roll out. The observed roll patterns may also serve a secondary function allowing changes in body pitch to contribute to the turn. Due to the banked orientation while turning (Warrick & Dial, 1998; Hedrick & Biewener, 2007; Chapter 2), nose-up pitch reorientations can contribute to reorienting the body into the desired direction. Theoretically, a full 90-degree bank and a subsequent 90-degree pitch-up, followed by a restoring 90-degree outward roll, would accomplish a net change in yaw of 90 degrees, meeting the reorientation requirement of the 90-degree turn. However, because of the dual function of body rotations, changing flight trajectory and reorienting the body (Chapter 2), substantial yaw rotations are simultaneously required.

The summed net wingbeat yaw reorientations never fully matched the 90 degrees of the turn (Fig. 3_2), again illustrating the need for a composite of body rotations components to simultaneously meet the rotational (acquisition of the desired, new flight orientation) and translational (flight path changes and offsetting of gravity) requirements of the turn (Chapter 2).

The consistent aerodynamic pitch accelerations related to the phase of the wingbeat cycle (Fig. 3_3, 3_5b), in combination with a "pitched-up" body posture and wing positions, strongly suggest that the center of pressure of the resultant aerodynamic force is positioned dorsally relative to the center of mass during the first half of the downstroke, and ventrally and anteriorly near the second half of the downstroke and the middle of the upstroke, respectively. These inferences corroborate the aerodynamic activity of the tip-reversal upstroke (Crandell & Tobalske, 2011; Chapter 2) and agree with previous findings that aerodynamic forces acting dorsal of the center of mass during the downstroke of the Japanese White-eye (Su *et al.,* 2011*).*

Contra-lateral differences in wing trajectory and axial wing orientation angles (Fig. 3_6; 3_7a) coincide with roll accelerations early in the downstroke directed towards the inside wing (Fig. 3_5b), and are likely indicative of the aerodynamic mechanism employed to generate the steering torque. Body accelerations that increase the angular momentum of the bird as a whole, likely require differential activation of contra-lateral flight muscles. In contrast to Warrick and Dial (1998), these 'active' body accelerations do not correlate with contra-lateral asymmetries in either wing speed relative to the body (relevant from a control perspective), or in the inertial frame (relevant for aerodynamics). Furthermore, contra-lateral differences in wing length (a proxy for wing area), angle of attack, wingbeat amplitude, or timing also do not relate to body accelerations. Instead, the pigeons simply reorient the flapping sweep of their wing trajectories toward the desired direction, which likely redirects the aerodynamic force into the turn. Assuming the aerodynamic force produced by the wings indeed acts above the center of mass,

the redirected aerodynamic force would therefore generate the observed roll towards the inside wing, in addition to the consistently observed nose-down pitch.

Considering the similarities in body plan across avian species, especially compared to flying insects, and the fairly simple nature of the aerodynamic torque generating mechanism described here, it is likely that other bird species use the observed mechanism to generate aerodynamic torques during slow turning flight. For example, cockatoos turning at low speeds displayed contralateral differences wing kinematics similar to those described in this study for pigeons, even though these differences did not relate significantly to roll accelerations in the cockatoos (Hedrick & Biewener, 2007).

The observed contra-lateral differences in wing trajectory and hand wing axial rotation angle corroborate the idea that fore-arm musculature is involved in low speed flight maneuvers (Bilo, 1985; 1994; Dial, 1992). The current results, however, do not exclude involvement of differential forces between the pectoralis muscles of the inside and outside wing (Warrick et al, 1998) or corresponding differential wing speeds (Warrick & Dial, 1998) as additional or complementary torque generating mechanisms. Here, we found that differences in wing speed occur near the middle and end of the downstroke (Fig. 3_7b), when roll velocities are substantial and being arrested, respectively (Fig. 3_5a). The rotational speed of the body could passively increase the speed of the wing on the side of the bird that moves with the wingbeat (the inside wing). Such a mechanism has been termed passive rotational damping (Hedrick et al, 2009), and could be responsible for arresting the roll velocity near the end of the downstroke.

Additionally, the more lateral projection angle of the inside wing in the second half of the downstroke (Fig. 3_6; 3_7c), resulting from the differential wing trajectory established earlier in the downstroke likely gives the aerodynamic force produced by the inside wing a greater moment arm about the roll axis, adding to even stronger rotational damping. Body rotations that are passively damped would not require differential activation of contra-lateral wing muscles.

To further understand the neuro-muscular components of flight control, we are currently examining activation and strain patterns of flight muscles throughout aerial turns. Differential activation of distal wing muscles has been found to relate to steering in simulated flight in pigeons (Bilo & Bilo, 1983), in addition to which an antebrachial hand wing extensor, the extensor metacarpus radialis, was found to predict lower frequency components of turning (Hedrick and Biewener, 2007). Combined with the torque generating mechanisms observed here, differential activation of inside and outside wing muscles involved in turning maneuvers can be expected for muscles related to wing trajectory, such as the scapulohumeralis caudalis and pectoralis pars sternobrachialis muscles (Dial *et al.* 1991), and hand wing pronation, such as the extensor metacarpi radialis and the ulnometacarpalis ventralis muscles (Vasquez, 1995).

Lastly, investigating torque generating mechanisms in different maneuvers, such as those employed during turns at higher flight speeds, and in different (avian) species may provide insight into the generality of the currently observed mechanism. Furthermore, such investigations will elucidate the breadth of the repertoire of turning mechanisms not only available, but actually employed by birds (see also Warrick and Dial, 1998).

Acknowledgements

We thank P.A. Ramirez for care of the animals, D.E. Lieberman for kindly sharing the use of the Qualisys cameras, and A.N. Ahn, T.E. Higgins, A. Eberle, C. Gastil, A. Randall, and C.A. Moreno for helpful discussions and informal contributions to this work. This study was funded by grants from NSF (IOS-0744056) and ONR (N0014-10-1-0951) to AAB.

CHAPTER 4

Head stabilization and visual control of turning flight in the pigeon

Control inputs for avian turning flight

Ivo G. Ros, Andrew A. Biewener

Summary

Growing recognition that similar flight control principles operate across insect and vertebrate fliers indicates that robust solutions have evolved to meet complex behavioral challenges. To examine potential similarities in visual and cervical feedback control of flight between birds and insects, we investigate the role of head stabilization in providing feedback cues for controlling turning flight in the pigeon. Based on previous observations that the eyes remain fixed relative to the head, we inferred control inputs from detailed head and body orientations and velocities during 90-degree aerial turns. Periods of angular head stabilization alternated with rapid repositioning movements (head saccades), confirming that control of head motion is decoupled from aerodynamic and inertial forces acting on the body during flapping flight. Moreover, visual cues induced by these head saccades predicted changes in flight trajectory, whereas the magnitude of neck bending predicted changes in angular positioning of the body. Controlling head motion to stabilize the visual field may therefore not only facilitate extraction of important motion cues but also offer mechanisms for controlling body and wing movements. Similarities between sensory flight control of birds and insects can inspire novel designs of robust controllers for autonomous aerial vehicles.

Introduction

The ability to maneuver, turn and maintain stable flight has been critical to the evolutionary diversification and success of flying animals. Rapid integration of sensing with the actuation and motion of the wings or other control surfaces is required for active flight control. However, the mechanisms by which sensory input is coupled to motor output for maneuvering flight in birds has been understudied compared to studies of avian functional anatomy, neural organization and sensory neurophysiology (for review, see (Zeigler & Bischof, 1993)).

Sensory input clearly shapes behavior, but behavior can also shape sensory perception (Zeil *et al*., 2008). For instance, fly flight is characterized by brief, sharp turns alternated with periods of straight, translational flight (Schilstra & Van Hateren, 1998), confining visual motion induced by self-rotation, or angular optic flow, to these rapid turns. As a consequence, course, speed, and distance information is more easily extracted from the translational optic flow during straight flight periods (Land, 1999). This flight behavior is inferred to be adapted to improving sensory perception in flies (Zeil *et al*., 2008). Understanding the relationship between sensory input and behavioral output is a key first step in identifying the underlying components of behavior that represent specific sensory adaptations.

Translational optic flow appears to guide the flight behavior of several unrelated species, indicating that it may provide a general visuomotor control stimulus. When flying down a corridor, budgerigars and honeybees follow flight paths that balance left and right lateral optic flow (Bhagavatula *et al.*, 2011; Srinivasan *et al.*, 1991). Furthermore, as optic flow increases, budgerigars, bees, moths, fruit flies, and blowflies reduce their flight speed to maintain an optic

flow rate below a possible internal limit (Bhagavatula *et al.*, 2011; Srinivasan *et al.*, 1991; David, 1979; Fry *et al*., 2009; Verspui & Gray, 2009; Kern *et al*., 2012).

By moving their head backwards and forwards relative to the body just before landing (but not after take-off), pigeons may similarly use fluctuations in translational head speed relative to their surroundings to increase close-range perception of a landing site (Green *et al*., 1994). These in-flight head speed fluctuations are reminiscent of the head bobbing readily observed during walking in many birds. However, in contrast to the periods of stationary head 'hold' phases that occur during walking (Dunlap & Mowrer, 1930; Friedman, 1975; Frost, 1978), the pigeon's head never comes to a complete stop during landing flight. Based on associations of head orientations during turning in pigeons (Bilo *et al*., 1985), ascending and descending flight in pigeons, as well as during jumping and slope walking in domestic chicks, the control of head movements has been proposed as an essential underlying component of the visual control of avian locomotion (Green, 1998).

In addition to optic flow, cervical mechano-receptors assist flight control in insects, including dragonflies (Mittelstaedt, 1950), flying locusts (Goodman, 1965), and blowflies (Land, 1973; Liske, 1977). Similarly, reflexes related to cervical and vestibular systems in normal and labyrinthectomized hand-held pigeons led to comparing the flight control system of birds to the autopilot of an airplane. Groebbels (1926; 1929) proposed that birds control body motion by tracking head motion, essentially 'following their turning heads'. In support of this hypothesis, certain wing and tail muscles in the pigeon react to vestibular stimulation, angular visual stimulation, and passive or active lateral head deflections when under simulated flight conditions

(Bilo & Bilo, 1978; Bilo & Bilo, 1983). Observations of maneuvering pigeons and zebra finches provide further evidence that head stabilization during flight may play a role in flight control (Bilo *et al*., 1985; Warrick *et al*., 2002; Eckmeier *et al*., 2008). Finally, the importance of head stabilization for flight control is reinforced by the inability of pigeons to recover from perturbations when wearing restraining neck collars (Warrick *et al*., 2002).

Head stabilization and visual control of locomotion may therefore be tightly linked in flying birds. Nearly all animals "foveate," changing their gaze, or viewing direction, in an alternating pattern of stable gaze fixations and fast saccades, defined as rapid movements of the eye (Land, 1999). However, in most birds, gaze changes are primarily driven by head (rather than eye) movements (Gioanni . Furthermore, pigeons actively maintain the direction of their eyes within their head, referred to as the primary gaze position (Wallman & Pettigrew, 1985; Wallman & Velez, 1985; Nalbach *et al*., 1990). Thus, head orientation is often used as an indicator of gaze in birds (see Kjearsgaard *et al*., 2008).

Here, we use head orientation to investigate the potential link between head stabilization and sensory inputs for the control of turning flight in pigeons, by analyzing detailed 3D movements of the head and body during low-speed, 90 degree, level turns (Fig. 4_1). Measurements of head velocity and gaze direction are used to infer visual feedback during turning flight. A flying animal's trajectory (velocity direction) determines the focus of expansion (FOE), resulting from the optic flow induced by its translational movement. Any deviation between the FOE and the head's mid-sagittal plane, therefore, produces a "FOE offset" (Fig. 4_2A). Additionally, cervical proprioceptive feedback is inferred from cervical flexure and/or

twisting, defined here as “head offset” (Fig. 4_2B). Using these estimates of visual and proprioceptive feedback, we examine how these two sensory inputs predict body rotations that redirect aerodynamic force to control turning flight. We use body rotations as the output of flight control, given that pigeons change their flight trajectory and orientation through body attitude changes, much like helicopters and fruit flies (Fry & Dickinson, 2003), during low speed flight (Chapter 2).

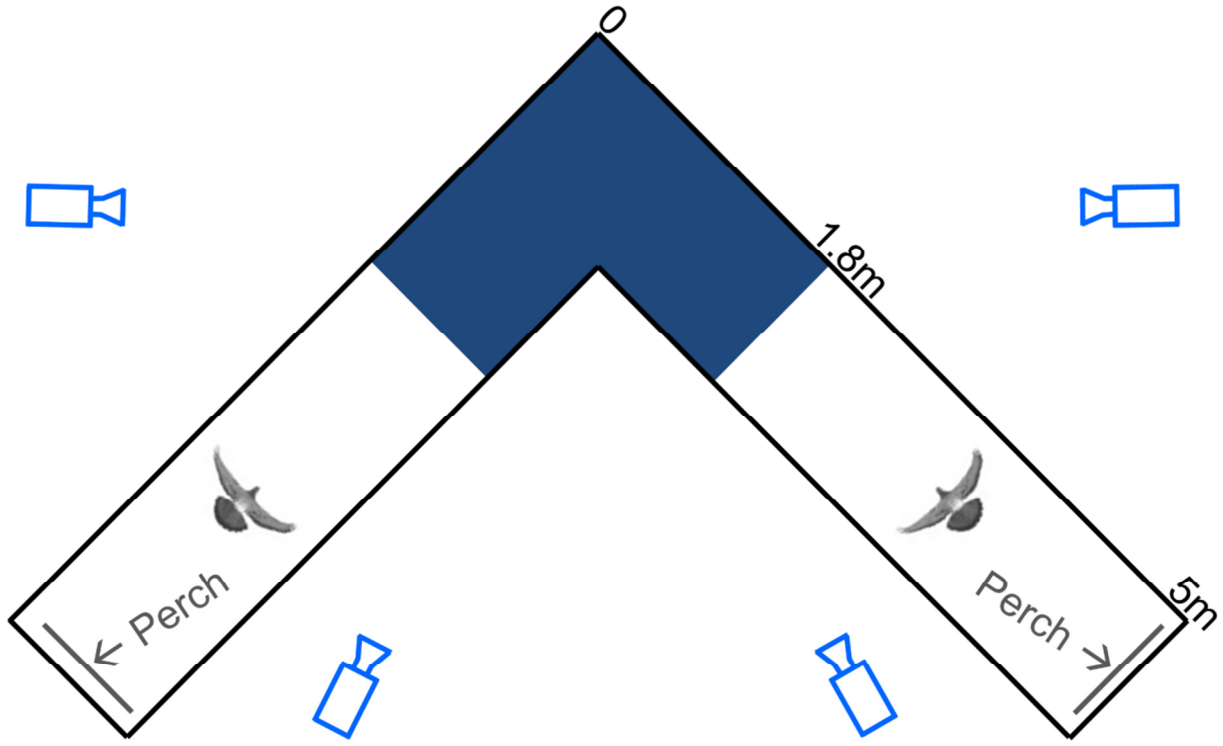

Figure 4_1. Schematic top view of the flight corridor. Light blue camera outlines represent viewing angles, with camera distances underrepresented by 50%. The spatially calibrated section of the 90-degree turn (dark blue), the pigeon silhouettes, and the perches (grey lines) are drawn to scale. Dimensions are noted along the outside of one leg of the symmetrical corridor.

We expect that visual feedback will more accurately predict these body rotations, because the most direct measure of the required amount of steering is the deviation between the animal's current and desired flight trajectory. By directing its gaze in the desired flight direction, a bird creates an offset between its gaze and the current velocity-induced FOE, proportional to the amount of steering required. In contrast, we hypothesize that cervical flexure, or head offset, correlates with subsequent re-orientation of the body to re-align with the head and not with changes in flight trajectory.

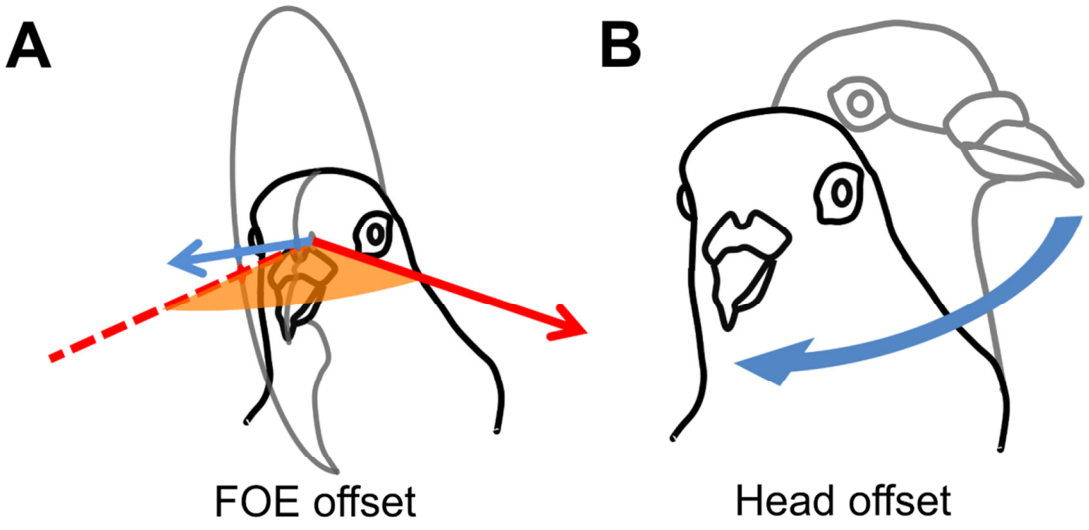

Figure 4_2. Representations of visual and cervical proprioceptive feedback. (A) Visual feedback is represented by the FOE offset (orange, shaded wedge); the angle between the head velocity (red vector) and its projection (dashed red line) on the mid-sagittal plane of the head (grey partial circle). Head orientation indicates gaze (blue vector), or viewing direction. (B) Cervical proprioceptive feedback is represented by head offset (blue curved arrow); the 3D angle between a straight flight head orientation (grey outline of the head) and the instantaneous head orientation (black outline of the head).

Materials and Methods

Three wild-type pigeons (*Columba livia*) were housed and studied at the Concord Field Station (Bedford, MA) in accordance with protocols approved by Harvard University's Institutional Animal Care and Use Committee. The pigeons were trained to fly back and forth between two perches situated at either end of two 5-m-long by 1-m-wide by 2-m-high netted sections, connected by a 90° turn midway (Fig. 4_1). The symmetrical, square-corner corridor was constructed of lightweight, 2-cm mesh nylon deer netting supported by a PVC frame consisting of 4-cm diameter piping.

The pigeons were marked at seven anatomical locations, and the bill tip was used as an additional, natural marker. All artificial markers consisted of polystyrene foam and were attached using thermoplastic adhesive. On the head, two 4-mm diameter spheres were attached to feathers near the lateral ends of the coronal suture of the skull. On each wing, at 67% of the length of the ninth primary feathers, 4-mm diameter spheres were attached to the dorsal side of the rachis. On the body, three 19-mm diameter hemi-spheres were attached to 5-cm by 10-cm strips of elastic tape (to reduce feather movement). One marker was placed ventrally over the rostral end of the keel, and two markers were placed on the left and right rump (4-cm lateral to the vertebral column, over the synsacrum).

Using four synchronized high-speed cameras, 3D positions of the markers were reconstructed within a calibrated 2.9 m^3 volume that encompassed the turn. Only trials in which the birds did not contact the netting were accepted for analysis. The synchronized video system, consisting of one FastCam 1024 PCI, and three FastCam SA3 cameras (Photron USA Inc.),

recorded at 250 Hz with 0.001 sec exposure time. A total of 10,624 video frames were digitized using DLTdv5 (Hedrick, 2008) in Matlab (Mathworks Inc.). Data processing and calculations were also performed in Matlab using custom-written scripts. Positional data were filtered with a fourth-order Butterworth filter using a low-pass cutoff frequency four times the wingbeat frequency. The cutoff frequency was determined by residual analysis (Winter, 2005).

Wingbeats were partitioned into upstroke and downstroke phases, based on reversal of the major bending direction of the primary feathers. This bending reversal of the primary feathers coincided with the instant the primary feather markers moved laterally relative to the body, in both ventral (start of upstroke) and dorsal (start of downstroke) positions.

Visual feedback can be deduced from head velocity and orientation, assuming that the eyes maintain a constant orientation within the head; this is generally the case in pigeons and many other species of birds (Bloch *et al*., 1984; Wallman & Pettigrew, 1985; Wallman & Velez, 1985; Nalbach *et al*., 1990). The head velocity vector relative to the mid-sagittal plane of the head therefore indicates the retinal location of the focus of expansion (FOE) resulting from translational optic flow. Head position was represented by the midpoint between the eyes, and calculated based on the three head markers. Head velocity was determined by the time-derivative of 3D head position.

Gaze indicates where the bird's head is 'facing', defined as the direction of a head-fixed vector in the mid-sagittal head plane and 30 degrees above the line running through the center of the head and the bill-tip (Fig. 4_2A). Gaze lies within the plane formed by the lateral canals of

the vestibular systems, which are held close to horizontal during level flight (Erichsen *et al*., 1989).

Angular head saccades were identified objectively whenever the angular speed of the head surpassed the propagated spatial (1 mm) and temporal (0.04 μs) measuring errors. The spatial measuring error was based on the average deviation of the measured length of an object from its known size, whereas the temporal measuring error was obtained from Photron USA Inc. Saccade duration was measured over the period during which gaze changed outside of the noise level with respect to the phases of head stabilization. However, saccades started before and stopped after gaze changed outside of the noise level on either side of saccades. Therefore, to obtain a more accurate saccade duration, we added an average-based period of gaze change within the noise level at the start and end of saccades.

Estimates of both visual and cervical proprioceptive feedback were tested as predictors of body rotations. FOE offset, the angle between the head velocity vector and the mid-sagittal plane of the head, represented visual feedback (Fig. 4_2A). Head offset, the angle between the instantaneous head orientation and the straight flight head orientation, both relative to the body, represented cervical proprioceptive feedback (Fig. 4_2B). FOE offset and head offset were measured at the end of a saccade, or, for wingbeat cycles without saccades, at the average phase of the end of a saccade, which was 34% into the upstroke (Fig. 4_5A).

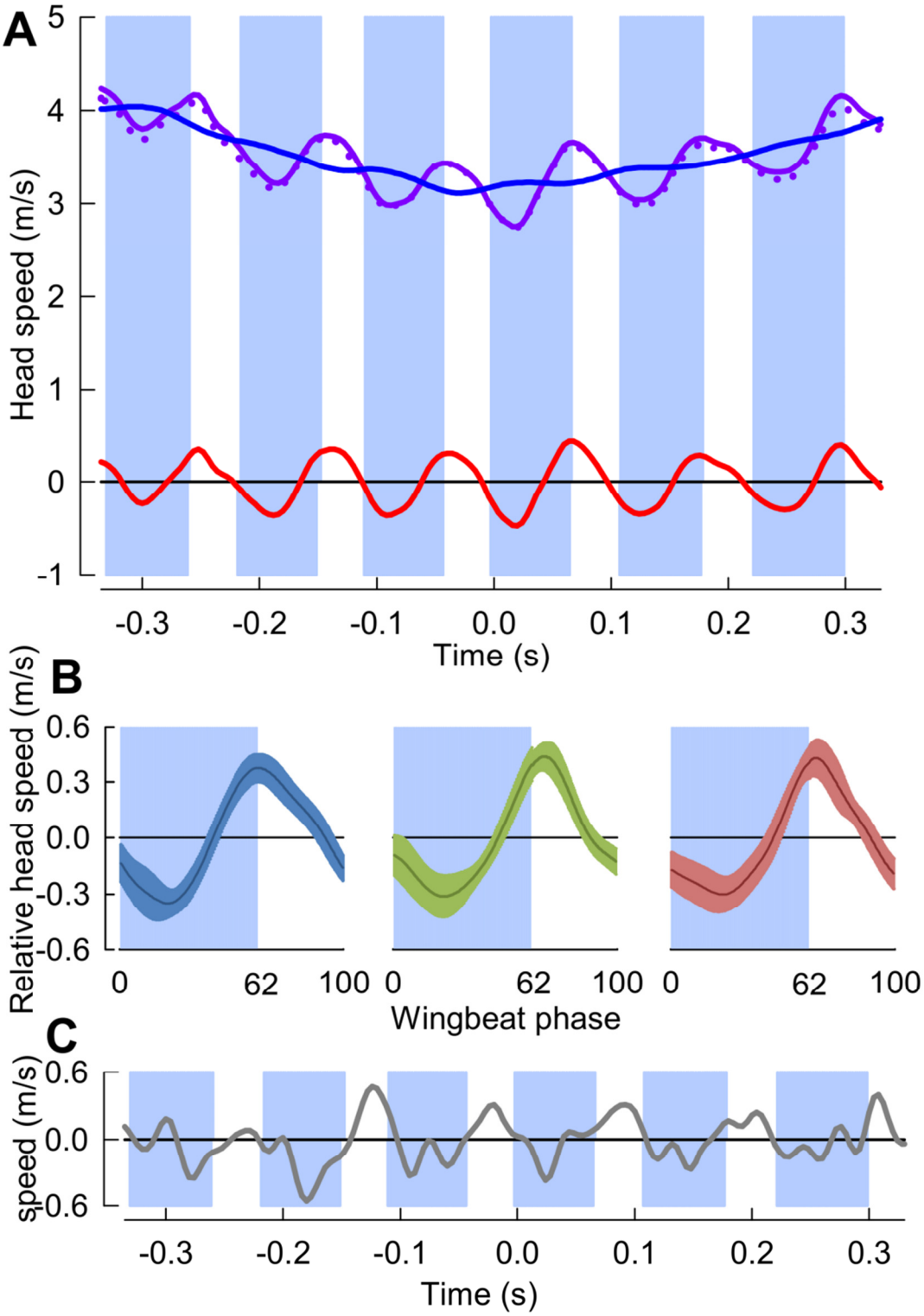
A
Head speed (m/s)
5
4
3
2
1
0
-1
-0.3
-0.2
-0.1
0.0
0.1
0.2
0.3
Time (s)
B
Relative head speed (m/s)
0.6
0.3
0.0
-0.3
-0.6
0
62
100
Wingbeat phase
C
speed (m/s)
0.6
0.0
-0.6
-0.3
-0.2
-0.1
0.0
0.1
0.2
0.3
Time (s)

Figure 4_3.

Figure 4_3 (Continued). Head speed fluctuates phasically throughout aerial turns. (A) Head speed (solid purple trace), and its horizontal component (dotted purple trace), fluctuate throughout a representative turn. Downstroke periods (blue shading) are defined relative to the center of the turn (time = 0 s). Subtraction of the running-average (blue trace) from the instantaneous head speed gives the relative head speed (red trace). (B) Relative head speeds (mean ± sd) normalized to wingbeat period for three individuals (blue, n=18; green n=16; and red n=16). Head speed peaks immediately after the down-upstroke transition (4 ± 6 ms). (C) Head speed relative to the body (grey trace) throughout the same turn shows no clear pattern, indicating an absence of mechanical coupling between the head and body.

These estimates of sensory feedback were compared to two functionally separate body rotation components, based on previous findings that pigeons produce aerodynamic forces in a uniform direction relative to their body during turns: 1) A*erodynamic roll / pitch*: body rotations that redirect the aerodynamic force, analogous to helicopter roll and pitch, and 2) *aerodynamic yaw*: body reorientations about the direction of the aerodynamic force, analogous to helicopter yaw (Chapter 2).

The analyses were based on a total of forty-nine wingbeat cycles from nine turns, both left and right, in three individuals. Unless noted otherwise, results were expressed as mean± SD. Correlations were tested with standard least squares regression models with individual effect leverage (JMP, SAS Institute). To account for multiple comparisons (n=28) a Bonferroni corrected significance level of $p_c < 0.00179$ was used to identify statistically significant trends.

Results

The three pigeons flew through the 90° level turn in 5.5 ± 0.5 wingbeat cycles over a period of 0.63 ± 0.06 s. Throughout the turns, the 3D translational speed of the head fluctuated with an amplitude of 0.79 ± 0.14 m/s, consistently peaking 4 ± 6 ms following the down-upstroke transition (Fig 3 A,B). Fluctuations in head speed were predominantly horizontal (99.4 ± 0.6%), for head speeds ranging from 2.2 to 4.5 m/s. Head speeds relative to the body were comparable in magnitude to overall head speed fluctuations and exhibited no consistent relation to the wingbeat cycle (Fig. 4_3C).

Although translational head speed fluctuated continuously, pigeons displayed distinct periods of 3D angular head stabilization, despite continuous rotations of the body (Fig. 4_4A, B). Periods of angular head stabilization were interrupted by brief head repositioning movements lasting 25.9 ± 5.8 % of the wingbeat period in nearly two-thirds (63 ± 7 %) of the turning wingbeats. These angular head saccades were characterized by step-wise changes in horizontal gaze (Fig. 4_3C). All head saccades were directed away from the flight trajectory and into the turn. Peaks in speed of gaze change occurred near the downstroke-upstroke transition, immediately following peaks in translational head speed (Fig. 4_4D, 4_5A). Identification of head saccades was based on the speed of horizontal gaze change surpassing the propagated kinematics measuring error (Fig. 4_4D). Saccades varied in magnitude (5-30 deg), duration (14-39 ms), and speed (400-1200 deg/s). Larger saccades occurred earlier in the wingbeat cycle ($p<0.0001$) (Fig 5B), lasted longer ($p<0.0001$), and reached higher peak speeds ($p<0.0001$) (Fig. 4_5C).

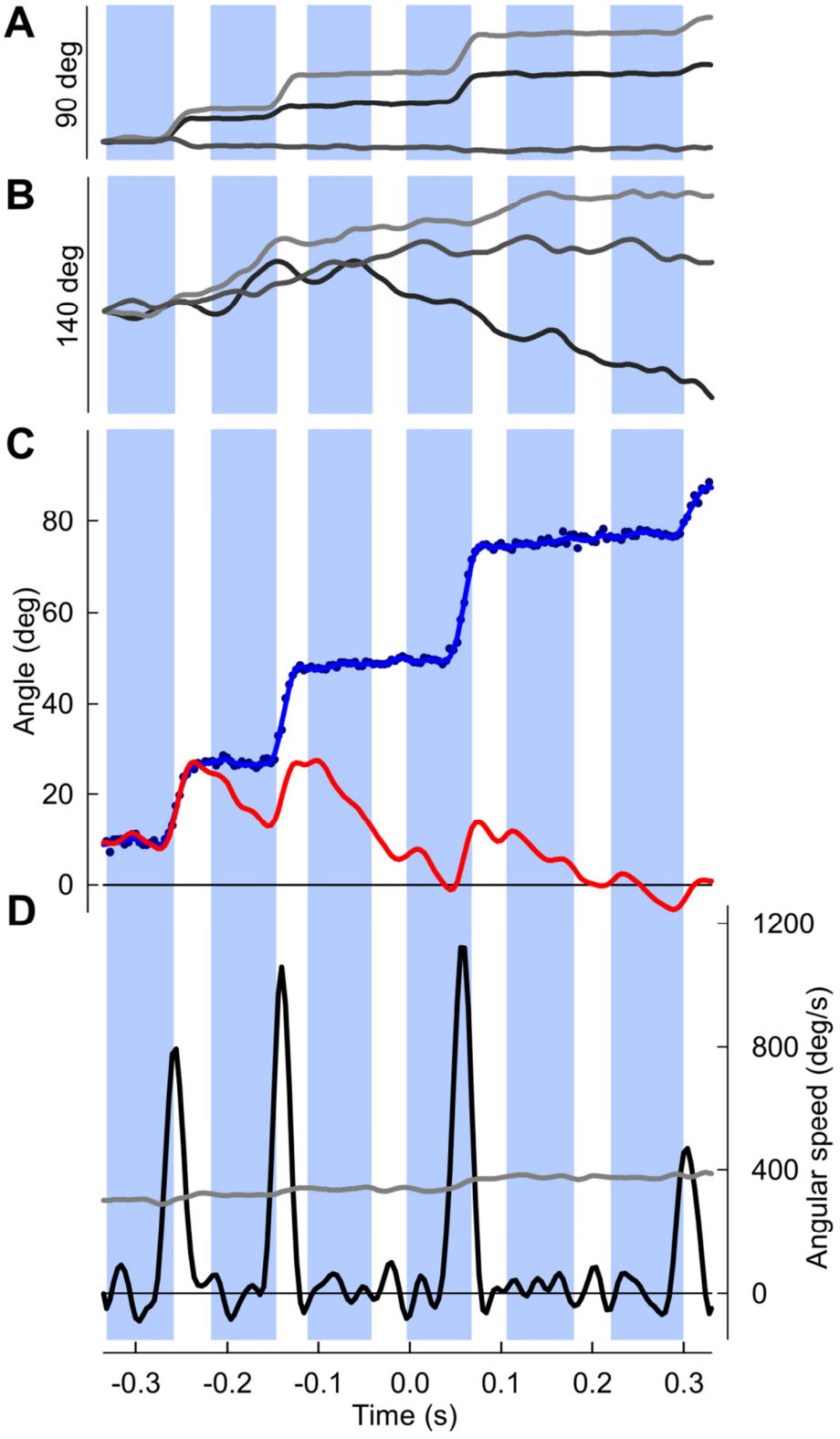
A
90 deg
B
140 deg
C
Angle (deg)
80
60
40
20
0
D
1200
800
400
0
Angular speed (deg/s)
-0.3
-0.2
-0.1
0.0
0.1
0.2
0.3
Time (s)

Figure 4_4.

Figure 4_4 (Continued). Angular head stabilization and saccades during aerial turns. (A) Rotations about the roll, pitch, and yaw axes of the head (dark, medium and light grey traces, with positive roll, pitch, and yaw defined as right ear down, bill up, and bill right, respectively). Downstroke is indicated by blue shading. (B) Roll, pitch and yaw of the body, defined as in (A). (C) Unfiltered (blue dots) and low-pass filtered (blue trace) horizontal component of gaze (head direction). Gaze changes are directed into the turn (positive). The focus of expansion (FOE) offset (red trace) defined as the angle between the head velocity and the mid-sagittal plane of the head peaks following successive saccades. (D) Peaks in horizontal head angular speed (black trace, n=4) that surpass the measuring error (grey trace) indicate angular head saccades.

Saccade amplitude was modulated 1.99 times more strongly by speed than by duration. Saccades were predominantly horizontal (slope between 3D saccade amplitude and its horizontal component = 0.995, N=3; Fig. 4_5C), consistent with the level nature of the flight turns that were studied.

Estimates of visual and cervical proprioceptive inputs were compared to body rotations during turning flight. These body rotations, representing behavioral outputs, were calculated discretely over whole wingbeat cycles to integrate over finer scale body motions that occur within wingbeats, but which are unrelated to net changes in body orientation (Fig. 4_4B, (Warrick & Dial, 1998; Hedrick & Biewener, 2007)). Based on prior analysis of body rotations that underlie changes in flight trajectory versus body orientation (Chapter 2), two orthogonal body rotation components were calculated: (i) *aerodynamic roll/pitch*, which changes the direction of the aerodynamic force and (ii) *aerodynamic yaw*, which reorients the body about the aerodynamic force but does not affect flight trajectory (Fig. 4_6).

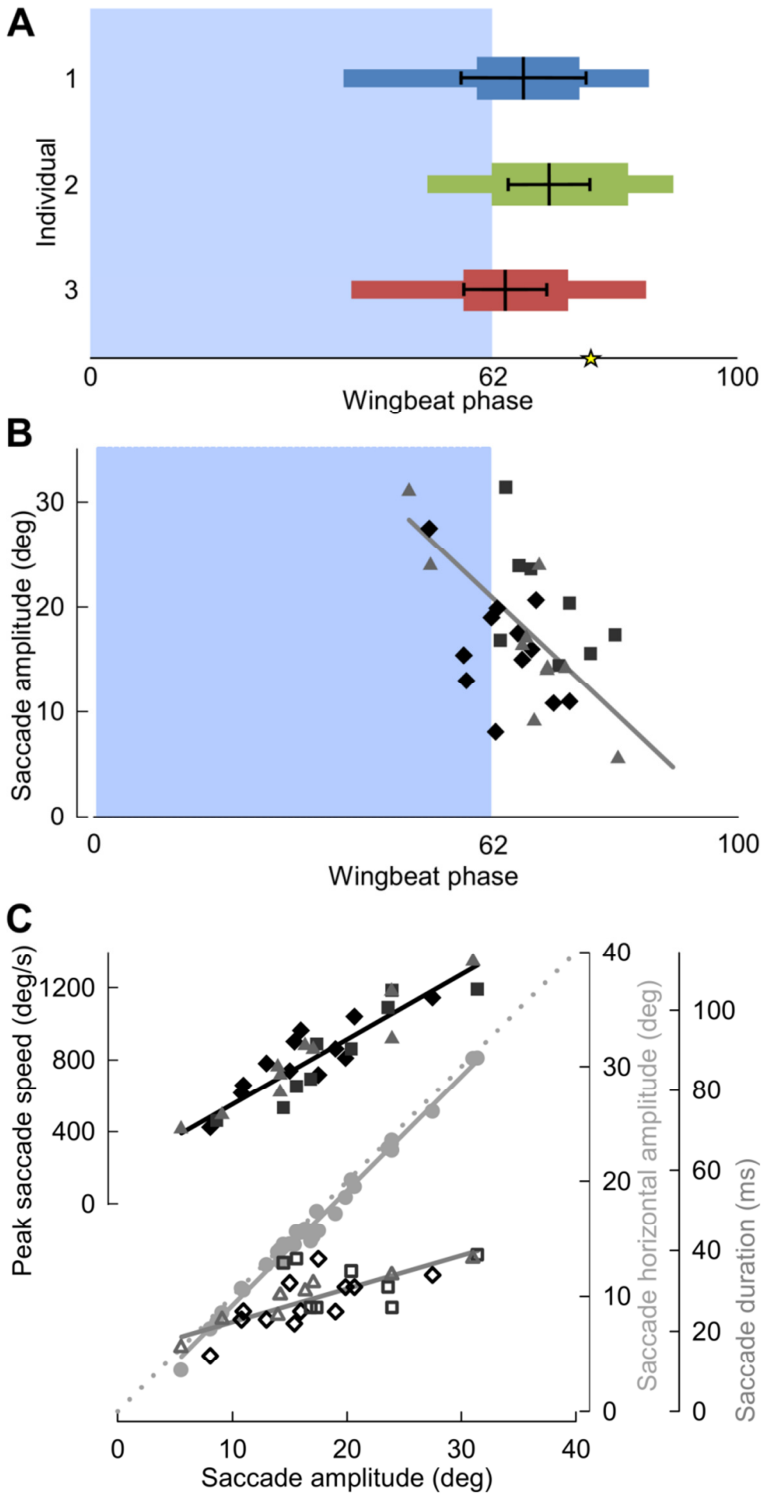
A
Individual
1
2
3
0
62
100
Wingbeat phase
B
Saccade amplitude (deg)
30
20
10
0
0
62
100
Wingbeat phase
C
Peak saccade speed (deg/s)
1200
800
400
0
40
30
20
10
0
Saccade horizontal amplitude (deg)
100
80
60
40
20
0
Saccade duration (ms)
0
10
20
30
40
Saccade amplitude (deg)

Figure 4_5.

Figure 4_5 (Continued). Characteristics of angular head saccades in turning pigeons. (A) The timing of angular head saccades normalized to wingbeat duration, for three individuals (blue, green and red). Narrow colored bars indicate the ranges of saccade start and end phases, whereas wide colored bars indicate average saccade duration, measured from average saccade start to end phases. Thick black lines indicate the mean ± sd phase of the saccade angular speed peaks. The asterisk indicates the average end phase of a saccade. (B) Saccade amplitude as a function of wingbeat phase, with symbols indicating three different individuals. Larger saccades occur earlier in the wingbeat cycle. (B and C) Solid lines represent standard least squares regressions, corrected for individual effects ($p<0.001$ for all four trends). (C) Both saccade speed and saccade duration (filled and unfilled symbols, respectively) increase with saccade amplitude. Saccade peak speed and duration trend lines indicate their relative contributions to saccade amplitude. Their scaling relative proportionality (dotted grey line) based on constant average duration and speed shows that saccade amplitude is modulated 1.99 times more strongly by speed than by duration. Saccades are predominantly horizontal, as indicated by a slope of 0.995 between 3D saccade amplitude and its horizontal component (grey circles).

Whereas FOE offset resulting from a saccade positively predicted subsequent aerodynamic roll / pitch body rotations, head offset positively predicted subsequent aerodynamic yaw body rotations (Fig. 4_7). However, associations of FOE offset and head offset with aerodynamic body rotations were of opposite sign and occurred at different relatively timed wingbeat cycles. FOE offset was associated with aerodynamic roll/pitch over the wingbeat cycle immediately following a saccade (Fig. 4_7A, B), whereas head offset was associated with aerodynamic yaw, but phase delayed over the second full wingbeat cycle following the saccade (Fig. 4_7A, C). Neither estimate of sensory input predicted 3D body rotations (Fig. 4_7).

Notably, changes in angular horizontal head velocity direction that occurred over the subsequent 1.5 wingbeat cycles were also strongly predicted by FOE offset (Fig. 4_8).

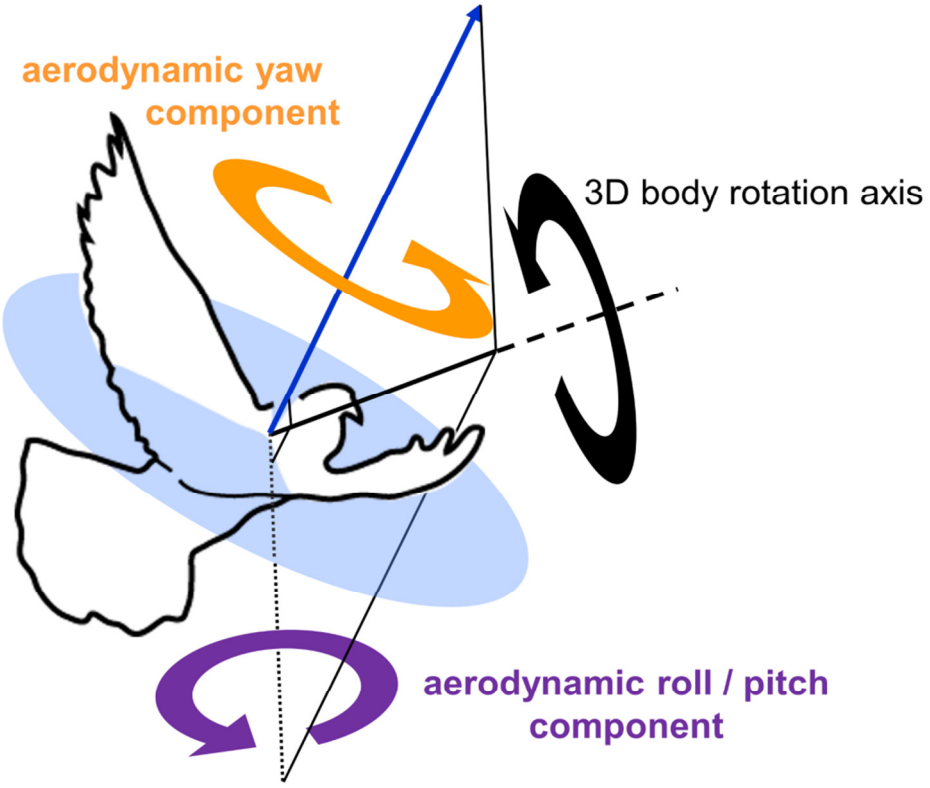

Figure 4_6. Two functionally separate body rotation components of a turning pigeon. Outline of a pigeon, superimposed with the average direction of aerodynamic force production during the downstroke (blue arrow, after Ros *et al.* 2011). An exemplary 3D body rotation is represented by a single axis of rotation (thick black solid line with dashed extension, and black circular arrow). The 3D rotation is decomposed into two perpendicular components: aerodynamic roll/pitch (ARP, purple circular arrow), and aerodynamic yaw (AY, orange circular arrow). Note that the axis describing ARP lies within the circular blue plane, which is normal to the aerodynamic force. ARP is therefore the component of the body rotation that redirects the aerodynamic force, whereas AY represents re-orientation of the body about the aerodynamic force and, therefore, does not cause changes in flight trajectory.

Discussion

Throughout low-speed aerial turns pigeons stabilize angular motions of their head, despite continuous and independent oscillations of their body (Fig. 4_4A, B). For level turns, translational fluctuations in head speed are horizontal and peak in-phase with the wingbeat cycle near the ventral stroke transition (Fig. 4_3). Angular head saccades occur in nearly two-thirds of turning wingbeats (Fig. 4_4), allowing pigeons to stabilize their gaze during intervening periods. Angular head saccades are also nearly horizontal, being directed into the turn and away from the bird's flight trajectory. Saccade magnitude correlates with saccade timing and duration: larger saccades occur earlier in the wingbeat cycle, reach higher peak speeds and last slightly longer (Fig. 4_5). The focus of expansion (FOE) offset induced immediately after a saccade significantly predicts body rotations that underlie flight trajectory changes (Chapter 2) over the wingbeat cycle immediately following the head saccade, as well as the resulting change in flight trajectory over the subsequent wingbeat cycle (Fig. 4_7, 4_8). Conversely, the head offset induced by neck bending immediately after a saccade predicts changes in body orientation over the subsequent 1.5 wingbeat cycles that realign the bird's body with the new flight trajectory, but which do not affect the flight trajectory itself (Chapter 2) (Fig. 4_7).

The predominantly horizontal fluctuations in head speed likely serve a visual function. These translational head movement patterns during low-speed turns are similar to the head bobbing observed in pigeons prior to landing (Davies & Green, 1988) and reminiscent of the head bobbing observed during walking in many bird species (Frost, 1978), both of which are thought to serve a primarily visual function. Consequently, translational head speed peaks that

occur during turning flight (Fig. 4_3) may also serve to improve parallax-based perception of speed and depth by either increasing translational optic flow, or by dishabituating ganglion cells involved in motion sensing (Frost & DiFranco, 1976). In addition, head speed troughs may serve to reduce motion blur and facilitate detection of independently moving objects (Fig. 4_3; (Land, 1999; Frost & DiFranco, 1976; Necker, 2007; Frost, 2009)). Furthermore, the consistent phase relationships of head speed fluctuations (Fig. 4_3) and angular saccades (Fig. 4_4) with respect to the wingbeat cycle suggest that head motions and gaze changes are likely coupled to the central pattern generator network driving the flapping wings (Grillner, 2006).

Importantly, the pigeon's head stabilization strategy isolates its head from body motions (Fig. 4_3C; 4_4A, B (Warrick *et al*., 2002; Videler *et al.* 1983)). As a result head and body movements, both translational and angular, are uncorrelated, illustrating the absence of mechanical coupling (Fig. 4_3C; 4_4A, B). The transmission of strong, impulsive aerodynamic and inertial flight forces from the wings to the body suggests that head stabilization is actively mediated through cervical muscles controlled by optomotor and vestibulocollic reflexes (Gioanni, 1988).

One advantage of fixating gaze though head orientation, as birds do, rather than by optical nystagmus of the eyes, as in humans and other animals (Land, 1999), is that a stationary head may enable cervical sensors to provide information about the orientation of the body relative to the surroundings. Fast and robust control could be achieved by using cervical feedback as a single control input to steering muscles, as suggested by Groebbels (1929), effectively integrating visual and vestibular information. Alternatively, cervical feedback could

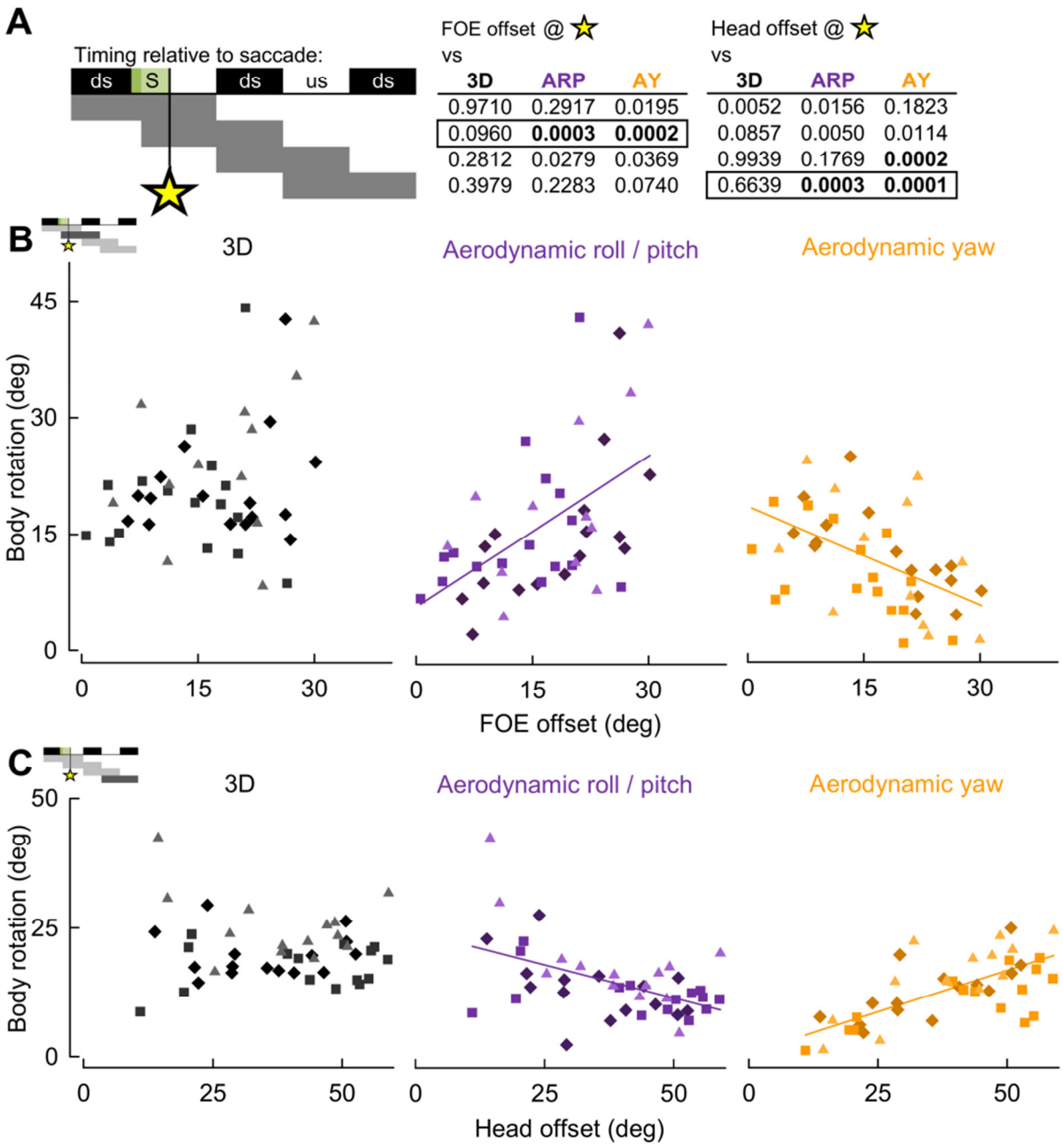
A
Timing relative to saccade:
ds
S
ds
us
ds
FOE offset @ ☆
vs
3D ARP AY
0.9710 0.2917 0.0195
0.0960 0.0003 0.0002
0.2812 0.0279 0.0369
0.3979 0.2283 0.0740
Head offset @ ☆
vs
3D ARP AY
0.0052 0.0156 0.1823
0.0857 0.0050 0.0114
0.9939 0.1769 0.0002
0.6639 0.0003 0.0001
B
3D
Aerodynamic roll / pitch
Aerodynamic yaw
Body rotation (deg)
45
30
15
0
0
15
30
FOE offset (deg)
C
3D
Aerodynamic roll / pitch
Aerodynamic yaw
Body rotation (deg)
50
25
0
0
25
50
Head offset (deg)

Figure 4_7.

Figure 4_7 (Continued). Temporal correlations between potential sensory inputs and body rotations. (A) A representation of the relative timing between FOE and head offset measured at the end of saccades (green area, S), and subsequent body rotations. Downstroke (ds) and upstroke (us) timing is shown in black and white, respectively. Grey rectangles indicate periods over which body rotations were calculated, relative to each saccade (four rows for four discrete progressive regressions). The asterisk indicates the end of the saccade. P-values for least squares regression analyses, corrected for individual effects, are shown in upper right table for correlations with 3D, aerodynamic roll/pitch (ARP) and aerodynamic yaw (AY) body rotations. Statistical significance was corrected for multiple comparisons (p_c= 0.00179). Regressions for outlined p-values are plotted in (B) and (C). (B) FOE offset, the angle between head velocity and the mid-sagittal plane of the head, is positively associated with ARP over the wingbeat cycle immediately following saccades. AY over the same relative wingbeat cycle is negatively associated with FOE offset. (C) Head offset, the degree of neck bending and/or twisting, is negatively associated with aerodynamic roll/pitch over the subsequent wingbeat cycle. AY over the same relative wingbeat cycle is positively predicted by head offset. (B) and (C) Significant regressions are represented by solid purple and orange lines.

be used to transform steering directions relative to the head into steering directions relative to the body. Such a coordinate system transformation from the head to the body is necessary because external perception occurs within the head (eyes and vestibular systems), whereas steering motor output occurs within the body (wings and tail). Therefore, controlling head motion to stabilize the bird's visual field could not only facilitate extraction of important motion cues, but also offer a mechanism for controlling body and wing movements.

Our results show for the first time that offsets in visual feedback are primarily determined by head saccades during turning flight in pigeons (Fig. 4_4). Because head saccades are consistently directed into the turn and away from the flight trajectory, the saccades generally lead to increases in focus of expansion offset. Although saccades do not consistently start from a zero FOE offset and not all of head rotation necessarily results in FOE offset, the majority of FOE offset is determined by head saccade movement. The pattern of angular gaze stabilization

observed here is similar to that observed in pigeons held fixed while stimulated with an artificial visual surround under simulated flight conditions (Gioanni & Sansonetti, 1999), as well as in freely flying blowflies (Schilstra & Van Hateren, 1998). Whereas pigeons mediate angular gaze stabilization largely through head movements, blowflies additionally use their whole body to stabilize gaze.

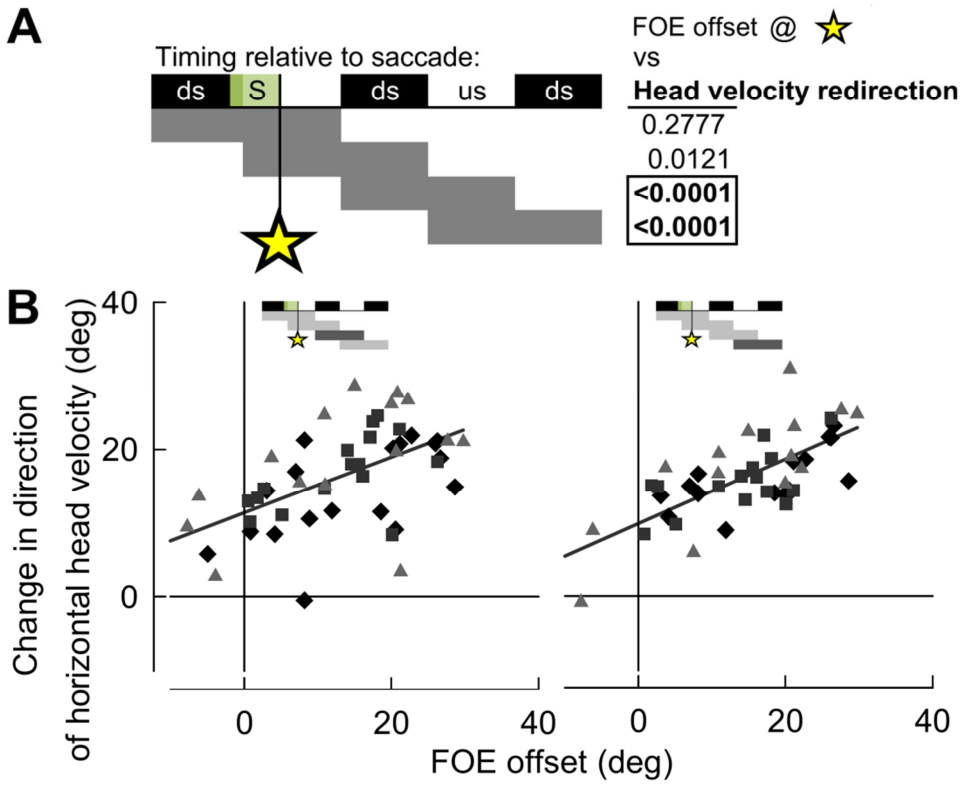

Figure 4_8. FOE offset predicts subsequent changes in flight velocity. (A) Representation of the relative timing between FOE offset at the end of a saccade (green area, S) and changes in direction of horizontal head velocity. Grey rectangles indicate periods over which changes in head velocity direction where calculated relative to each saccade. Regressions for highlighted significant p-values are plotted in (B). (B) FOE offset is positively associated with changes in horizontal velocity direction over the subsequent 1.5 wingbeat cycles following a saccade.

FOE offset predicts subsequent aerodynamic roll/pitch motions of the pigeon, whereas head offset predicts subsequent aerodynamic yaw, yet neither predicts full 3D body rotations (Fig. 4_7). Based on our analysis of the potential sensory inputs that guide turning flight in pigeons, these key relationships indicate that flight trajectory and flight orientation are individually, yet concurrently, controlled through visual and cervical afferent inputs, respectively. Further, the timing of aerodynamic roll/pitch body rotations predicted by FOE offset over the wingbeat cycle immediately following a head saccade suggests that they may be sufficiently delayed to be controlled through a dedicated visuomotor pathway. Recordings of *in vivo* muscle activation referenced to wing stroke timing (Ros *et al*. in prep.) show that the onset of pectoralis muscle activation powering the downstroke occurs 23 ± 9 ms after the end of a saccade when FOE offset is maximal. At present, temporal delays involved in optic flow processing via the accessory optic system in birds are unknown (Arends & Zeigler, 1991; Frost *et al.*, 1990). Thus, additional study of visuomotor timing is needed to determine whether the delay between head saccade and aerodynamic roll/pitch is sufficient for FOE offset control of flight muscles.

FOE offset resulting from angular head saccades also predicts changes in flight trajectory over the subsequent wingbeat cycle (Fig. 4_8). The temporal delay between the timing of aerodynamic roll/pitch rotations and of actual changes in flight trajectory indicates that pigeons first need to change the direction of aerodynamic force production before substantially changing the flight trajectory. Therefore, this temporal delay indicates a significant mechanical component in the total delay between visual input and desired mechanical output.

The correlation of head offset with subsequent aerodynamic yaw body rotations (Fig. 4_7) similarly suggests that head offset may control flight re-orientation of the bird's body after it has changed its flight trajectory. Thus, in-flight head stabilization may indirectly couple visual cues that guide changes in flight trajectory through aerodynamic roll/pitch, with afferent cervical feedback that subsequently guides body re-orientation through aerodynamic yaw (Chapter 2). The possible role of cervical afferents in controlling flight orientation is consistent with wing muscle activity in response to neck bending in pigeons under simulated flight conditions (Bilo & Bilo, 1978).

Our kinematic analysis of head, body and wing motions indicates that pigeons use visual information to guide their flight trajectory and use head deviations relative to their body to control body re-orientation during turning flight. Future work is needed to test the predictions that emerge from these kinematic patterns and the sensorimotor control mechanisms they suggest. Nevertheless, our results suggest that visual and proprioceptive offsets are used as steering inputs for turning flight in birds as well as insects, providing new insight into widespread flight control principles that can inspire design of robust controllers for autonomous aerial vehicles.

Acknowledgments

We thank P.A. Ramirez for care of the animals, Prof. S.A. Combes for use of high speed cameras, Profs. A.N. Ahn and B.P. Ölveczky for comments on the manuscript, Drs. A.M. Berg Robertson and M.E. de Boef Miara for help with experiments, Profs. D.V. Lee and R.L. Tedrake for general suggestions, and R.J. Ros for additional assistance. This study was funded by grants from the National Science Foundation (IOS-0744056) and the Office of Naval Research (N0014-10-1-0951) to AAB.

CHAPTER 5

Ruby-throated hummingbirds use optic flow in flight stabilization

Hummingbirds go with the flow

Ivo G. Ros, Andrew A. Biewener

Summary

Within birds, hummingbirds excel at hovering, being the only group able to sustain aerobic hovering and feed from swaying flowers while doing so. Flight stabilization, a key component of flight control, requires measurement of self-motion as a negative feedback signal. Vision is the dominant sense used for gaze stabilization in birds and relays information about self-motion through optic flow, or movement of the visual panorama across the retina. Whether generated through actual motion of a bird or through projection of moving images, if vision is used to stabilize flight, birds should reduce optic flow through corrective flight maneuvers. To test this hypothesis, we present freely hovering ruby-throated hummingbirds with projected virtual panoramas, or surrounds, rotated in different directions and at different speeds. The birds counter these illusory self-motions by rotating their head and body, and by flying with the surround. The hummingbirds apparently separate rotational from translational optic flow and use both these visual cues to stabilize their vision and control hovering flight.

Introduction

Flight control is crucial in ecologically relevant flight behaviors such as predator-prey interactions, courtship, and foraging in dynamically and geometrically complex environments (Dudley, 2002). An underlying component of flight control is the detection of self-motion as a control-input for flight stabilization.

Birds fly in three-dimensionally complex environments and can detect self-motion using various sensory modalities, most notably the visual, vestibular and somatosensory systems (Warren & Wertheim, 1990). In cases of conflicting signals, the visual system overrules other modalities (Friedman, 1975). The visual cue indicating self-motion is optic flow: the resulting movement of the panorama, or visual surround, across the retinae (Simpson, 1984). Optic flow resulting from rotations (angular movement) and translations (movement along a straight line) are processed separately by the avian visual system (Wylie &Frost, 1990).

Birds use optic flow to guide various sensorimotor behaviors. Budgerigars choose flight paths that balance optic flow between the left and right sides and reduce their flight speed to maintain the optic flow rate below a possible internal limit (Bhagavatula *et al*., 2011). Optic flow parameters are also used by hawks and pigeons to land, and by hummingbirds to approach feeders (Davies & Green, 1990; Lee *et al.*, 1993; Lee *et al*, 1991).

Optomotor responses, as observed in a variety of animals ranging from vertebrates to arthropods, serve to prevent rotation of the eyes, head and/or body (Simpson, 1984), resulting in gaze stabilization through active negation of optic flow (e.g. Collet & Land, 1975). Gaze

stabilization not only improves image resolution and the ability to detect relative object motion, but also facilitates the extraction of direction, speed and distance information (Land, 1999). The optomotor response in pigeons, in which the gaze is reflexively stabilized by moving the eyes and head in response to visual stimuli, is another example of the use of optic flow by birds (Bilo, 1992; Gioanni &Vidal, 2012).

Here, we test whether illusory visual sensations of self-motion in hummingbirds elicit corrective responses in flight speed and body orientation. By projecting moving images that result in a combination of rotational and translational optic flow under untethered flight conditions, we expect natural (closed-loop) behavioral response dynamics (see Gioanni &Vidal, 2012). In pigeons, certain wing and tail muscles react to rotational visual stimulation during simulated flight (Bilo, 1992), indicating that optic flow (in addition to gaze stabilization) is involved in flight control, much like in insects (*e.g.* Collet & Land, 1975). Following from these earlier studies, we hypothesize that hummingbirds will orient and fly to reduce perceived self-motion imposed by a rotating visual surround. Alternatively, the birds may only track the virtual surround through smooth head rotations following the visual surround until a fast saccade returns the head to its original orientation, without any change in body orientation or flight path. This null-hypothesis would predict that optic flow is merely used for vision stabilization, whereas orienting the body and flying with the virtual surround would indicate that optic flow also functions to control flight.

Materials and Methods

Five female ruby-throated hummingbirds, *Archilocus colubris*, were trapped, housed and studied at the Concord Field Station (Bedford, MA, USA) in accordance with protocols approved by Harvard University's Institutional Animal Care and Use Committee. Each bird was acclimatized within the experimental setup and subsequently studied during two 2-hour flight sessions.

To generate virtual surround rotations (VSR), four projectors (MW663, BenQ Corporation, Taipei, Taiwan) were positioned equidistantly around a 1.2 m inner diameter, vertically oriented, acrylic cylinder. The acrylic cylinder wall was coated for rear-projection and had black fabric extending above and below to eliminate extraneous visual cues (Fig.1). The birds were prevented from ascending beyond two-thirds of the cylinder height by an acrylic ceiling, supporting a 3 cc syringe with artificial nectar (Nekton GmbH, Pforzheim, Germany) at its center. A total of 32 equal-width vertical bars (alternating black and white) were projected synchronously at 120 Hz. Given the short photoreceptor response time expected of hummingbirds (Healey, 2013), we projected under low-light conditions to lower their critical fusion frequency (CFF). The projected images resulted in an illuminance of 38 lux at the center, and a contrast of 47 lux measured at the perimeter of the cylinder. The VSR was either held stationary or rotated horizontally in either direction at 62, 98 or 134 deg/s, resulting in seven experimental conditions. All quantified motions and directions were normalized to the VSR direction.

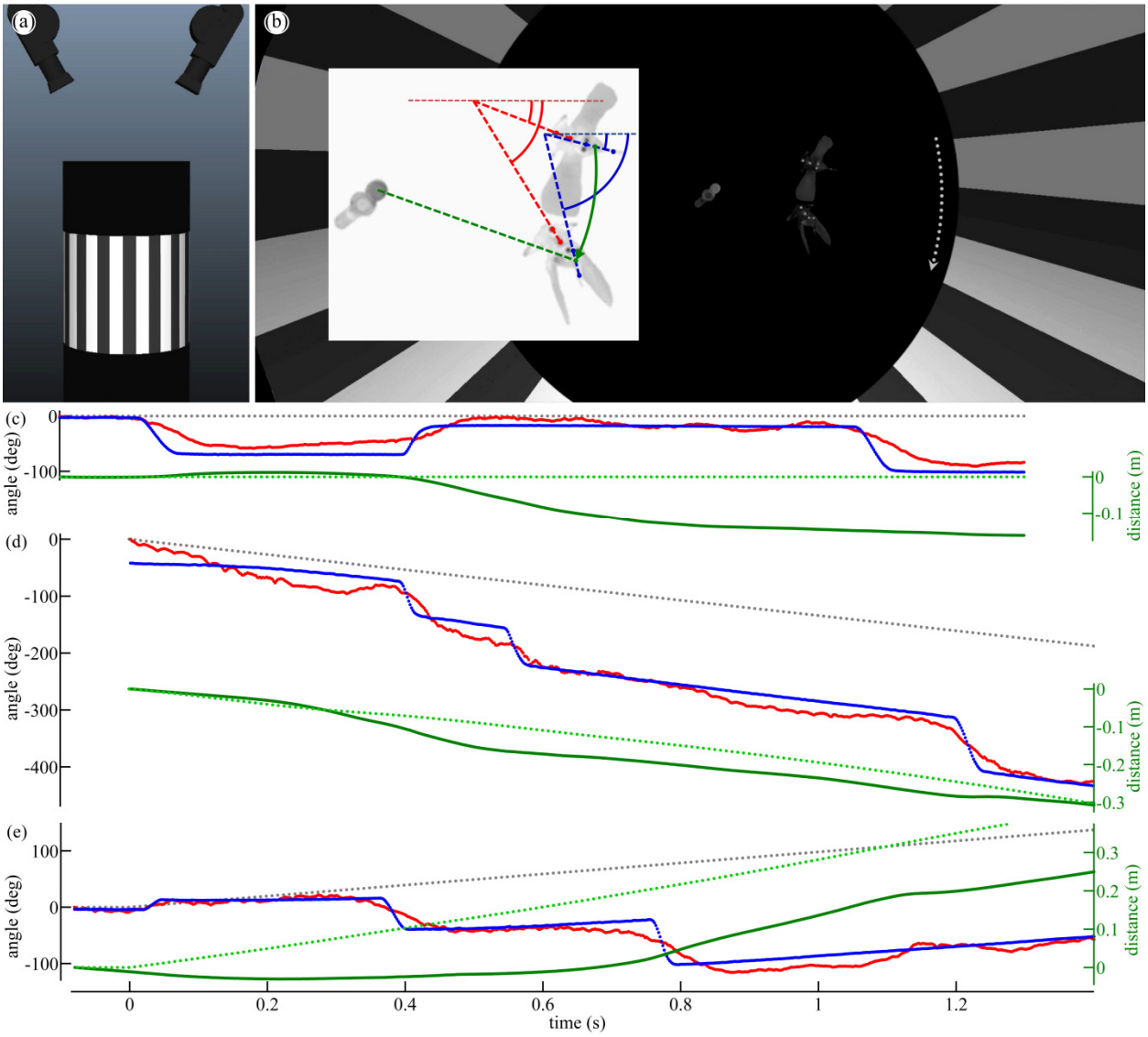

Figure 5 1. Free-flying hummingbirds track virtual surround rotations, negating apparent self-motion. (a, b) Two high-speed video cameras, black silhouettes, aimed at the center of a vertical, hollow cylinder record hummingbirds flying near a centrally suspended feeder. (b) Top view. The hummingbird rotates clockwise with the virtual surround (dotted grey arrow) and is depicted at two instances separated by 0.02 s. Inset (greyscale inverted): body orientation (red) and head orientation (blue), as well as circumferential flight distance (green), all within the horizontal plane, are referenced against arbitrary starting positions (corresponding darker dashed lines). (c-e) Representative trials at VSR speeds of 0 deg/s (c), -98 deg/s (d), and 134 deg/s (e), with the VSR projected at 120 Hz (grey trace). To completely negate translational optic flow, the hummingbirds must fly circumferentially (green dotted trace), depending on their radial position within the cylinder and the imposed VSR velocity.

The hummingbirds flew freely within the cylinder and were recorded with two FastCam 1024 PCI cameras (Photron USA Inc., San Diego, CA, USA) operating in synchrony at 500 Hz (Fig. 1a), for which sufficient illumination was provided by two 850 nm wavelength infra-red LED arrays, imperceptible to the hummingbirds.

Using thermoplastic and cyanoacrylate adhesives, four light-weight white polystyrene markers, 2-3 mm in diameter, were attached to each individual: on the head, two markers were positioned near the lateral ends of the coronal suture of the skull, and on the body, two markers were positioned dorsally over the spine, separated by 14 mm (Fig. 5_1b). Additionally, a 2 mm diameter dot of white non-toxic correction fluid was deposited on the bill. The maximum mass added to a bird was 0.04g, or 1% of the body mass.

Using the high speed camera images and DLTdv5 (Hedrick, 2008) in Matlab (Mathworks Inc., Natick, MA), 3D positions of the markers were determined within a calibrated 0.2 m^3 volume at the center of the cylinder. Calculations were performed in Matlab using custom-written scripts. The circumferential component of flight velocity was calculated using a virtual head center marker. For both head and body, the azimuth, or angle between a global horizontal reference and the horizontal projection of a direction-vector based on marker positions is hereafter simply referred to as ‘orientation’ (Fig. 5_1b, inset).

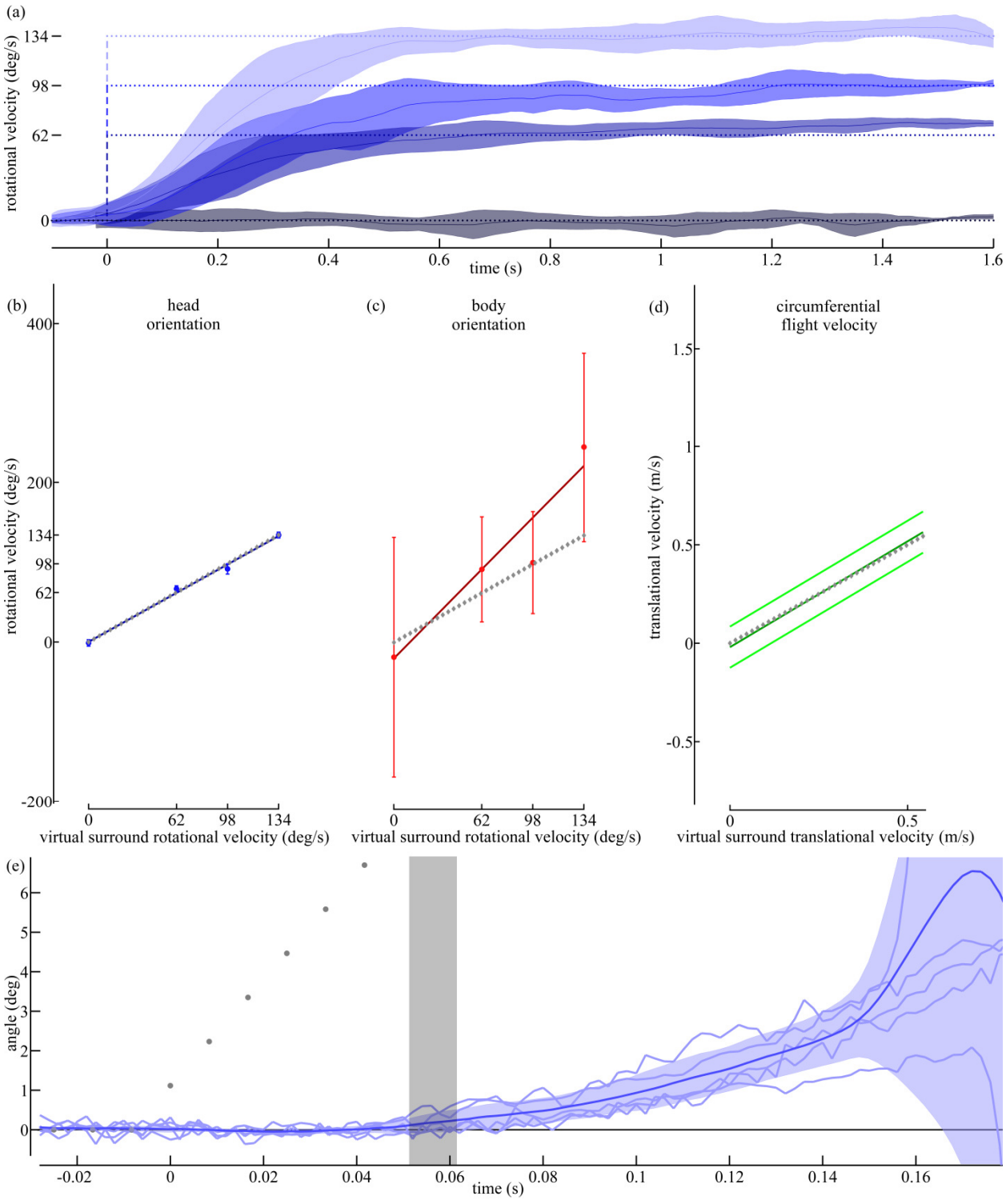
(a)
rotational velocity (deg/s)
134
98
62
0
0
0.2
0.4
0.6
time (s)
0.8
1
1.2
1.4
1.6
(b)
head
orientation
400
200
134
98
62
0
-200
rotational velocity (deg/s)
0
62
98
134
virtual surround rotational velocity (deg/s)
(c)
body
orientation
0
62
98
134
virtual surround rotational velocity (deg/s)
(d)
circumferential
flight velocity
1.5
1
0.5
0
-0.5
translational velocity (m/s)
0
0.5
virtual surround translational velocity (m/s)
(e)
angle (deg)
6
5
4
3
2
1
0
-0.02
0
0.02
0.04
0.06
time (s)
0.08
0.1
0.12
0.14
0.16

Figure 5_2.

Figure 5_2 (Continued). Rotational velocities of the head and body, and translational flight velocities match projected virtual surround speeds. (a) Head orientation velocity, averaged across individuals (solid traces ± shading (SD)), begins matching imposed VSR speed (dotted traces) approximately 0.5 seconds following VSR onset (t = 0 s), for all three VSR speeds. Note that head saccades are omitted to illustrate tracking during the slow phases. (b-d) Between 0.5 s to 1.5 s after VSR onset, head (blue) and body (red) orientation velocities, as well as circumferential flight velocities (green), correlate with corresponding VSR velocities (multiple least squares regressions with individual effect leverages (solid dark prediction lines; $p<0.001$ for all three variables), although variation in body orientation tracking (c) is considerably greater than tracking of head orientation (b) to the virtual surround. Means per VSR speed (dark colors) ± SD (light error bars and light green traces) illustrate VSR tracking (grey dashed lines). (e) Unfiltered head orientations of five individuals for a VSR speed of 134 deg/s (light blue lines), as well as the mean ± SD (dark blue trace and shaded area). Conservatively, the range of visuo-mechanical delay (grey shading) between stimulus onset and kinematic response was estimated from the instant when mean head orientation superseded one SD of the steady head orientation and the instant when the mean superseded twice that amount.

Results

The five hummingbirds hovered near the center of the cylinder with a wingbeat frequency of 42.7 ± 1.3 Hz. For each individual, the VSR was initiated randomly for a period between 0.8 s and 1.8 s for each non-zero surround speed condition. During stationary surround trials, voluntary fast turns of the head, or head saccades, alternated with periods of rotational head stabilization (Fig. 5_1c). During the non-zero VSR trials (± 62, 98 and 134 deg/s), fast phases (saccades) alternated with slow phases of rotational head motion (Fig. 5_1d, e). During the slow phases, the head rotated in the same direction as the VSR (Fig. 5_1c-e). Furthermore, after approximately 0.5 s following VSR onset, the speed of the slow phases matched that of the VSR, differing less than the propagated measuring error (26 deg/s for the three-wingbeat running-average measure of head orientation velocity) (Fig. 5_2a). Between 0.5 to 1.5 s after VSR onset,

head orientation velocity correlated with the projected VSR speed (adjusted $R^2 = 0.98$; $p<0.001$; multiple least-squares linear regression with individual effect leverage; Fig. 5_2b).

Among the 81 head saccades at non-zero VSR speeds, the hummingbirds tended to saccade in the direction of the projected rotations, making 12.2 ± 5.5 (individual mean ± SD) saccades with the VSR direction and 4 ± 3 saccades against (*e.g.* Fig. 5_1e) (two-sample t-test $P < 0.05$).

Fluctuations in body orientation were more continuous, but generally tracked low-frequency changes in head orientation (Fig. 5_1c-e). VSR speed during the period 0.5 to 1.5 s after stimulus onset predicted body orientation velocity ($R^2 = 0.17$; $P < 0.001$; Fig. 5_2b), though not as strongly as head orientation. When both slow and fast phases of head orientation velocity were included (and temporally corrected for a cross-correlation lag of -0.020 ± 0.002 s), the correlation with body orientation velocity was even stronger ($R^2 = 0.40$; $P < 0.001$). Circumferential flight velocity of the hummingbirds followed similar trends (Fig. 5_1c-e) and was correlated with the circumferential VSR speed corrected for the bird's radial position ($R^2 = 0.53$; $P < 0.001$).

Table 5_1. Measured velocities are all directed with the VSR (+).

tracking gain (measured/VSR) across individuals (N=5)	between individuals (mean ± SD)	within individuals (mean SD)
head orientation velocity (slow phases)	1.01 ± 0.04	0.10
body orientation velocity	1.48 ± 0.68	2.32
circumferential flight velocity	0.93 ± 0.22	0.66

Consistently, variation in all three variables between individuals (head and body orientation velocity, and circumferential flight velocity) as a function of VSR speed was smaller than the variation observed throughout a given trial within individuals (Fig. 5_2b-d; Table 5_1).

After VSR onset, a temporal latency of 52 to 62 ms was observed before changes in head orientation began tracking the motion of the virtual surround. This temporal latency range was estimated from the instants at which head orientation changed more than one and two standard deviations of head orientation during phases of head stabilization (Fig. 5_2e).

Discussion

When presented with a virtual visual surround rotated in different directions and at different speeds, hummingbirds counter this apparent self-motion by rotating their head and body, and by flying with the surround (video S1; Fig. 5_2b-d). These results suggest that hummingbirds separate rotational from translational optic flow and use both visual cues to stabilize hovering flight.

The greater variability of the body orientation tracking of the virtual surround compared with the slow phases of the head orientation (Table 5_1) likely has multiple causes. First, control of body orientation is not clearly compartmentalized between slow phases of stabilization relative to the surround and rapid saccades, as is control of head orientation. The higher degree of stabilization and more faithful tracking observed for head orientation may reflect greater control authority of the head by direct action of neck muscles, whereas rotational and translational stabilization of the body, with its larger mass and moment of inertia, depends on aerodynamic forces generated by the wings. Second, body rotations are likely needed to change flight speed in order to move with the surround (Chapter 1), as observed here. Third, spontaneous brief reorientations and changes in hovering position occur during normal hummingbird hovering (Greenewalt, 1960) and can, therefore, also be expected relative to a virtual rotating surround. Whereas slow phase head orientation tracking of VSR exhibits a gain of almost precisely 1.0, the higher tracking gain of body orientation relative to VSR (1.48, Table 5_1) likely reflects the cross-correlation of body orientation and head orientation that includes the fast phases (head saccades) in combination with the tendency of birds to saccade with the VSR.

Not surprisingly, all three flight variables related to virtual surround rotational tracking and underlying flight stabilization (head orientation velocity, body orientation velocity and circumferential flight speed) display a temporal latency relative to the instantaneous onset of the visual stimulus. This latency is likely comprised of multiple components, including visuomotor processing delay, muscle actuation electromechanical delay, and body and head rotational inertia. Furthermore, separate types of neurons involved in optic flow processing tuned to different magnitudes of optic flow may contribute to the temporal lag in establishing VSR tracking (see Crowder *et al.*, 2003). As observed here, the pure 'visuomechanical' delay between stimulus onset and the *initiation* of head rotations, was estimated to be between 52 and 62 ms (Fig 2e). Such a delay is longer than visuomechanical delays observed in insects, which are approximately 20 ms (e.g. Collet & Land, 1975), consistent with their smaller size and higher wingbeat frequencies (Healey, 2013).

Acknowledgements

We thank A.N. Ahn for comments on the manuscript, C.D. Williams, A. Mountcastle and S. Ravi for discussions, as well as Y. Hong for help with digitization. This study was funded by grants from NSF (IOS-0744056) and ONR (N0014-10-1-0951) to AAB.

BIBLIOGRAPHY

Aldridge HDJN (1986) Kinematics and aerodynamics of the Greater Horseshoe Bat (*Rhinolopus ferrumequinum*) in horizontal flight at various flight speeds. *J Exp Biol* 126, 479–497.

Alexander RM (1968) *Animal mechanics*. London: Sidgwick & Jackson.

Arbib MA, Érdi P & Szentágothai J (1997) *Neural Organization: Structure, Function, and Dynamics*, Cambridge, MA: Bradford Book/MIT.

Arends JJA & Zeigler HP (1991) Organization of the cerebellum in the pigeon (*Columba livia*): I. Corticonuclear and corticovestibular connections. *J Comp Neurol* 306: 221–224.

Azuma A (1992) *The Biokinetics of Flying and Swimming,* New York: Springer.

Baptista LF, Trail PW & Horblit HM (1997) Family Columbidae. Pp. 60–243 in del Hoyo J, A Elliot, & J Sargatal (eds.). *Handbook of the birds of the world. Vol.4: Sandgrouse to cuckoos.* Lynx Edicions, Barcelona.

Berg AM & Biewener AA (2010) Wing and body kinematics of takeoff and landing flight in the pigeon (*Columba livia*) *J Exp Biol* 213: 1651-1658.

Berg, van den, C & Rayner JMV (1995) The moment of inertia of bird wings and the inertial power requirement for flapping flight. *J Exp Biol* 198: 1655-1664.

Bhagavatula PS, Claudianos C, Ibbotson MR & Srinivasan MV (2011) Optic Flow Cues Guide Flight in Birds. *Curr Biol* 21: 1794-1799. (doi:10.1016/j.cub.2011.09.009)

Biewener AA, Corning WR & Tobalske BW (1998) *In vivo* pectoralis muscle force–length behavior during level flight in pigeons (*Columba livia*). *J Exp Biol* 201: 3293–3307.

Bilo D & Bilo A (1978) Wind stimuli control vestibular and optokinetic reflexes in the pigeon. *Naturwissenschaften* 65: 161–162.

Bilo D & Bilo A (1983) Neck flexion related activity of flight control muscles in the flow-stimulated pigeon. *J Comp Physiol* 153: 111-122.

Bilo, D (1994) Course control in flight. In MNO Davies and PR Green (eds.), *Perception and motor control in birds*, pp. 227–247. Springer-Verlag, Berlin.

Bilo, D (1992) Optocollic reflexes and neck flexion related activity of flight control muscles in the airflow-stimulated pigeon. In: Berthoz A, Graf W, Vidal PP (Eds). The head-neck sensory motor system. Oxford: Oxford University Press.

Bilo D, Bilo A, Muller M, Theis B & Wedekind F (1985) Neurophysiological-cybernetic analysis of course control in the pigeon. *Biona Report* 3: 445-477.

Bloch S, Rivaud S, Martinoya C (1984) Comparing frontal and lateral viewing in the pigeon. III. Different patterns of eye movements for binocular and monocular fixation. *Behav Brain Res* 13: 173–182. doi:10.1016/0166-4328(84)90147-5.

Blondeau J (1981) Aerodynamic capabilities of flies, as revealed by a new technique. *J Exp Biol* 92: 155-163.

Brown RHJ (1948) The flapping cycle of the pigeon. *J Exp Biol* 25: 322-333.

Brown RHJ (1963) The flight of birds. *Biol Rev* 38: 460-489.

Bundle MW & Dial KP (2003) Mechanics of wing-assisted incline running (WAIR). *J Exp Biol* 206: 4553-4564.

Collett TS & Land MF (1975) Visual control of flight behaviour in the hoverfly, *Syritta pipiens* L. *J Comp Physiol A* 99: 1–66.

Crandell KE & Tobalske BW (2011) Aerodynamics of tip-reversal upstroke in a revolving pigeon wing. *J Exp Biol* 214: 1867-1873.

Crowder NA, Dawson MR & Wylie DR **(**2003) Temporal frequency and velocity-like tuning in the pigeon accessory optic system. *J Neurophysiol* 90: 1829-1841.

David CT (1979) Optomotor control of speed and height by free-flying drosophila. *J Exp Biol* 82: 389-392.

Davies MNO, Green PR (1988) Head-bobbing during walking, running and flying: relative motion perception in the pigeon. *J Exp Biol* 138:71-91.

Davies MNO & Green PR (1990) Optic flow-field variable trigger landing in hawk but not in pigeons. *Naturwissenschaften* 77: 142-144.

Davies MNO & Green PR (1994) *Perception and motor control in birds*. Springer-Verlag, Berlin.

Dial KP, Goslow GE & Jenkins FA (1991) The functional anatomy of the shoulder in the European starling (*Sturnus vulgaris*). *J Morphol* 207: 327–344.

Dial KP, Jackson BE & Segre P (2008) A fundamental avian wing-stroke provides a new perspective on the evolution of flight. *Nature* 451: 985-990.

Dial KP (1992) Avian forelimb muscles and nonsteady flight: Can birds fly without using the muscles in their wings? *Auk* 109: 874–885.

Dial KP & Gatesy SM (1993) Neuromuscular control and kinematics of the wings and tail during maneuvering flight. *American Zoologist* 33: 5.

Dial KP, Goslow GE JR, Jenkins FA JR (1991) The functional anatomy of the shoulder in the European starling (*Sturnus vulgaris*). *Journal of Morphology* 207: 327-344. doi:10.1002/jmor.1052070309.

Dial KP, Kaplan SR, Goslow GE JR & Jenkins, FA JR (1988). A functional analysis of the primary upstroke and downstroke muscles in the domestic pigeon (*Columba livia*) during flight. *J Exp Biol* 134: 1–16.

Dudley R (2000) *The Biomechanics of Insect Flight. Form, Function, Evolution* (Princeton University Press, Princeton).

Dudley R (2002) Mechanisms and implications of animal flight maneuverability. *Integr Comp Biol* 42: 135 -140.

Dunlap K, Mowrer OH (1930) Head movements and eye functions of birds. *J Comp Psychol* II: 99-113.

Eckmeier D, Geurten BRH, Kress D, Mertes M, Kern R, Egelhaaf M, Bischof HJ (2008) Gaze strategy in the free flying zebra finch (*Taeniopygia guttata*). *PLOS ONE* 3: e3956. doi:10.1371/journal.pone.0003956.

Erichsen JT, Hodos W, Evinger C, Bessette BB, Phillips SJ (1989) Head orientation in pigeons: postural, locomotor and visual determinants. *Brain Behav Evol* 33: 268–278.

Friedman MB (1975) Visual control of head movements during avian locomotion. *Nature* 255: 67–69.

Frohlich C (1980) Physics of somersaulting and twisting. *Scientific American* 242(3): 155.

Frost BJ (1978) The optokinetic basis of head-bobbing in the pigeon. *J Exp Biol* 74: 187–195.

Frost BJ (2009) Bird head stabilization. *Curr Biol* 19: R315-316. doi:10.1016/j.cub.2009.02.002.

Frost BJ, DiFranco DE (1976) Motion characteristics of single units in the pigeon optic tectum. *Vision Res* 16: 1229-1234.

Frost BJ, Wylie DR, Wang YC (1990) The processing of object and self-motion in the tectofugal and accessory optic pathways of birds. *Vis Res* 30: 1677-1688.

Fry SN, Rohrseitz N, Straw AD, Dickinson MH (2009) Visual control of flight speed in Drosophila melanogaster. *J Exp Biol* 212: 1120–1130. doi:10.1242/jeb.020768.

Fry SN, Sayaman R, Dickinson MH (2003) The aerodynamics of free-flight maneuvers in *Drosophila*. *Science* 300: 495–498.

Gatesy SM & Baier DB (2010) The origin of the avian flight stroke: a kinematic and kinetic perspective. *Paleobiology* 31: 382-399.

Gatesy SM & KP Dial (1996) Tail muscle activity patterns in walking and flying pigeons (*Columba livia*). *J Exp Biol* 176: 55–76.

Gill FB (1995) *Ornithology*. New York: W. H. Freeman & Company.

Gioanni H (1988) Stabilizing gaze reflexes in the pigeon (*Columba livia*). I. Horizontal and vertical optokinetic eye (OKN) and head (OCR) reflexes. *Exp Brain Res* 69: 567–582.

Gioanni H, Sansonetti A (1999) Characteristics of slow and fast phases of the optocollic reflex (OCR) in head free pigeons (*Columba livia*). Influence of flight behaviour. *Eur J Neurosci* 11: 155–166.

Gioanni H & Vidal PP (2012) Possible cues driving context-specific adaptation of optocollic reflex in pigeons (*Columba livia*). *J Neurophysiol* 107: 704-717. doi: 10.1152/jn.00684.2011.

Goodman LJ (1965) The role of certain optomotor reactions in regulating stability in the rolling plane during flight in the desert locust, *Schistocerca gregaria*. *J Exp Biol* 42: 385-407.

Götz KG, Wandel U (1984) Optomotor control of force and light in *Drosophila* and *Musca*, II Covariance of lift and thrust in still air. *Biol Cyb* 51: 135–139.

Green PR (1998) Head Orientation and Trajectory of Locomotion during Jumping and Walking in Domestic Chicks. Brain Behav Evol 51:48-58. doi:10.1159/000006529.

Green PR, Davies MNO, Thorpe PH (1994) Head-bobbing and head orientation during landing flights of pigeons. *J Comp Phys A* 174: 249-256.

Greenewalt CH (1975) The Flight of Birds: The Significant Dimensions, Their Departure from the Requirements for Dimensional Similarity, and the Effect on Flight Aerodynamics of That Departure. *Transactions of the American Philosophical Society* 65: 1-67.

Greenewalt CH (1960) Hummingbirds. New York (NY): Doubleday.

Grillner S (2006) Biological pattern generation: The cellular and computational logic of networks in motion. *Neuron* 5211: 751–766.

Groebbels F (1926) Die Lage- und Bewegungsreflexe der Vögel. *Pflugers Arch* 214: 721-743.

Groebbels F (1929) Der Vogel als automatisch sich steuerndes Flugzeug. *Naturwissenschaften* 17: 890-893.

Healy K (2013) Metabolic rate and body size are linked with perception of temporal information, *Animal Behaviour* **x**, 1-12. doi: 10.1016/j.anbehav.2013.06.018.

Hedrick TL, Tobalske BW, Ros IG, Warrick DR & Biewener AA (2012) Morphological and kinematic basis of the hummingbird flight stroke: scaling of flight muscle transmission ratio. *Proceedings of the Royal Society B: Biological Sciences*, 279(1735): 1986-1992. doi: 10.1098/rspb.2011.2238.

Hedrick TL & Biewener AA (2007) Low speed maneuvering flight of the rose-breasted cockatoo (*Eolophus roseicapillus*). I. Kinematic and neuromuscular control of turning. *J Exp Biol* 210: 1897-1911. doi:10.1242/jeb.002055.

Hedrick TL, Cheng B & Deng XY (2009) Wingbeat time and the scaling of passive rotational damping in flapping flight. *Science* 324: 252–255.

Hedrick TL (2008) Software techniques for two- and three-dimensional kinematic measurements of biological and biomimetic systems. *Bioinspir. Biomim.* 3: 034001.

Hedrick TL & Biewener AA (2007) Low speed maneuvering flight of the rose-breasted cockatoo (*eolophus roseicapillus*). I. Kinematic and neuromuscular control of turning. *J Exp Biol* 210(11): 1897–1911.

Hedrick TL, Usherwood JR & Biewener AA (2007) Low speed maneuvering flight of the rose-breasted cockatoo (*eolophus roseicapillus*). II. Inertial and aerodynamic reorientation. *J Exp Biol* 210(11): 1912–1924.

Iriarte-Diaz J & Swartz SM (2008) Kinematics of slow turn maneuvering in the fruit bat *Cynopterus brachyotis J Exp Biol* 211: 3478-3489.

Iriarte-Diaz J, Riskin DK, Willis DJ, Breuer KS & Swartz SM (2011) Whole-body kinematics of a fruit bat reveal the influence of wing inertia on body accelerations. *J Exp Biol* 214: 1546-1553.

Iwaniuk AN & Wylie DR (2007) Neural specialization for hovering in hummingbirds: Hypertrophy of the pretectal nucleus lentiformis mesencephali. *Journal of Comparative Neurology* 500(2): 211-221.

Kern R, Boeddeker N, Dittmar L, Egelhaaf M (2012) Blowfly flight characteristics are shaped by environmental features and controlled by optic flow information. *J Exp Biol* 2015: 2501-2514. doi:10.1242/jeb.061713.

Kjaersgaard A, Pertoldi C, Loeschcke V, Witzner Hanzen D (2008) Tracking the gaze of birds. J *Avian Biol* 39: 466-469. doi: 10.1111/j.2008.0908-8857.04288.x.

Land MF (1973) Head movements of flies during visually guided flight. *Nature* 243: 299-300.

Land MF (1999) Motion and vision: why animals move their eyes. *J. Comp. Physiol. A* **185**, 341–352.

LaValle SM (2006) *Planning algorithms*. Cambridge: Cambridge Univ. Press.

Lee DN, Davies MNO, Green PR & Vanderweel FRR (1993) Visual control of velocity of approach by pigeons when landing. *J Exp Biol* 180: 85-104.

Lee DN, Reddish PE & Rand DT (1991) Aerial docking by hummingbirds. *Naturwissenschaften* 78: 526-527.

Liske E (1977) The influence of head position on the flight behavior of the fly *Calliphora erythrocephala*. *J Insect Physiol* 23: 375-379.

Lorenz KZ (1933) Beobachtetes über das Fliegen der Vögel und über die Beziehungen der Flügel- und Steuerform zur Art des Fluges. *Journal für Ornithologie* 81: 107–236.

Maurice M & Gioanni H (2004) Role of the cervico-ocular reflex in the “flying” pigeon: interactions with the optokinetic reflex. *Vis Neurosci* 21: 167–180.

Mitiguy P (2008) *Dynamics for Mechanical, Aerospace, and Biomechanical Engineers*.

Mittelstaedt H (1950) Physiologie des Gleichgewichtssinnes bei fliegenden Libellen. *Z Vergl Physiol* 32: 422-463.

Morrison IF (1928) Note on the inertia dyadic. *Science* 67: 630.

Nachtigall W (1979) Schiebeflug bei der Schmeißfliege *Calliphora erythrocephala* (Diptera: Calliphoridae). *Entom Gen* 5: 255–265.

Nalbach H-O, Wolf-Oberhollenzer F, Kirschfeld K (1990) The pigeon's eye viewed through an ophthalmoscopic microscope: orientation of retinal landmarks and significance of eye movements. *Vision Res* 30: 529-540.

Necker R (2007) Head-bobbing of walking birds. *J Comp Physiol A* 193: 1177-83.

Newman FH & VHL Searle (1957) *The general properties of matter*. London: Arnold.

Norberg UM (1976) Aerodynamics, kinematics, and energetics of horizontal flapping flight in the long-eared bat *Plecotus auritus*. *J Exp Biol* 65: 179-212.

Norberg UM (1990) *Vertebrate flight*. Berlin: Springer-Verlag.

Phillips WF (2004) *Mechanics of Flight*. Hoboken: Wiley.

Pratab R & Ruina A (2009) Introduction to Statics and Dynamics. Oxford: Oxford University Press.

Rayner JMV (1988) The evolution of vertebrate flight. *Biol J Linn Soc* 34: 269–287.

Ros IG, Ahn AA, Koh S, Biewener AA (in prep).

Ros IG, Bassman LC, Badger MA, Pierson AN & Biewener AA (2011) Pigeons steer like helicopters and generate down- and upstroke lift during low speed turns. *PNAS* 108: 19990-19995. (doi: 10.1073/pnas.1107519108)

Rüppell G (1977) *Bird flight*. New York: Von Nostrand Reinhold.

Schilstra C, van Hateren JH (1998) Stabilizing gaze in flying blowflies. *Natur*e 395: 654. doi:10.1038/27114.

Simpson JI (1984) The accessory optic system. *Ann Rev Neurosci* 7: 13–41.

Spedding GR, Rayner JMV & Pennycuick CJ (1984) Momentum and energy in the wake of a pigeon (*Columba livia*) in slow flight. *J Exp Biol* 111: 81-102.

Srinivasan MV, Lehrer M, Kirchner WH & Zhang SW (1991) Range perception through apparent image speed in freely flying honeybees. *Vis Neurosci* 6: 519–535.

Srinivasan MV, Zhang SW, Lehrer M & Collett TS (1996) Honeybee navigation en route to the goal: visual flight control and odometry. *J Exp Biol* 199: 237-244.

Stepniewski WZ & Keys CN (1984) *Rotary-wing Aerodynamics.* New York: Dover Publications.

Stolpe M & Zimmer K (1939) Der Schwirrflug des Kolibri im Zeitlupenfilm. *J Orn* 87: 136-155.

Su JY, Ting SC, Chang YH & Yang JT (2011) Aerodynamic trick for visual stabilization during downstroke in a hovering bird. *Physical Review E* 84: 012901.

Sugiura H & Dickinson MH (2009) The generation of forces and moments during visually-evoked steering maneuvers in flying *Drosophila*. *PLoS ONE* 4: e4883.

Sy M (1936) Funktionell-anatomische Untersuchungen am Vogelflügel. *Journal für Ornithologie* 84: 199–296.

Talbot PD & Corliss LD (1977) A Mathematical force and moment model of a UH-1H helicopter for flight dynamics simulations NASA Ames Research Center and Ames Directorate, USAAMRDL, AVRAD-COM.

Tobalske BW (2007) Biomechanics of bird flight. *J Exp Biol* 210: 3135–3146.

Tobalske BW, Hedrick TL, Dial KP & Biewener AA (2003) Comparative power curves in bird flight. *Nature* 421: 363-366.

Vazquez RJ (1995) Functional anatomy of the pigeon hand (*Columba livia*): a muscle stimulation study. *Journal of Morphology*, 226(1): 33-45.

Verspui R, Gray JR (2009) Visual stimuli induced by self-motion and object-motion modify odour-guided flight of male moths (*Manduca sexta* L.). *J Exp Biol* 212: 3272-3282. doi:10.1242/jeb.031591.

Videler JJ, Weihs D, Daan S (1983) Intermittent gliding in the hunting flight of the kestrel, *Falco tinnunculus L.*. *J Exp Biol* 102: 1-12.

Vogel S (1966). Flight in *Drosophila*. I. Flight performance of tethered flies. *J Exp Biol* 44: 567-78.

Wagner H (1986) Flight performance and visual control of flight of the free-flying housefly (*Musca domestica* L.). I. Organization of the flight motor. *Phil Trans R Soc Lond B* 312: 527-551.

Wallman J, Pettigrew JD (1985) Conjugate and disjunctive saccades in two avian species with contrasting oculomotor strategies. *J Neurosci* 5: 1418-1428.

Wallman J, Velez J (1985) Directional asymmetries of optokinetic nystagmus: developmental changes and relation to the accessory optic system and to the vestibular system. *J Neurosci* 5: 317–329.

Warren R & Wertheim AH (1990) Perception and control of self-motion. Hillsdale, NJ: Erlbaum.

Warrick DR, Bundle MW, Dial KP (2002) Bird maneuvering flight: blurred bodies, clear heads. *Integ Comp Biol* 42: 141–148. doi:10.1093/icb/42.1.141.

Warrick DR, Dial KP (1998) Kinematic, aerodynamic and anatomical mechanisms in the slow, maneuvering flight of pigeons. *J Exp Biol* 201: 655-672.

Warrick DR, Tobalske BW & Powers DR (2005) Aerodynamics of the hovering hummingbird. *Nature* 435: 1094-1097.

Warrick DR (1998) The turning and linear maneuvering performance of birds: The cost of efficiency for coursing insectivores. *Can J Zool* 76(6): 1,063–1,079.

Warrick DR & KP Dial (1998) Kinematic, aerodynamic, and anatomical mechanisms in the slow maneuvering flight of pigeons. *J Exp Biol* 201:655–672.

Warrick DR, Dial KP & Biewener AA (1998) Asymmetrical force production in the maneuvering flight of pigeons. *The Auk* 115(4):916–928.

Weis-Fogh T (1972) Energetics of hovering flight in hummingbirds and in *Drosophila*. *J Exp Biol* 56: 79-104.

Winchester J (2006) *The Encyclopedia of modern aircraft: from civilian airliners to military superfighters.* San Diego: Thunder Bay Press.

Winter DA (2005) *Biomechanics and Motor Control of Human Movement*. Hoboken: Wiley.

Wylie DR & Frost BJ (1990) Binocular neurons in the nucleus of the basal optic root (nBOR) of the pigeon are selective for either translational or rotational visual flow. *Vis Neurosci* 5: 489–495.

Zeigler HP, Bischof HJ (1993) *Vision, Brain, and Behavior in Birds*. Cambridge (MA): MIT Press.

Zeil J, Boeddeker N, and Hemmi JM (2008) Vision and the organization of behavior. *Curr Biol* 18: 320–323.

Zimmer K (1943) Der Flug des Nektarvogels (*Cinnyris*). *Journ F Orn* 91: 371-387.